Synthesis, pharmacological and solubility evaluation of antiplasmodial pyrido[1,2-*a*]benzimidazoles with cyclic and functionalized amine side chain substituents.

Ferdinand Wafula Ndubi

University of Cape Town

August 2016

Synthesis, pharmacological and solubility evaluation of antiplasmodial pyrido[1,2-*a*]benzimidazoles with cyclic and functionalized amine side chain substituents.

A dissertation submitted to the University of Cape Town in fulfillment of the requirements for the degree

Masters in Chemistry

by

Ferdinand Wafula Ndubi

Supervisor: Prof. Kelly Chibale

Co-supervisor: Prof. Mino R. Caira

Department of Chemistry

University of Cape Town

Rondebosch, 7701

Cape Town

South Africa.

August 2016

Declaration

I declare that ***Synthesis, pharmacological and solubility evaluation of antiplasmodial pyrido[1,2-a]benzimidazoles with cyclic and functionalized amine side chain substituents*** is my original work and has not been presented for the award of any degree at any university. I know the meaning of plagiarism and declare that all of the work in the document, except for that which is properly acknowledged, is my own.

_____

Ferdinand W. Ndubi

August 2016.

Acknowledgements

I would like to most sincerely thank Prof. Kelly Chibale for the opportunity as well as the support, guidance, assistance and supervisory input throughout this research project. I wish to thank Prof. Mino Caira for the support and advice I received from him. Your cumulative efforts have made this the most memorable learning phase of my life so far, and for that I am forever grateful.

I also wish to sincerely thank Dr. Kawaljit Singh, Dr. Peter Njogu, Paul Njaria and Dr. Nicholas Njuguna for introducing me and teaching me the ropes when I began this research project. Your guidance was invaluable. I also thank Elaine Rutherfoord-Jones and Deirdre Brooks for taking care of the administrative arrangements and ensuring my focus was fully on this project.

Special thanks to Carmen de Kock, Duane Knowles, Mathew Njoroge, Christel Brunschwig, Jill Combrinck, Nina Lawrence and John Okombo for the *in vitro* testing of my compounds. Also to Peter J. Smith, Sergio Wittlin (STPH), Lyn-Marie Birkholtz (UP) and Theresa Coetzer (Wits) for further testing of the analogues in this project. I wish to thank Dr. Hong Su (CSCR, UCT) and Pete Roberts (NMR) for their assistance with XRD and spectroscopic analysis.

A huge thank you goes out to the entire KC research group, especially the PBI group comrades (Linley, Godfrey, John and Peter) for the support and ideas. I also thank Terence Noonan, Vaughan Maurel, Richard Payne, Francoise Amombo Noa and Merrill Wicht (CSCR) for their assistance. Special thanks to Peter Cheuka and Dr. Sandile Simelane for proof-reading my chapters before submission.

To my mother, Mrs. Phoebe Ndubi, and my siblings Sammy, Fred, Cyrillah, Enock and Christabel; thanks for the support. Thank you all for always being there for me.

Finally, to my wife Joy and my little girl Cheryl; thank you both for helping me focus on the important things in life. Everything is a lot more meaningful with you guys around, and may God continue to bless you abundantly.

Conferences

January 2016 – Short talk and poster presentation:

Synthesis and antimalarial structure-activity relationship studies of cycloalkylamine functionalized pyrido[1,2-a]benzimidazoles presented at the **Keystone symposia 2016 conference: Drug discovery for parasitic diseases**, January 24-28 2016, Granlibakken resort, Tahoe city, California (USA).

ABSTRACT

Malaria continues to cause significant morbidity and mortality globally, especially in sub-Saharan Africa where the disease is endemic. Widespread resistance by *Plasmodium* parasites to chloroquine and sulphadoxine-pyrimethamine, once mainstays of malaria treatment, has further set back control efforts. Recent reports of emerging resistance to ACTs, the current first-line antimalarial drugs, present an even grimmer picture in regard to future control and eradication of malaria. Moreover, antimalarial medications in current clinical use are fraught with challenges of high cost, low availability and undesirable adverse effects associated with their use. This cocktail of factors calls for accelerated research efforts to identify novel, safe and efficacious agents for treatment of malaria. Pyrido[1,2-*a*]benzimidazoles (PBIs) have previously been shown to possess potent antiplasmodial activity, but their *in vivo* antimalarial activity is limited by poor oral bioavailability arising from low aqueous solubility. The mechanism of action of PBI antimalarials remains unknown. In an attempt to address these initial limitations associated with PBIs, and shed light on potential contributing mechanisms of action, PBI analogues containing aliphatic cyclic and functionalized amine side chain substituents bearing polar, hydrogen-bonding groups were synthesized and evaluated for pharmacological and beta-hematin inhibition activity. The functionalized and cyclic amine side chain substituents were envisaged to improve aqueous solubility of the new analogues while maintaining or improving antiplasmodial activity and metabolic stability. Aminopiperidine-based compounds were found to possess the most potent antiplasmodial and beta-hematin inhibition activity coupled with moderate to high turbidimetric solubility. Analogues with pyrrolidine and piperazine groups showed only moderate activity in the *in vitro* assays, and also showed lower solubility compared to the piperidines. Azetidine and cyclohexylamine substitution led to compounds with moderate to poor *in vitro* activity and solubility. Substitution with highly polar functions and reduced basicity of the second amino group on the cyclic amine moiety were found to be detrimental to both activity and solubility. Minimal substitution on the PBI core was also carried out, where dichloro groups were found to improve both antiplasmodial and beta-hematin inhibition activity, as well as microsomal metabolic stability. These analogues, however, showed increased cytotoxicity compared to their unsubstituted counterparts. Salt screening was also attempted for one of the frontrunner analogues, resulting in a total of five salts. All but one of the salts were moderately

soluble in the kinetic solubility assay, as was the free base form of the compound. Two of the five salts showed higher solubility than the free base.

List of Abbreviations

°C	Degrees Celsius
δ	Delta (NMR chemical shift)
μM	micromolar
ACT	Artemisinin Combination Therapy
API	Active Pharmaceutical Ingredient
ARU	Asymmetric Residue Unit
ASU	Asymmetric Unit
ATP	Adenosine Triphosphate
BCS	Biopharmaceutical Classification System
BHIA	Beta-hematin Inhibition activity
C Log P	Calculated Log P
CD	Cyclodextrin
CHO	Chinese Hamster Ovarian
CQ	Chloroquine
CQS	Chloroquine-sensitive
CSD	Cambridge Structural Database
CYP450	Cytochrome P450
DAD	Diode Array Detector
DCM	Dichloromethane
DHA	Dihydroartemisinin
DMF	*N*, *N*-dimethylformamide
DMSO	Dimethyl sulfoxide
DMSO-*d*	Deuterated dimethyl sulfoxide
DSC	Differential scanning calorimetry
Et_3N	Triethylamine
EtOAc	Ethyl acetate

G6PD	Glucose-6-phosphate dehydrogenase
GRAS	Generally regarded as safe
HEPES	4-(2-hydroxyethyl)-1-piperazineethylsulfonic acid
Hex	Hexane
HLM	Human liver microsomes
HPLC	High Performance Liquid Chromatography
HTS	High throughput screening
IC_{50}	Half-maximal inhibitory concentration
ip	intraperitoneal
LC-MS	Liquid chromatography-Mass spectrometry
LHS	Left-hand side
m/z	mass-to-charge ratio
MeCN	Acetonitrile
MeOH	Methanol
mg/kg	milligram per kilogram
$MgSO_4$	Magnesium sulfate
MHz	Megahertz
MLM	Mouse liver microsomes
MMV	Medicines for Malaria Venture
MP	Melting point
MS	Mass spectrometry
MSD	Mean survival days
MTS	Medium throughput screening
MTT	3-(4,5-dimethylthiazol-2-yl)-2,5-diphenyltetrazoliumbromide
MW	Molecular weight
NADPH	Nicotinamide Adenine Dinucleotide phosphate (reduced form)
$NaHCO_3$	Sodium bicarbonate

NCE	New Chemical Entity
NH_4OAc	Ammonium acetate
NME	New Molecular Entity
NMR	Nuclear Magnetic Resonance
ORTEP	Oak Ridge Thermal Ellipsoid Plot
PAMPA	Parallel artificial membrane permeability assay
PBI	Pyrido[1,2-*a*]benzimidazole
PBS	Phosphate-buffered saline
PK	Pharmacokinetic
pKa	Ionization constant
po	per oral
$POCl_3$	Phosphorus (V) oxychloride
PV	Parasitophorous vacuole
RLM	Rat liver microsomes
SAR	Structure-activity relationship
SI	Selectivity Index
SP	Sulfadoxine-pyrimethamine
TCAMS	Tres Cantos antimalarial set
TGA	Thermogravimetric analysis
THF	Tetrahydrofuran
TLC	Thin layer chromatography
tPSA	Topological polar surface area
VT-NMR	Variable Temperature Nuclear Magnetic Resonance
WHO	World Health Organization
XRD	x-ray diffraction

TABLE OF CONTENTS:

CHAPTER 1: INTRODUCTION AND LITERATURE REVIEW

1.1 MALARIA

1.1.1 Background information, history and aetiology

Malaria is an infectious parasitic disease caused by various protozoan species belonging to the genus *Plasmodium*.[1] The term "malaria" originates from the two Italian words "mal" (bad) and "aria" (air) owing to the early association of the disease with marshy areas and the assumption that the foul air was responsible for its causation.[1,2]

Malaria is a disease of the ancient world, and references to malaria-like infections are found as far back as 2700 BC from Chinese documents, 2000 BC from Mesopotamia clay tablets, 1570 BC from Egyptian papyrus hieroglyphics and Hindu texts originating from the 6th Century BC.[2-3] It was, however, only in 1880 that malaria parasites were first detected in a patient"s blood by the French army officer Charles Louis Alphonse Laveran. This was followed by discovery of sexual stages of the parasites in blood by William McCallum and elucidation of the transmission cycle in culicine mosquitoes and birds infected with *Plasmodium relictum* by Ronald Ross, both in 1897.[3] These events marked a significant step forward in understanding the cause and transmission of malaria. Conclusive evidence that human malaria was transmitted by Anopheline mosquitoes was demonstrated by a group of Italian malariologists in 1898.[4] In 1948, Henry Shortt and Cyril Garnham discovered the development of malaria parasites in the liver before entry into the bloodstream. Finally, presence of dormant stages of the parasite in the liver was demonstrated by Wojciech Krotoski in 1982.[2,4]

More than 100 species of *Plasmodium* have been identified, of which only five are known to cause human malaria: *P. falciparum, P. malariae, P. vivax, P. ovale* and *P. knowlesi*.[5] *P. falciparum* is responsible for causation of the most severe form of the disease.[6] Falciparum malaria, therefore, contributes most significantly to morbidity and mortality rates associated with the disease. The two species *P. vivax* and *P. ovale* cause a milder form of disease although they result in future relapses due to persistence of dormant hypnozoite forms in the liver.[7-9] *P. malariae* is usually associated with infections of chronic nature and can persist in blood asymptomatically for long periods of time.[10] The zoonotic parasite *P. knowlesi* was only previously known to cause malaria in Macaque monkeys (*Macaca fascicularis*), but has now

been shown to also infect humans.[11-13] Various species of *Anopheles* mosquitoes are responsible for human transmission of these parasites.[14]

Effective control of malaria worldwide has been greatly hampered by high cost, toxicity and severe adverse effects of existing antimalarials coupled with development of resistance to these agents.[15-17] Resistance to chloroquine and sulphadoxine-pyrimethamine is extensively mapped by now.[18,19] Of greater concern are recent reports of emerging resistance to artemisinin-combination therapies (ACTs) in South-East Asia, the current first line agents in malaria treatment.[20] Vector resistance to commonly used insecticides[21]and the unavailability of an effective malaria vaccine[22-24] have also impacted on the global fight against the disease.

1.1.2 Epidemiology

Malaria has a worldwide distribution; with tropical and sub-tropical regions of the world bearing the highest endemicity rates.[25] These regions include sub-Saharan Africa, Amazonia, Southern Asia and the Asia-Pacific locale. Lower rates are observable in Southern Africa, Europe, Australia and North America. However, even in endemic areas, the epidemiology of malaria is highly heterogeneous and determined by local factors including the predominant parasite species, vector characteristics, seasonal transmission patterns and transmission intensity.[26]

According to the World Health Organization (WHO) malaria report of 2015, a total of 214 million (range: 149-303 million) cases of malaria were recorded, resulting in 438,000 deaths (range: 236,000-635,000).[27] This represented an 18% reduction in comparison to the malaria incidences recorded in 2010 (262 million) and a 48% decline in the number of deaths in that year (839,000). Most of the cases (80%) and deaths (90%) occurred in sub-Saharan Africa.[27] Malaria case incidences are highest among children under five years of age and pregnant women, with the disease claiming the life of a child in sub-Saharan Africa every 2 minutes.[27-30]

In spite of the reported decline in global malaria cases, reports of emerging resistance to ACTs pose a significant threat to the gains made in fighting the disease.[20,31-33] Also, countries in sub-Saharan Africa still face a huge malaria burden due to the favorable tropical climatic conditions which foster mosquito breeding, coupled with social and political instability in some regions and resource-poor economies which limit investment in malaria prevention strategies.[34] Additionally,

Europe and other non-endemic areas are still grappling with the challenge of imported malaria.[35,36] This necessitates the need for development of new antimalarials.

1.1.3 Life cycle and pathophysiology

Malaria is transmitted by the bite of an infected female *Anopheles* mosquito.[37] Although there are approximately 400 known species of *Anopheles* mosquitoes globally, only about 60 are malaria vectors under natural conditions.[1,37] Of these, about 30 species are of significant public health concern.

When an infected mosquito takes a blood meal, *Plasmodium* sporozoites contained in its salivary glands are discharged into the punctured host dermis[1,5,37] (**Fig. 1.1**). The sporozoites are carried in the bloodstream to the liver.[38] Once in the liver, each sporozoite traverses various hepatocytes before finally infecting a specific hepatocyte with the formation of a parasitophorous vacuole (PV). The sporozoites, shielded away in the PV, undergo further development and maturation to form mature liver schizonts, each containing tens of thousands of first generation merozoites.[5,38] This initial stage of parasite development in the liver, known as the exoerythrocytic stage, is asymptomatic and lasts about 9-16 days.[1]

Upon maturation, the schizonts burst to release thousands of merozoites into the bloodstream.[5] In *P. vivax* and *P. ovale*, some liver schizonts transform to dormant tissue forms known as hypnozoites.[7-9] These persist in the liver for long periods and can cause relapses even after several years (**Fig. 1.1**). Hypnozoite formation does not occur in *P. falciparum* and *P. malariae* infections. Although numerous merozoites are destroyed by the immune system, a significant portion survive and infect erythrocytes.[39] This marks the beginning of the erythrocytic stage, which is accompanied by characteristic symptoms of the disease such as fever and chills. Invasion of human red blood cells (RBCs) by *Plasmodium* merozoites is a complex process involving various recognition mechanisms and proteins.[40] Intraerythrocytic asexual division continues to form more merozoites, which are released into the bloodstream and invade more erythrocytes. These invasion-multiplication-release-invasion cycles last about 48 hours in *P. falciparum*, *P. vivax* and *P. ovale*; and about 72 hours in *P. malariae* infections.[5] The cycles continue until the host succumbs or the blood-stage parasites are cleared by chemotherapy.

During the course of intraerythrocytic division, some merozoites differentiate to form male and female gametocytes.[41] These sexual forms of the parasite are ingested by a mosquito taking a blood meal, and in the mosquito‟s gut they undergo exflagellation to form microgametes which fuse and undergo fertilization to yield a zygote.[5,41] The zygote transforms into a motile stage, the ookinete[41], which then migrates to the mosquito midgut, secretes a wall and grows to form an oocyst.[1,5] The oocyst undergoes maturation with formation of hundreds of merozoites, and eventually ruptures to release the merozoites into the insect‟s hemocele. These are dispersed throughout the insect‟s system, including the salivary glands.[5] Upon ingesting its next blood meal, the infected mosquito inoculates the merozoites and thus a new life cycle begins (**Fig. 1.1**).

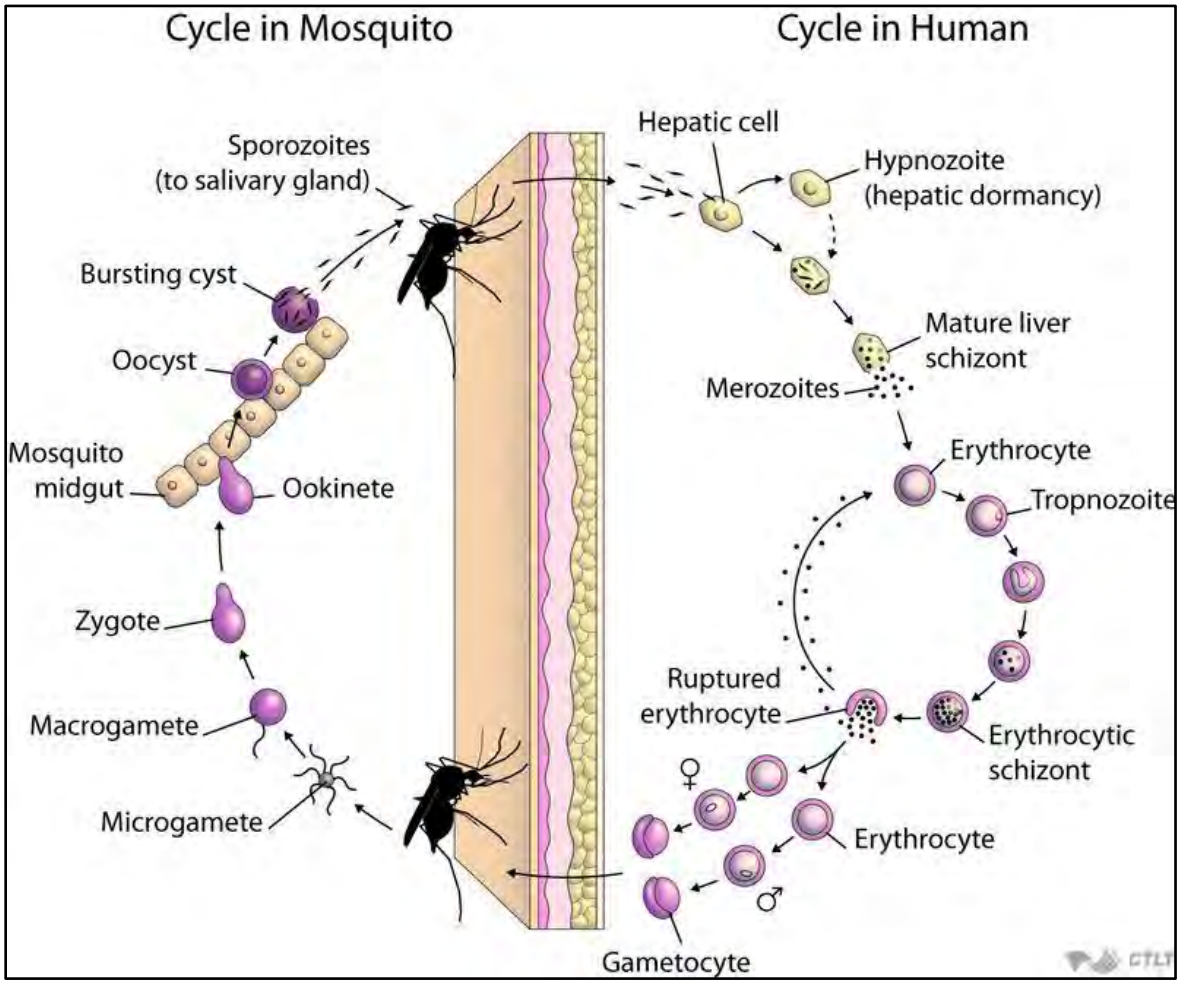

Fig. 1.1: Life cycle of *Plasmodium* parasites - adapted from CTLT (UBC) online resources.[42]

1.1.4 Treatment of malaria

With proper and timely diagnosis, malaria infections are largely treatable.[43,44]

The choice of a specific treatment regimen is determined by four main factors:[44]

- ✓ Species of the infecting *Plasmodium* parasite
- ✓ Clinical status of the patient (uncomplicated versus severe)
- ✓ Drug susceptibility of the infecting parasite depending on local and regional resistance patterns
- ✓ Special risk groups e.g. pregnant women, infants and non-immune travellers

According to the WHO malaria treatment guidelines of 2015, artemisinin-combination therapy (ACT) is the treatment of choice for adults and children diagnosed with uncomplicated *P. falciparum* malaria.[45] This consists of an artemisinin derivative e.g. artemether in combination with a longer-acting blood schizonticide such as lumefantrine. Examples of common ACT regimens used include artemether-lumefantrine, artesunate-amodiaquine, artesunate-mefloquine, dihydroartemisinin (DHA)-piperaquine and artesunate-sulfadoxine/pyrimethamine (SP) (**Figs. 1.2** and **1.3**). A novel, water-soluble artemisinin derivative, artelinic acid (or its sodium salt artelinate sodium, **Fig. 1.2**) is also currently undergoing trials as a potential antimalarial.[46,47] These regimens are usually optimized to suit the patient‟s body weight and are administered orally over a duration of three days.[45] Artemisinin derivatives are fast-acting blood schizonticides[48] and therefore are combined with the slower-acting agents to prevent development of resistance and also minimize chances of recrudescence after clearance of the initial blood parasite load.[49,50] Clearance of blood forms of *Plasmodium* effectively treats the clinical sequelae associated with the disease.

ACT is also recommended in treating uncomplicated *P. falciparum* malaria in pregnant women excluding those in the first trimester as well as in infants, patients co-infected with HIV, non-endemic travellers returning from endemic settings and cases of hyperparasitemia.[45]

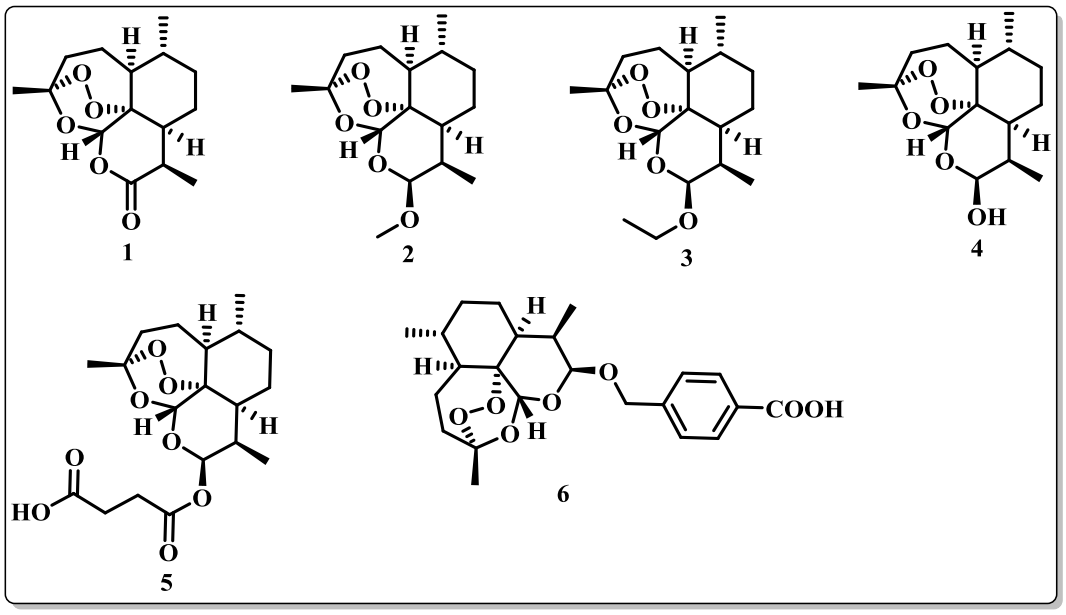

Fig. 1.2: Chemical structures of artemisinin (**1**) and its derivatives used in malaria treatment – artemether (**2**), arteether (**3**), DHA (**4**), artesunic acid (**5**) which is usually used as the salt form artesunate sodium and artelinic acid (**6**).

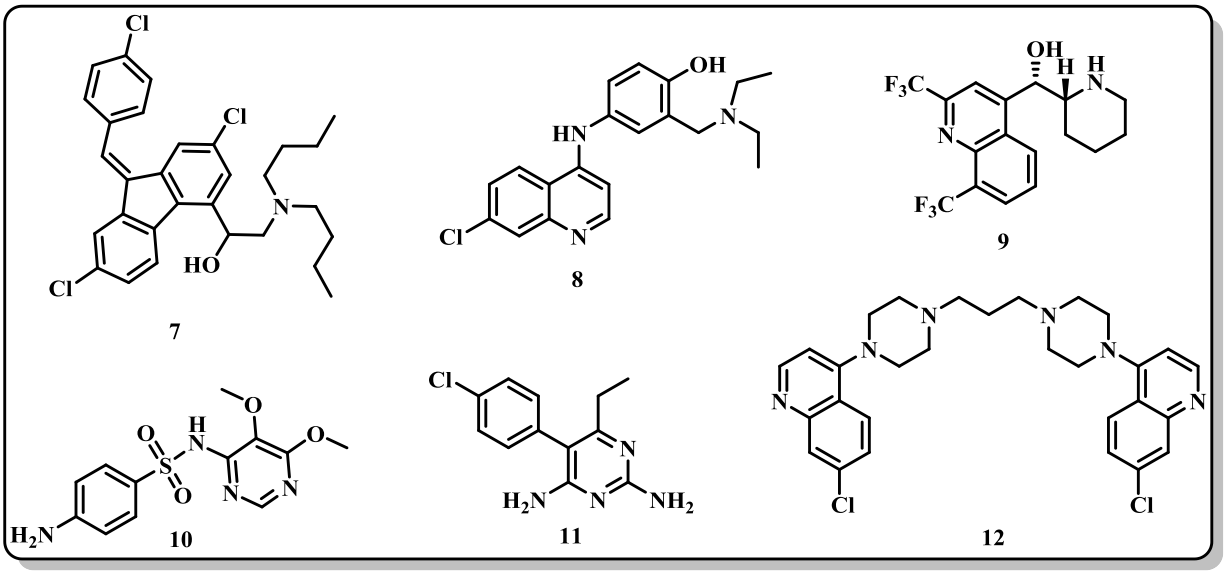

Fig. 1.3: Chemical structures of agents used in ACT regimens – lumefantrine (**7**), amodiaquine (**8**), mefloquine (**9**), sulfadoxine (**10**), pyrimethamine (**11**) and the symmetrical bisquinoline piperaquine (**12**).

The treatment of choice for uncomplicated cases of *P. vivax*, *P. ovale*, *P. malariae* or *P. knowlesi* malaria in areas with prevalent chloroquine resistance is a suitable ACT.[45] Otherwise, chloroquine (**Fig. 1.4**) is used in areas where it retains activity against these parasites. Pregnant

women in the first trimester who have chloroquine-resistant *P. vivax* malaria are treated with quinine[44] (**Fig. 1.5**). Primaquine (**Fig. 1.4**), an 8-aminoquinoline and the only antimalarial currently known to be active against the hypnozoite stage of *Plasmodium*, is used to achieve radical cure and prevent relapses in *P. vivax* and *P. ovale* malaria.[45,51,52] Primaquine is also the only antimalarial known to possess activity against *P. falciparum* gametocytes, and can therefore be used to prevent transmission of the parasite.[52] The drug, however, causes severe hemolysis in individuals with glucose-6-phosphate dehydrogenase (G6PD) deficiency.[53] Therefore, the G6PD status of patients has to be known before initiation of primaquine therapy.

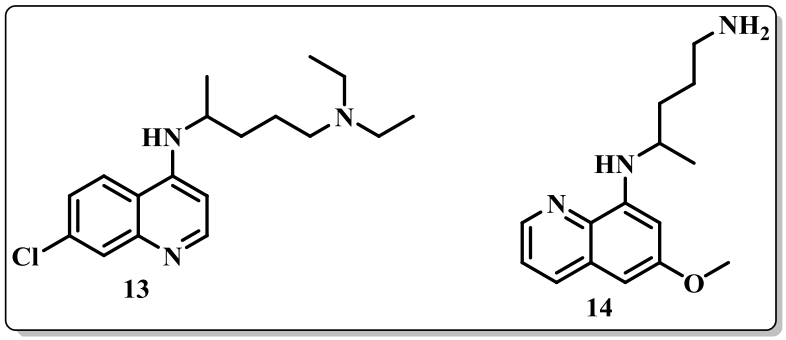

Fig. 1.4: Chemical structures of chloroquine (**13**) and primaquine (**14**).

The treatment of choice for uncomplicated *P. falciparum* malaria in pregnant women in the second and third trimesters is a 7-day course of ACT combined with Clindamycin.[45] For travellers returning to non-endemic countries, atovaquone-proguanil, a suitable ACT or quinine plus sulfadoxine-pyrimethamine are recommended.

Second line options for treatment of *P. falciparum* malaria generally consists of an ACT or quinine in combination with an antibiotic (**Fig. 1.6**), usually clindamycin, tetracycline or doxycycline.[45]

Even though significant resistance has developed to sulfadoxine-pyrimethamine, the combination is used for intermittent preventive therapy, a chemoprophylactic measure against malaria during pregnancy in endemic countries.[54,55]

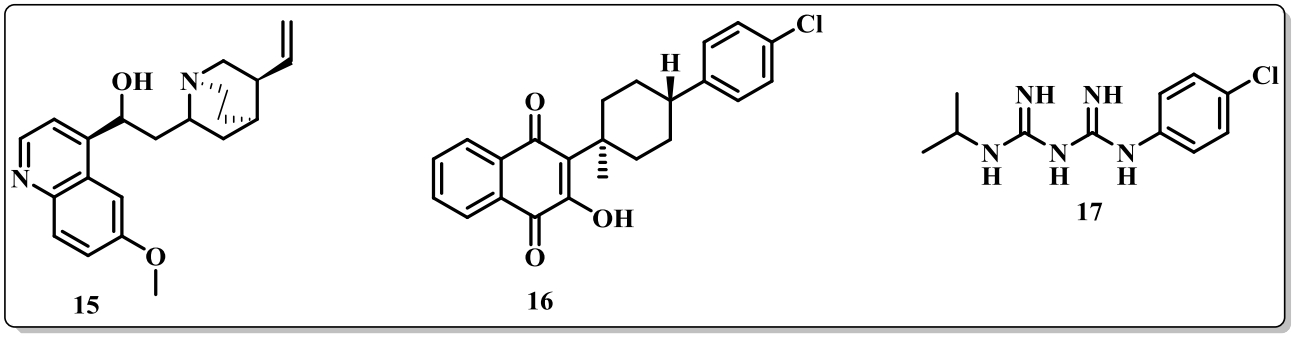

Fig. 1.5: Chemical structures of second line agents used in treatment of malaria – quinine (**15**), atovaquone (**16**) and proguanil (**17**).

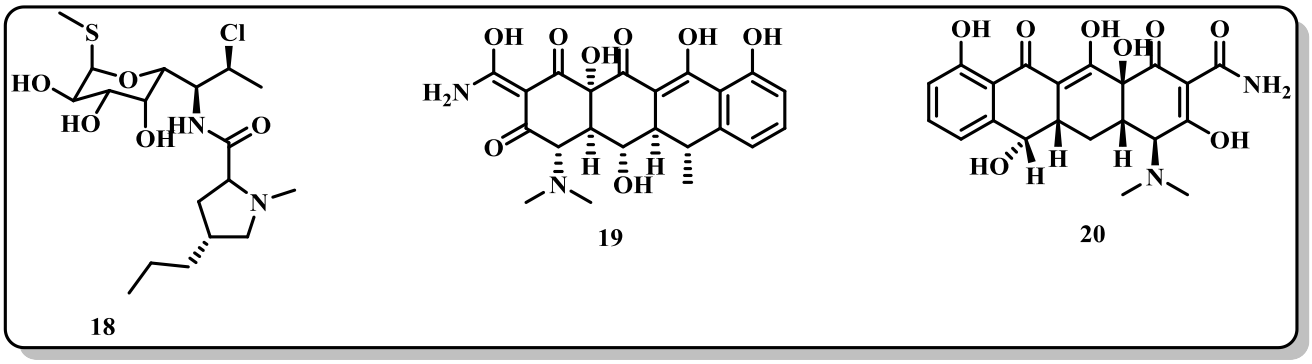

Fig. 1.6: Chemical structures of antibiotics used as second line agents in treatment of malaria – clindamycin (**18**), doxycycline (**19**) and tetracycline (**20**).

1.1.5 Challenges in treatment and control of malaria

Development of resistance to commonly used antimalarials is perhaps the biggest setback facing effective treatment and control of malaria today.[56] Resistance to chloroquine and sulfadoxine-pyrimethamine, once effective agents in malaria treatment, has almost invalidated their usefulness in many parts of the world.[18,19] Emerging resistance to artemisinins in South East Asia paints an even grimmer picture as ACT regimens are the current first-line agents in treatment of malaria.[16,20] This calls for an active malaria drug discovery pipeline to replace potent antimalarials that may be rendered ineffective by parasite resistance.

The utility of antimalarials currently in clinical use is also impacted upon by high cost, toxicity and adverse effects arising from their use.[15,17] Mosquito resistance to commonly used insecticides[21]coupled with the lack of an effective malaria vaccine as yet also greatly set back the fight against malaria globally.[22-24]

In the face of these drawbacks, efforts need to be made to develop new antimalarial drugs that will be:

- ✓ Affordable, so as to benefit a large segment of societies especially in resource-poor settings
- ✓ Active against drug-resistant mutants of *Plasmodium*
- ✓ Safe and effective to use with minimal adverse effects
- ✓ Possess novel mechanisms of action so as to forestall development of resistance
- ✓ Orally active, for convenience of administration.

1.2 PHENOTYPIC WHOLE CELL SCREENING AS A STRATEGY IN ANTIMALARIAL DRUG DISCOVERY.

1.2.1 Introduction

Various strategies have been employed in the search for novel antimalarial drugs. One such approach is high-throughput screening of large numbers of small molecules with high chemical diversity against whole parasite cells.[57] Compound libraries commonly available for public use are utilized to screen hundreds to thousands of compounds in automated screening systems, usually yielding leads that can then be progressed by medicinal chemistry optimization.[57,58] The most well-known of these compound libraries include the Genomics Institute of the Novartis Research Foundation malaria box, the GlaxoSmithKline Tres-Cantos Antimalarial Set (TCAMS) library and the Medicines for Malaria Venture (MMV) malaria box.

Over the last few years, phenotypic whole-cell screening has proven to be more successful in yielding antimalarial leads as compared to target-based screening.[57,59] This can be attributed to the fact that leads identified by phenotypic screening already possess the necessary features to interact with their targets, as opposed to those from target-based screening campaigns which utilize an isolated and purified target. Membrane permeability characteristics and the general cellular physiological conditions are, therefore, already catered for by phenotypic screens.[60] Phenotypic screens also possess the advantage of being able to identify leads which act on novel targets, or more than a single parasite target.[58,60] This can be extremely vital in instances where the disease biology is not well understood as it can expose new biological pathways and also forestall selection of resistant mutants.

As part of an MMV-University of Cape Town drug discovery collaboration, phenotypic high-throughput screening (HTS) of a BioFocus DPI SoftFocus® kinase library for antiplasmodial hits identified the 3,5-Diaryl-2-aminopyridine hit compound **21** (**Fig. 1.7**).[61,62] Medicinal chemistry optimization of **21** led to development of the candidate MMV048 (**22**), currently at the human volunteer stage of translational development.[63] The pyridobenzimidazole class of antimalarials, the subject of this research thesis, were also identified via a phenotypic high throughput screen. Details are discussed in the next chapter.

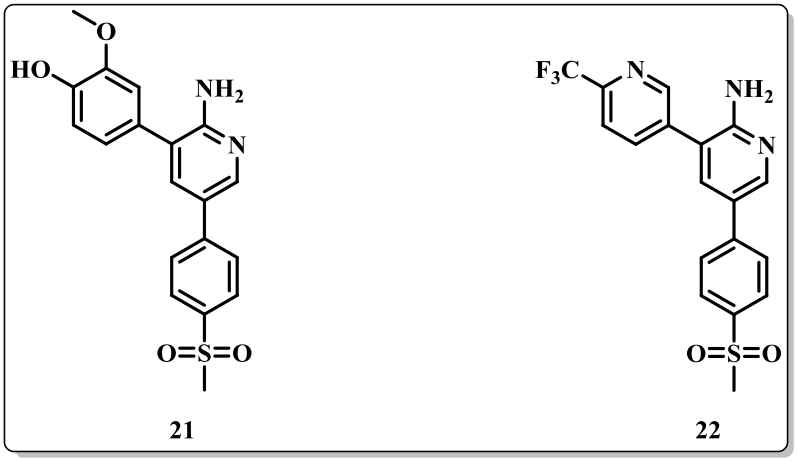

Fig. 1.7: Chemical structures of the screening hit compound **21** and MMV048 (**22**).

1.2.2 Phenotypic whole cell versus target based screening

Unlike phenotypic whole cell screening, target based screening utilizes known parasite drug targets against which compounds are tested to identify a lead.[57] This requires a parasitic drug target to be fully characterized and validated for such screening to be carried out. In essence, a drug target is only said to be fully validated when there exists a drug in current clinical use for which it has been proven that the main mechanism of action is by interaction with the target in question.[57,63]

In such cases where a drug target is fully validated, target based screening is usually combined with *in silico* methods, rational drug design and virtual screening so as to take full advantage of the properties of the drug target.[59,63,64]

Compared to phenotypic screening, target based screens have the advantage of being able to fully incorporate the latest developments in genomics and computational drug design for lead optimization.[65] The precise mechanism of action is also well understood. Additionally, target based screening is more aptly applicable in high-throughput screening programs as the purified target can be tested against a large number of compounds.[59,65] However, leads obtained by target based screening often fail to produce *in vivo* activity, usually due to physiological differences between the biological system and the isolated target.[65]

As mentioned earlier, phenotypic screening has the advantage of identifying leads which already possess some of the features necessary to exert activity at cellular level.[57-60] These are, therefore, more amenable to medicinal chemistry optimization to exert their activity at the tissue and whole organism levels. The absence of target bias in these screens also allows for testing against complex, multifaceted biological systems where exact disease mechanisms may not be fully understood.[59,65] A significant downside of using phenotypic screens in lead identification is that further deconvolution studies are usually required to elucidate the mechanism(s) of action for purposes of lead optimization.[65] These screens are also less applicable to large compound libraries, and physiological assay variables may affect their reproducibility.[65] Additionally, where multiple cellular targets are involved, multiple efficacy studies may need to be employed to fully elucidate the activity profile of a lead compound.[65]

1.2.3 Life cycle stage-specific screening in antimalarial drug discovery

Most antimalarials in clinical use today target the blood stage (merozoite) forms of the parasite.[5,44,45,48] By eliminating blood forms of the parasite which are responsible for the symptoms of malaria, clinical cure is achieved. However, malaria relapse is rife in patients infected with *P. vivax* and *P. ovale* due to persistence of hypnozoites in the liver.[7-9] Also, presence of gametocytes in patients‟ blood means they can still act as a reservoir for transmission of infection to other healthy individuals.[41]

Currently, primaquine is the only antimalarial active against gametocytes of *P. falciparum* and hypnozoite forms of *P. vivax* and *P. ovale*. It is, therefore, the only agent that can be used to achieve radical cure, prevent relapses and prevent malaria transmission.[45,51,52] Use of primaquine is, however, associated with serious, potentially fatal hemolysis especially in individuals with genetic G6PD deficiency.[53] This calls for development of new antimalarials to circumvent these challenges.

Modern antimalarial drug discovery programs, therefore, incorporate life cycle stage-specific screening at the early development phase to identify compounds that are:

- ✓ Active against gametocytes of *P. falciparum*, indicating potential for development as transmission-blocking agents
- ✓ Active against liver forms of the parasite, therefore potentially developable as agents that will achieve radical cure or prevent development of clinical malaria by clearing liver forms
- ✓ Active against hypnozoite forms of *P. vivax* and *P. ovale* to prevent relapses.

1.3 SOLUBILITY OF DRUG CANDIDATES

1.3.1 Introduction

With recent advances in high throughput screening techniques, compounds with extremely low aqueous solubility are increasingly making their way into early drug development.[57-60,66] Numerous low molecular weight, highly lipophilic compounds with poor aqueous solubility are continually being identified as leads and progressed into medicinal chemistry optimization programs.[66,67] Drug solubility is a significant factor in absorption, and therefore bioavailability, of orally-administered drugs.[67] Compounds with low aqueous solubility usually present a number of setbacks in drug discovery programs. These include poor absorption and bioavailability following oral doses, inability to be administered intravenously, inaccurate low activity from bioassays due to compound precipitation from solution and erratic bioassay results. They also present challenges in formulation development and even increased propensity for adverse effects owing to the need for frequent, high-dose administration.[68] Since oral administration is the cheapest and most convenient route for patients, the focus has to be on developing new drugs with adequate aqueous solubility so as to achieve the desired oral bioavailability. This, therefore, calls for drug development scientists to prioritize optimization of solubility, among other physicochemical properties, in the early stages of discovery.[67]

The Biopharmaceutical Classification System (BCS)[69] classifies drugs and new molecular entities (NMEs) in four groups based on their *in vitro* solubility and permeability properties:

- ✓ Class I - High solubility, high permeability
- ✓ Class II- Low solubility, high permeability
- ✓ Class III - High solubility, low permeability
- ✓ Class IV - Low solubility, low permeability

This mode of classification is usually based on *in vitro* kinetic solubility data and parallel artificial membrane permeability assays (PAMPA).[69,70] Compounds that fall under BCS classes II and IV are especially amenable to solubility improvement in the initial stages of development. Excluding first-pass metabolism in the liver, oral bioavailability is highly dependent on intestinal absorption, which is a function of the compound‟s solubility and permeability.[70]

Various physical, chemical and supramolecular methods can be employed to improve solubility of drug candidates, as outlined in the following section.

1.3.2 Methods used to improve solubility of drug candidates

1.3.2.1 Physical methods

Solubility of chemical entities can be influenced by the physical nature of the substance.[71] Methods such as micronization, selection of a different polymorph and use of solid dispersions have been used to improve compound solubility.[71,72]

Micronization or milling usually reduces the drug particle size to increase its surface area to volume ratio, therefore improving the compound‟s interaction with the solvent and resulting in improved dissolution rate. Solid dispersions can be defined as molecular mixtures of hydrophobic, poorly water soluble drugs with hydrophilic carriers.[72] This provides a drug release profile that is driven by the hydrophilic carrier polymer‟s properties.

Different polymorphs of the same compound usually have different solubilities and dissolution profiles.[71,73] By selecting the most favorable polymorph or polymorphic mixture, solubility of a given NME can be optimized.

1.3.2.2 Chemical methods

The intrinsic solubility of a compound is usually related to its chemical structure.[68] Chemical structure and specific functional groups on a molecule usually determine the compound‟s lipophilicity, size, ionizability (pK_a) and crystal lattice energy. To improve aqueous solubility, synthetic chemistry strategies such as introduction of ionizable groups, introduction of polar groups, inclusion of hydrogen-bonding groups, reduction of lipophilicity and disruption of planarity have been employed.[68,71,74-76]

Inclusion of ionizable groups generally increases solubility of hydrophobic compounds especially at pH ranges where these groups exist in their ionized forms.[71] Common groups used include amine and carboxylic acid functions, which in their ionized state improve the compound‟s interaction with water and therefore improve aqueous solubility.

Polar groups such as ester, amide and carboxylic acid functionalities are also used to improve solubility.[74] These tend to reduce the log P of hydrophobic compounds, improving their ability to interact with water and therefore improving their solubility. Hydrogen bonding between solute

molecules and water plays a significant role in enhancing aqueous solubility.[74] Introduction of hydrogen bond donors and acceptors such as hydroxyl and amino groups on highly lipophilic compounds can thus be employed to improve aqueous solubility.

Reduction in lipophilicity e.g. by replacement of phenyl groups with pyridyl or pyrimidinyl functions can also be used as a chemical means of improving aqueous solubility.[75] Reduced lipophilicity can also be achieved by saturation of aromatic functionalities, e.g. replacement of phenyl groups with cyclohexyl groups.[75] Generally, lipophilic molecules tend to self-associate and only interact minimally with water. A reduction in lipophilicity leads to better association with the aqueous environment. Also, numerous hydrophobic molecules possessing large, planar polycyclic aromatic hydrocarbon structures tend to associate by π-stacking interactions.[68,76] Substitution patterns that disrupt the planarity of such molecules usually disrupt the crystal packing characteristics, resulting in a higher-energy crystal lattice that is then more easily solubilized.[76]

A final approach involving improvement of solubility by modification of chemical structure utilizes prodrugs.[77] Prodrugs with superior aqueous solubility as compared to the parent drug are usually prepared for oral administration, and after absorption these are hydrolyzed to yield the parent drug.[78,79] Ester, acyl and amino acid-conjugated prodrugs are common examples in this regard. The prodrug is usually designed to achieve improved solubility and permeability, thus achieving better absorption.[78] Once absorbed, it is then cleaved by plasma enzymes to release the free drug.

1.3.2.3 Salt formation

Formation of salts is the cheapest, most common and most effective method used to improve aqueous solubility of lipophilic drugs.[66] The majority of drugs and new chemical entities (NCEs) under development today are weakly basic or acidic molecules possessing one or more ionizable groups.[66,80] These can be utilized to form salts with appropriate counterions. Owing to their ionic nature, the salts have optimal interaction with water molecules and this results in improved aqueous solubility compared to the free base or acid form.

Selection of an appropriate counterion to use in forming a salt for a specific active pharmaceutical ingredient (API) can usually be done using a high-throughput microplate

assembly.[81] This involves screening the API(s) in question against a range of possible counterions, and selection of the best candidates for scale-up and further characterization.

In spite of their large capacity to improve solubility of lipophilic molecules, salts present unique challenges especially in terms of physical stability.[82,83] Compared to the free base or acid form of a drug, salts usually have a different melting point, mechanical properties (e.g. flowability), stress stability, hygroscopicity and overall water content. These physical properties have to be taken into account when selecting a suitable salt for formulation.[82] Therefore, a balance has to be obtained between improvement of solubility and the desirable physical attributes necessary for formulation.

1.3.2.4 Co-crystals and cyclodextrin inclusion complexes

Co-crystals and cyclodextrin inclusion complexes represent supramolecular derivatives of APIs where no covalent or ionic bonding exists between the constituent molecules.

In general terms, co-crystals are multicomponent crystals composed of two or more molecular and/or ionic compounds in which all the components are solid under ambient conditions when in their pure form.[84,85] These usually exist in a stoichiometric ratio in the co-crystal assembly. A pharmaceutical co-crystal will, therefore, be composed of the API and one or more co-former(s). A number of „generally regarded as safe" (GRAS) co-formers are now listed for use in pharmaceutical co-crystals.[85] Pharmaceutical co-crystals usually utilize common supramolecular synthons (**Fig. 1.8**) obtained from the Cambridge Structural Database (CSD) to select suitable co-formers for specific API molecules.[74,84,86] Hydrogen bonding between the API and co-former synthon sustains the co-crystal architecture.

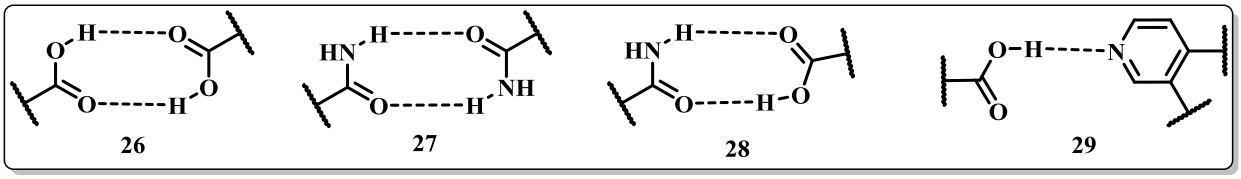

Fig. 1.8: Examples of common supramolecular synthons used in pharmaceutical co-crystals – carboxylic acid (**26**) and amide (**27**) homosynthons; carboxylic acid-amide (**28**) and carboxylic acid-pyridyl (**29**) heterosynthons.

Co-crystal formation between lipophilic APIs and more polar co-formers has been shown to improve both solubility and oral bioavailability of such molecules.[84-87]

Cyclodextrins (**Fig. 1.9**), on the other hand, are a family of naturally occurring cyclic oligosaccharides with hydrophobic inner cavities and hydrophilic groups on the exterior.[74,88] They are classified as α-, β- or γ-cyclodextrin depending on the number of sugar moieties in the ring. When dissolved in aqueous solution, the inner cavities of cyclodextrins are occupied by water molecules at high enthalpy. These are readily substituted by more hydrophobic guest molecules to form cyclodextrin inclusion complexes.[89] Upon saturation, the CD-drug inclusion complex exists in equilibrium with the free drug, thus enhancing solubility and bioavailability of the drug by its release from the cyclodextrin cavity.[88,90] Naturally occurring cyclodextrins and their semisynthetic derivatives used in pharmaceuticals are fairly non-toxic and upon dissociation of the CD-drug inclusion complex to yield the free drug, the cyclodextrin can be safely metabolized and excreted.[91]

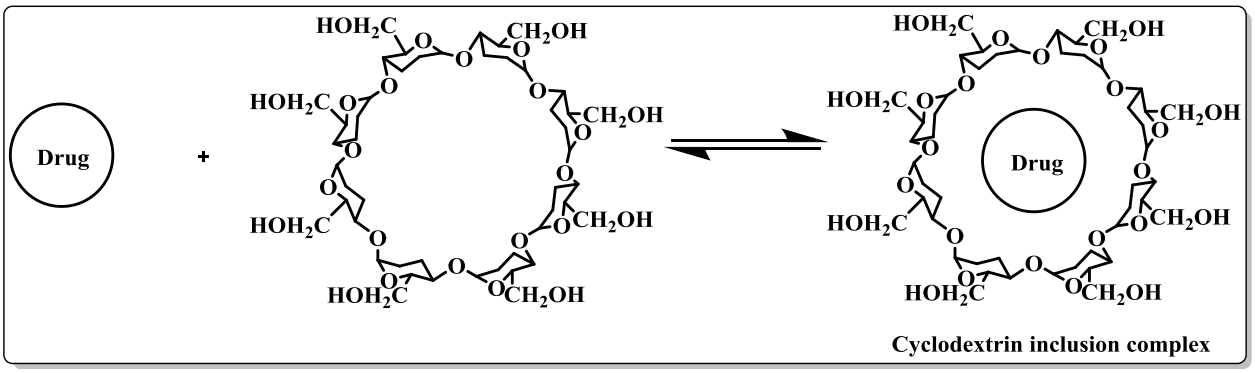

Fig. 1.9: Simple representation of formation of a cyclodextrin inclusion complex.

In this research project, attempts have been made to improve the aqueous solubility by chemical modification involving introduction of polar, hydrogen bonding groups. Salt formation was also attempted for the frontrunner compound. Details of these strategies are outlined in subsequent chapters.

1.4 AIMS AND OBJECTIVES

1.4.1 Main objective

Synthesis of antiplasmodial pyrido[1,2-*a*]benzimidazoles with cyclic and functionalized amine side chain substituents for pharmacological, physicochemical and SAR studies.

1.4.2 Research question/hypothesis

Is it possible to identify pyrido[1,2-*a*]benzimidazole (PBI) analogues with improved solubility while maintaining or improving antiplasmodial activity and metabolic stability?

1.4.3 Specific aims

i) Synthesis of pyrido[1,2-*a*]benzimidazole derivatives designed to improve solubility by introduction of polar groups for structure-activity relationship (SAR) studies.

ii) Characterization of the target compounds using various analytical, physical and spectroscopic techniques.

iii) Salt screening for selected compounds.

iv) Submission of the compounds synthesized for *in vitro* antiplasmodial activity testing, as well as cytotoxicity and *in vitro* metabolic stability testing for the most potent compounds.

v) Solubility assessment of all compounds synthesized and salt screening for selected compounds.

REFERENCES

1. Tuteja, R. Malaria – An overview. *FEBS J,* **2007**, *274*, 4670-4679.
2. Cox, E. F. G. History of the discovery of malaria parasites and their vectors. *Parasit. Vec.,* **2010**, *3*, 2-9.
3. Schlagenhauf, P. Malaria: From pre-history to present. *Infect. Dis. Clin. North Am.*, **2004**, *18*, 189-205.
4. Bruce-Chwatt, L. J. Alphonse Laveran‟s discovery 100 years ago and today‟s global fight against malaria. *J. Roy. Soc. Med.*, **1981**, *74*, 531-537.
5. Garcia, L.S. Malaria. *Clin. Lab. Med.*, **2010**, *30*, 93-129.
6. Bousema, T.; Drakeley, C. Epidemiology and infectivity of *Plasmodium falciparum* and *Plasmodium vivax* gametocytes in relation to malaria control and elimination. *Clin. Microbiol. Rev.*, **2011**, *24*, 377-410.
7. Howes, E. R.; Reiner, E. R.; Battle, K. E.; Longbottom, J.; Mappin, B.; Ordanovich, D.; Tatem, A. J.; Drakeley, C.; Gething, P. W.; Zimmerman, P. A.; Smith, D. L.; Hay, S. I. *Plasmodium vivax* transmission in Africa. *PLoS Negl. Trop. Dis.*, **2015**, *9*, 1-27.
8. Liu W, et al. African origin of the malaria parasite *Plasmodium vivax*. *Nat. Commun.*, **2015,** *8*, 1699-1712.
9. Dembele, L.; Franetich, J.; Lorthiois, A.; et al. Persistence and activation of malaria hypnozoites in long-term primary hepatocyte cultures. *Nat. Med.*, **2014**, *20*, 307-312.
10. Collins, W. E.; Jeffery, G. M. *Plasmodium malariae*: Parasite and disease. *Clin. Microbiol. Rev.*, **2007**, *20*, 579-592.
11. Muller, M.; Schlagenhauf, P. *Plasmodium knowlesi* in travellers, update 2014. *Int. J. Microbiol. Rev.*, **2014**, *22*, 55-64.
12. Tang, T.; Salas, A; Ali-Tammam, M; et al. First case of detection of *Plasmodium knowlesi* in Spain by real time PCR in a traveller from Southeast Asia. *Malar. J.*, **2010**, *9*, 219-225.
13. Antinori, S.; Galimberti, L.; Milazzo, L.; Corbellino, M. *Plasmodium knowlesi*: The emerging zoonotic malaria parasite. *Acta Tropica*, **2013**, *125*, 191-201.
14. Neafsey, D. E.; Waterhouse, R. M.; Abai, M. R.; et al. Highly evolvable malaria vectors: The genomes of 16 *Anopheles* mosquitoes. *Science*, **2016**, *21*, 1-29.

15. Talisuna, A.; Grewal, P.; Rwakimari, J. B.; Mukasa, S.; Jagoe, G.; Banerji, J. Cost is killing patients: Subsidizing effective antimalarials. *Lancet*, **2009**, *374*, 1224-1226.
16. Paloque, L.; Ramadani, A.; Mercereau-Puijalon, O.; et al. *Plasmodium falciparum*: Multifaceted resistance to artemisinins. *Malar. J.*, **2016**, *15*, 149-161.
17. Nevin, R. L. Idiosyncratic quinoline central nervous system toxicity: Historical insights into the chronic neurological sequelae of mefloquine. *Int. J. Parasit.*, **2014**, *4*, 118-125.
18. Wellems, T. E.; Plowe, C. V. Chloroquine-resistant malaria. *J. Infect. Dis.*, **2001**, *184*, 770-776.
19. Koussounda, F. K.; Bakoua, D.; Fesser, A.; Nkombo, M.; Vouvoungui, C.; Ntoumi, F. High prevalence of sulphadoxine-pyrimethamine associated mutations in *Plasmodium falciparum* field isolates from pregnant women in Brazzaville, Republic of Congo. *Infect. Gen. Evol.*, **2015**, *33*, 32-36.
20. Ashley, E.; Dhorda, M.; Fairhurst, R; et al. Spread of artemisinin resistance in *Plasmodium falciparum* malaria. *N. Engl. J. Med.*, **2014**, *371*, 411-423.
21. Kleinschmidt, I.; Mnzava, A. P.; Kafy, H. T.; et al. Design of a study to determine the impact of insecticide resistance on malaria vector control: A multi-country investigation. *Malar. J.*, **2015**, *14*, 282-295.
22. Li, S.; Plebanski, M.; Smooker, P.; Gowans, E. J. Editorial: Why vaccines to HIV, HCV and malaria have so far failed – Challenges to developing vaccines against immunoregulating pathogens. *Front. Microbiol.*, **2015**, *6*, 1318-1321.
23. Mueller, I.; Shakri, A. R.; Chitnis, C. E. Development of vaccines for *Plasmodium vivax* malaria. *Vaccines*, **2015**, *33*, 7489-7495.
24. Hoffman, S. L.; Vekemans, J.; Richie, T. L.; Duffy, P. E. The march towards malaria vaccines. *Vaccines*, **2015**, *33*, D13-D23.
25. Cotter, C.; Sturrock, H. J. W.; Hsiang, M. S.; Liu, J.; Phillips, A. A.; Hwang, J.; Gueye, C. S.; Fullman, N.; Gosling, R. D.; Feachem, R. G. A. The changing epidemiology of malaria elimination: New strategies for new challenges. *Lancet*, **2013**, *382*, 900-911.
26. Moss, W.; Dorsey, G.; Mueller, I.; et al. Malaria epidemiology and control within the international centers of excellence for malaria research. *Am. J. Trop. Med. Hyg.*, **2015**, *93*, 5-15.

27. WHO World malaria report, 2015. World Health Organization, Geneva, Switzerland, **2015**.
28. Seydel, K. B.; Kampondeni, S. D.; Valim, C.; et al. Brain swelling and death in children with cerebral malaria. *N. Engl. J. Med.*, **2015**, *372*, 1126-1137.
29. Rogerson, S. J.; Hviid, L.; Duffy, P. E.; Leke, R. F. G; Taylor, D. W. Malaria in pregnancy: Pathogenesis and immunity. *Lancet Infect. Dis.*, **2007**, *7*, 105-117.
30. Goncalves, B. P.; Huang, C. Y.; Morrison, R.; Holte, S.; Kabyemela, E.; Prevots, R.; Fried, M.; Duffy, P. E. Parasite burden and severity of malaria in Tanzanian children. *N. Engl. J. Med.*, **2014**, *370*, 1799-1808.
31. Dondorp, A.; Nosten, F.; Yi, P.; et al. Artemisinin resistance in *Plasmodium falciparum* malaria. *N. Engl. J. Med.*, **2009**, *361*, 455-467.
32. Leang, R.; Taylor, W.; Bouth, D.; et al. Evidence of *Plasmodium falciparum* multidrug resistance to artemisinin and piperaquine in western Cambodia: Dihydroartemisinin-piperaquine open-label multicenter clinical assessment. *Antimicrob. Agents Chemother.*, **2015**, *59*, 2-5.
33. Mbengue, A.; Bhattarjee, S.; Pandharkar, T.; et al. A molecular mechanism of artemisinin resistance in *Plasmodium falciparum* malaria. *Nature*, **2015**, *520*, 683-687.
34. Yeka, A.; Gasasira, A.; Mpimbaza, A.; Achan, J.; Nankabirwa, J.; Nsobya, S.; Staedke, S. G.; Donnelly, M. J.; Mangen, F. W.; Talisuna, A.; Dorsey, G.; Kamya, M. R.; Rosenthal, P. J. Malaria in Uganda: Challenges to control on the long road to elimination. I. Epidemiology and current control efforts. *Acta Trop.*, **2012**, *121*, 184-195.
35. Askling, H.; Bruneel, F.; Burchard, G.; et al. Management of imported malaria in Europe. *Malar. J.*, **2012**, *11*, 328-343.
36. Sturrock, H. J. W.; Roberts, K. W.; Wegbreit, J.; Ohrt, C.; Gosling, R. D. Tackling imported malaria: An elimination endgame. *Am. J. Trop. Med. Hyg.*, **2015**, *93*, 139-144.
37. Kumar, A.; Hosmani, R.; Jadhav, S.; et al. *Anopheles subpictus* carry human malaria parasites in an urban area of western India and may facilitate perennial malaria transmission. *Malar. J.*, **2016**, *15*, 124-132.
38. Vaughan, A.; Mikolajczak, S.; Wilson, E.; et al. Complete *Plasmodium falciparum* liver-stage development in liver-chimeric mice. *J. Clin. Invest.*, **2012**, *122*, 3618-3628.

39. Cowman, A. F.; Crabb, B. S. Invasion of red blood cells by malaria parasites. *Cell*, **2006**, *124*, 755-766.
40. Koch, M.; Baum, J. The mechanics of malaria parasite invasion of the human erythrocyte – Towards a reassessment of the host cell contribution. *Cell. Microbiol.*, **2016**, *18*, 319-329.
41. Alano, P. *Plasmodium falciparum* gametocytes: Still many secrets of a hidden life. *Mol. Microbiol.*, **2007**, *66*, 291-302.
42. CTLT online resources (http://wiki.ubc.ca/CTLT_Resource_Room). Centre for Teaching, Learning and Technology. University of British Columbia, Vancouver, Canada.
43. CDC Treatment guidelines – Treatment of malaria (Guidelines for Clinicians), 2013. Centers for disease control and prevention, Atlanta, GA, **2013**.
44. CDC Treatment guidelines – Treatment of malaria (Guidelines for Clinicians), 2015. Centers for disease control and prevention, Atlanta, GA, **2015**.
45. WHO Malaria treatment guidelines, 2015. World Health Organization, Geneva, Switzerland, **2015**.
46. Tripathi, R.; Puri, S. K.; Dutta, G. P. Sodium artelinate – A new potential gametocytocide. *Exp. Parasitol.*, **1996**, *82*, 251-254.
47. Li, Q.; Xie, L. H.; Johnson, T. O.; Si, Y.; Haeberle, A. S.; Weina, P. J. Toxicity and evaluation of artesunate and artelinate in *Plasmodium berghei*-infected and uninfected rats. *Trans. R. Soc. Trop. Med. Hyg.*, **2007**, *101*, 104-112.
48. O'Neill, P. M.; Barton, V. E.; Ward, S. A. The molecular mechanism of action of artemisinin – The debate continues. *Molecules*, **2010**, *15*, 1705-1721.
49. Giobbia, M.; Tonon, E.; Zanatta, A.; Cesaris, L.; Vaglia, A. Late recrudescence of *Plasmodium falciparum* malaria in a pregnant woman: A case report. *Int. J. Infect. Dis.*, **2005**, *9*, 234-235.
50. Ittarat, W.; Pickard, A.; Rattanasinganchan, P.; et al. Recrudescence in artesunate-treated patients with falciparum malaria is dependent on parasite burden, not on parasite factors. *Am. J. Trop. Med. Hyg.*, **2003**, *68*, 147-152.
51. Galappaththy, G. N. L.; Tharyan, P.; Kirubakaran, R. Primaquine for preventing relapse in people with *Plasmodium vivax* malaria treated with chloroquine. *Cochrane*, **2013**, *10*, CD004389.

52. Ashley, E .A.; Recht, J.; White, N. J. Primaquine: The risks and the benefits. *Malar. J.*, **2014**, *13*, 418-425.
53. Burgoine, K. L.; Bancone, G.; Nosten, F. The reality of using primaquine. *Malar. J.*, **2010**, *9*, 376-381.
54. Mace, K.; Chalwe, V.; Katalenich, B.; et al. Evaluation of sulphadoxine-pyrimethamine for intermittent preventive treatment of malaria in pregnancy: A retrospective birth outcomes study in Mansa, Zambia. *Malar. J.*, **2015**, *14*, 69-80.
55. Briand, V.; Cottrell, G.; Massougboji, A.; Cot, M. Intermittent preventive treatment for the prevention of malaria during pregnancy in high transmission areas. *Malar. J.*, **2007**, *6*, 160-167.
56. Farooq, U.; Mahajan, R. C. Drug resistance in malaria. *J. Vect. Borne Dis.*, **2004**, *41*, 45-53.
57. Sykes, M. L.; Avery, V. M. Approaches to protozoan drug discovery: Phenotypic screening. *J. Med. Chem.*, **2013**, *56*, 7727-7740.
58. Gamo, F.; Sanz, L.; Vidal, J.; et al. Thousands of chemical starting points for antimalarial lead identification. *Nature*, **2010**, *465*, 305-310.
59. Njoroge, M.; Njuguna, N. M.; Mutai, P.; Ongarora, D. S. B.; Smith, P. W.; Chibale, K. Recent approaches to chemical discovery and development against malaria and the neglected tropical diseases Human African Trypanasomiasis and Schistosomiasis. *Chem. Rev.*, **2014**, *114*, 11138-11163.
60. Guiguemde, W. A.; Shelat, A. A.; Garcia-Bustos, J. F.; Diagana, T.; Gamo, F. J.; Guy, R. K. Global phenotypic screening for antimalarials. *Chem. Biol.*, **2013**, *19*, 116-129.
61. Paquet, T.; Gordon, R.;Waterson, D.; Witty, M. J.; Chibale, K. Antimalarial aminothiazoles and aminopyridines from phenotypic whole-cell screening of a SoftFocus® library. *Future Med. Chem.*, **2012**, *4*, 2265-2277.
62. Younis, Y.; Douelle, F.; Feng, T.; et al. 3,5-Diaryl-2-aminopyridines as a novel class of orally active antimalarials demonstrating single-dose cure in mice and clinical candidate potential. *J. Med. Chem.*, **2012**, *55*, 3479-3487.
63. MMV – Research and development portfolio http://www.mmv.org/research-development/interactive -rd-portfolio (accessed 29th March, 2016).

64. Ferreira, G. L.; Oliva, G.; Andricopulo, A. D. Target based molecular modeling strategies for Schistosomiasis drug discovery. *Future Med. Chem.*, **2015**, *7*, 753-764.
65. Butera, J. A. Phenotypic screening as a strategic component of drug discovery programs targeting novel antiparasitic and antimycobacterial agents: An editorial. *J. Med. Chem.*, **2013**, *56*, 7715-7718.
66. Serajuddin, A. T. M. Salt formation to improve drug solubility. *Adv. Drug Deliv. Rev.*, **2007**, *59*, 603-616.
67. Lipinski, C. A.; Lombardo, F.; Dominy, B.W.; Feeney, P.J. Experimental and computational approaches to estimate solubility and permeability in drug development settings. *Adv. Drug Deliv. Rev.*, **2001**, *64*, 4-17.
68. Kerns, E. H and Di, L. Drug-like properties: Concepts, structure design and methods – From ADME to toxicity optimization. 1st Ed., **2008**.
69. Benet, L. Z. The role of BCS (Biopharmaceutics Classification System) and BDDCS (Biopharmaceutics Drug Disposition Classification System) in drug development. *J. Pharm. Sci.*, **2013**, *102*, 34-42.
70. Wexler, D. S.; Gao, L.; Anderson, F.; Ow, A.; Nadasdi, L.; McAlorum, A.; Urfer, R.; Huang, S. G. Linking solubility and permeability assays for maximum throughput and reproducibility. *J. Biomol. Screen.*, **2005**, *10*, 383-390.
71. Savjani, K. T.; Gajjar, A. K.; Savjani, J. K. Drug solubility: Importance and enhancement techniques. *ISRN Pharmaceutics*, **2012**, *2012*, 1-10.
72. Vasconcelos, T.; Sarmento, B.; Costa, P. Solid dispersions as a strategy to improve oral bioavailability of poorly water soluble drugs. *Drug Discov. Today*, **2007**, *12*, 1068-1075.
73. Censi, R.; Di Martino, P. Polymorph impact on the bioavailability and stability of poorly soluble drugs. *Molecules*, **2015**, *20*, 18759-18776.
74. Williams, H. D.; Trevaskis, N. L.; Charman, S. A.; Shanker, R. M.; Charman, W. N.; Pouton, C. W.; Porter, C. J. H. Strategies to address low drug solubility in discovery and development. *Pharmacol. Rev.*, **2013**, *65*, 315-499.
75. Le Manach, C.; Paquet, T.; Gonzalez Cabrera, D.; Younis, Y.; Taylor, D.; Wiesner, L.; Lawrence, N.; Schwager, S.; Waterson, D.; Witty, M. J.; Wittlin, S.; Street, L. J.; Chibale, K. Medicinal chemistry optimization of antiplasmodial imidazopyridazine hits

from high-throughput screening of a SoftFocus® kinase library: Part 2. *J. Med. Chem.*, **2014**, *57*, 8839-8848.

76. Ishikawa, M.; Hashimoto, Y. Improvement in aqueous solubility in small molecule drug discovery programs by disruption of molecular planarity and symmetry. *J. Med. Chem.*, **2011**, *54*, 1539-1554.
77. Fleisher, D.; Bong, R.; Stewart, B.H. Improved oral drug delivery: Solubility limitations overcome by the use of prodrugs. *Adv. Drug Deliv. Rev.*, **1996**, *19*, 115-130.
78. Stella, V. J.; Nti-Addae, K. W. Prodrug strategies to overcome poor water solubility. *Adv. Drug Deliv. Rev.*, **2007**, *59*, 677-694.
79. Hecker, S. J.; Calkins, T.; Price, M. E.; Huie, K.; Chen, S.; Glinka, T. W.; Dudley, M. N. Prodrugs of cephalosporin RWJ-333441 (MC-04,546) with improved aqueous solubility. *Antimicrob. Agents Chemother.*, **2003**, *47*, 2043-2046.
80. Paulekuhn, G. S.; Dressman, J. B.; Saal, C. Trends in active pharmaceutical ingredient salt selection based on analysis of the orange book database. *J. Med. Chem.*, **2007**, *50*, 6665-6672.
81. Korn, C.; Balbach, S. Compound selection for development – Is salt formation the ultimate answer? Experiences with an extended concept of the "100 mg approach". *Eur. J. Pharm. Sci.*, **2014**, *57*, 257-263.
82. Seo, J. H.; Park, J. B.; Choi, W. K.; Park, S.; Sung, Y. J.; Oh, E.; Bae, S. K. Improved oral absorption of cilostazol via sulfonate salt formation with mesylate and besylate. *Drug Design Dev. Ther.*, **2015**, *9*, 3961-3968.
83. O'Connor, K. M.; Corrigan, O. I. Preparation and characterization of a range of diclofenac salts. *Int. J. Pharm.*, **2001**, *26*, 163-179.
84. Shan, N.; Zaworotko, M. J. The role of co-crystals in pharmaceutical science. *Drug Discov. Today*, **2008**, *13*, 440-446.
85. Duggirala, M. K.; Perry, M. L.; Almarsson, O.; Zaworotko, M. J. Pharmaceutical co-crystals: Along the path to improved medicines. *Chem. Commun.*, 2016, *52*, 640-655.
86. Thakuria, R.; Delori, A.; Jones, W.; et al. Pharmaceutical co-crystals and poorly soluble drugs. *Int. J. Pharm.*, **2013**, *453*, 101-125.
87. Hickey, M.; Peterson, L.; Scoppettuolo, L.; et al. Performance comparison of a co-crystal of carbamazepine with marketed product. *Eur. J. Pharm. Biopharm.*, **2007**, *67*, 112-119.

88. Uekama, K.; Hirayama, F.; Irie, T. Cyclodextrin drug carrier systems. *Chem. Rev.*, **1998**, *98*, 2045-2076.
89. Salustio, P.; Pontes, P.; Conduto, C.; et al. Advanced technologies for controlled oral release: Cyclodextrins for controlled oral release. *AAPS Pharmsci.*, **2011**, *12*, 1276-1293.
90. Nair, A. B.; Attimarad, M.; Bandar, E.; Al-Dhubaib, A.; Wadhwa, J.; Harsha, S.; Ahmed, M. Enhanced oral bioavailability of acyclovir by inclusion complex formation using hydroxypropyl-β-cyclodextrin. *Drug Deliv.*, **2014**, *21*, 540-547.
91. Loftsson, T.; Jarho, P.; Masson, M.; Jarvinen, T. Cyclodextrins in drug delivery. *Expert Opin. Drug. Deliv.*, **2005**, *2*, 335-351.

CHAPTER 2: DESIGN, SYNTHESIS AND BIOLOGICAL EVALUATION OF PYRIDO[1,2*a*]BENZIMIDAZOLES WITH CYCLIC AND FUNCTIONALIZED AMINE SUBSTITUENTS.

2.1 INTRODUCTION

This chapter describes the design, synthesis as well as spectroscopic and physical characterization of compounds based on the **pyrido[1,2-*a*]benzimidazole** (PBI) general structure (**Fig. 2.1**). Cyclic amine substituents appropriately functionalized with polar, hydrogen-bonding groups were incorporated at position R_1 of the scaffold in an attempt to improve aqueous solubility. Established organic synthetic routes were utilized for this purpose. All the derivatives synthesized were evaluated for *in vitro* antiplasmodial activity against the chloroquine-sensitive NF54 strain of *P. falciparum* and apparent solubility by the turbidimetric assay. The most active analogs were tested for cytotoxicity and microsomal metabolic stability. Selected analogues were also tested for activity in the *P. berghei* liver stage assay and for gametocidal activity.

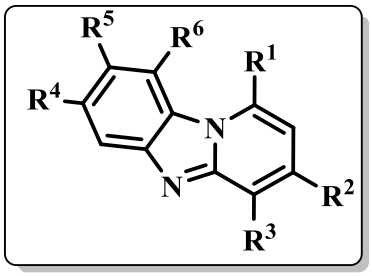

Fig. 2.1: General structure of the pyrido[1,2-*a*]benzimidazole scaffold.

2.2 BACKGROUND INFORMATION

A benzimidazole (**Fig. 2.2**) is a benzannulated bicyclic ring system consisting of benzene fused to an imidazole ring.[92] Even though the benzimidazole nucleus contains eight π-electrons which would violate Huckel‟s rule for aromaticity, the lone pair on N1 is readily delocalized into the ring.[93] This satisfies Huckel‟s rule and accounts for its aromaticity. The PBI scaffold consists of a benzimidazole fused across the N1-C2 (1,2) bond to pyridine on the N1-C2 bond (the *a* side) of the pyridine ring. The scaffold is, therefore, named as such in accordance with the Hantzsch-Widman rules.[93] It retains aromaticity associated with the benzimidazole core owing to electron delocalization as explained above.

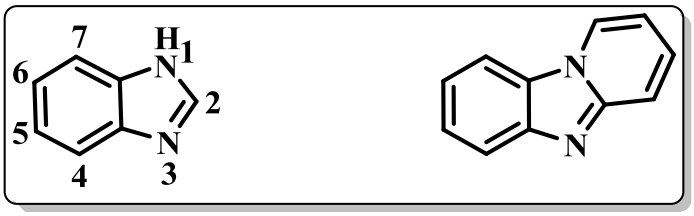

Fig. 2.2: Benzimidazole and the PBI nucleus.

The benzimidazole nucleus is a structural unit of naturally occurring purine nucleotides.[94] As such, it possesses the capacity to interact with numerous biological systems, leading to a wide variety of biological activities. The scaffold is found in a number of commercially available medications in different therapeutic classes including antihistamines (e.g. astemizole **30**), antiulcers (e.g. omeprazole **31**), antivirals (e.g. enviradine **32**), antihelmintics (e.g. albendazole **33**) and antihypertensives (e.g. telmisartan **34**).[94] Recent research and optimization of substituents around the benzimidazole core has also demonstrated that the compounds possess antitumor, anti-inflammatory, antifungal, antimicrobial, antitubercular and anxiolytic activity.[94,95-101]

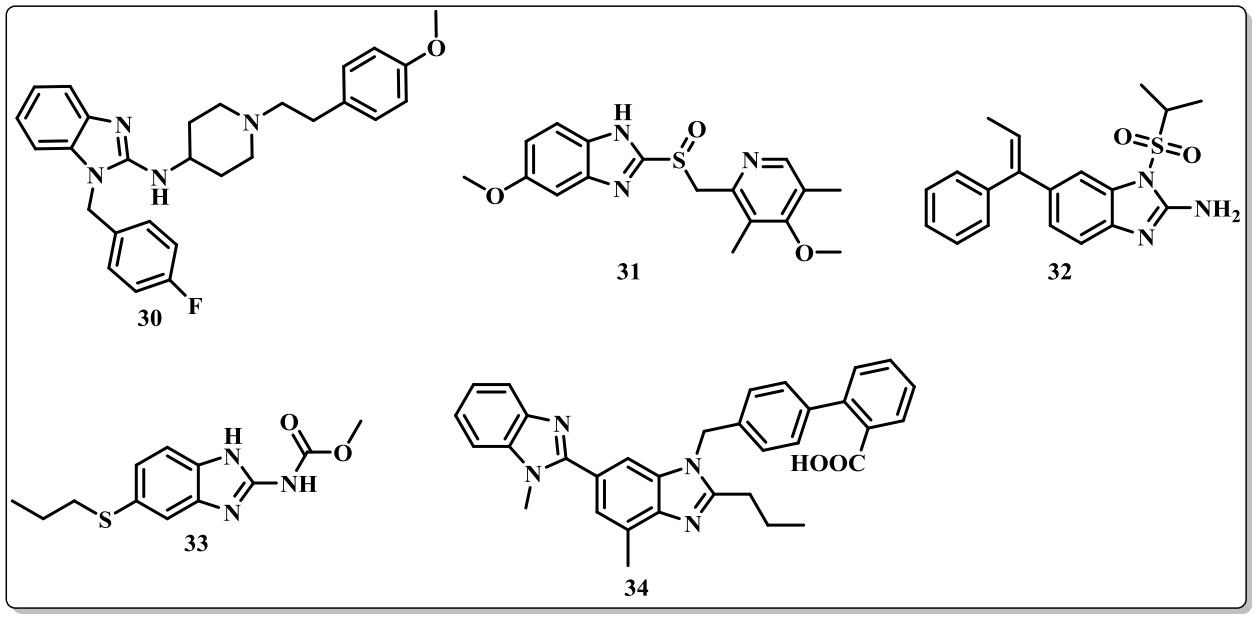

Fig. 2.3: Structures of some benzimidazole-containing drugs – astemizole (**30**), omeprazole (**31**), enviradine (**32**), albendazole (**33**) and telmisartan (**34**).

2.3 PREVIOUS STUDIES ON ANTIPLASMODIAL ACTIVITY OF BENZIMIDAZOLES

Recent studies have demonstrated that benzimidazole analogues possess potent *in vitro* antiplasmodial activity.[102] Musonda *et al.*, reported on the antiplasmodial activity of chloroquine-astemizole hybrids **35** and **36** (**Fig. 2.4**) in 2009.[103] In this study, compounds with *in vitro* antiplasmodial activity (IC_{50} values 0.023-0.6 μM) against the chloroquine resistant K1 strain of *P. falciparum* (CQ IC_{50} 0.23 μM) were identified. Benzimidazole derivatives with different substitution patterns have also been shown to possess potent antiplasmodial activity in recent studies.[102,104-106] Keurulainen *et al.*, illustrated the synthesis and potent antiplasmodial activities of benzimidazole aminopropylamides (e.g. analogues **37** and **38**) in 2015 while potent benzimidazole-5-carbohydrazide derivatives (e.g. **39**) were investigated by Camacho *et al.* in 2011. Highly potent benzimidazole-2-pyridinyl analogues with *in vitro* antiplasmodial IC_{50} values of 0.16-3 μM against *P. falciparum* (e.g. **40**) were synthesized and evaluated by Saify *et al.* in 2012 (**Fig. 2.4**).

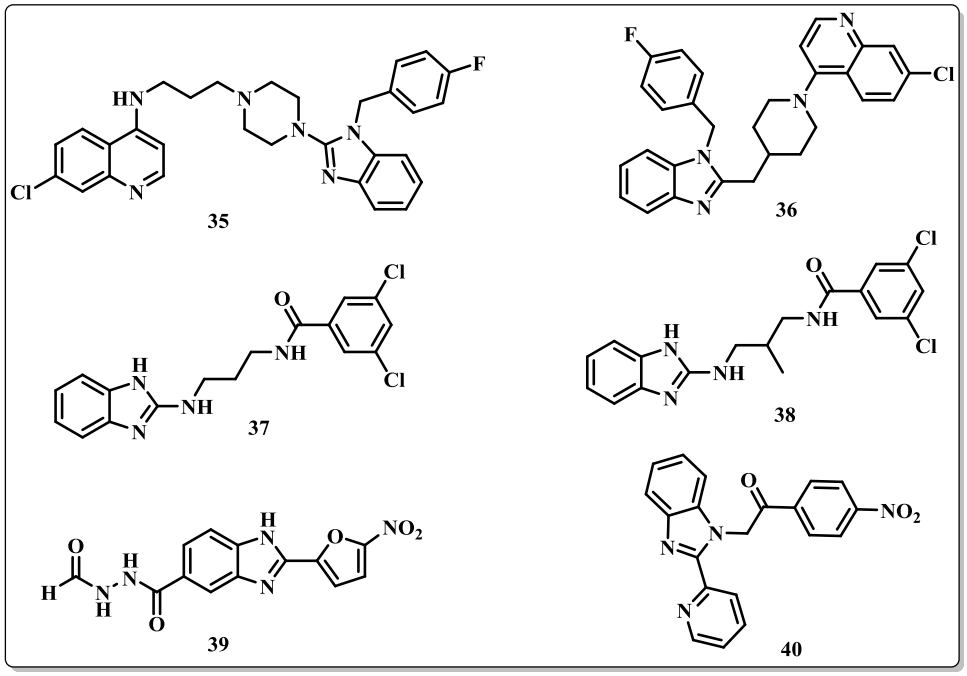

Fig. 2.4: Benzimidazole analogues with antiplasmodial activity from previous studies – chloroquine-benzimidazole hybrids **35** and **36**, benzimidazole aminopropylamides **37** and **38**, benzimidazole-5-carbohydrazide **39** and benzimidazole-2-pyridinyl analogue **40**.

2.4 PREVIOUS STUDY ON THE ANTIMALARIAL ACTIVITY OF PBI ANALOGUES

In 2011, Ndakala *et al.* reported on the synthesis and antimalarial activity of pyrido [1,2-*a*] benzimidazoles.[107] As part of a collaboration between TDR (Special Programme for Research and Training in Tropical Diseases) and the Belgian pharmaceutical firm Tibotec in 2000, a library of 1,440 chemically diverse nonproprietary chemicals were screened against a protozoa panel *in vitro*. From this screening, the PBI compound **TDR15087** (**Fig. 2.5**) with moderate activity against *P. falciparum* GHA and W2 strains (IC_{50} 0.17 and 0.37 μM respectively) was identified. To further explore the antiplasmodial SAR around the PBI core, an additional 535 PBI analogues were evaluated in a medium throughput-screen (MTS) against the chloroquine-resistant K1 strain of *P. falciparum*. This led to identification of 49 compounds with IC_{50} below 0.1 μg/ml, notably the benzylpiperazine analogs **TDR35885** and **TDR44047** (**Fig. 2.5**).

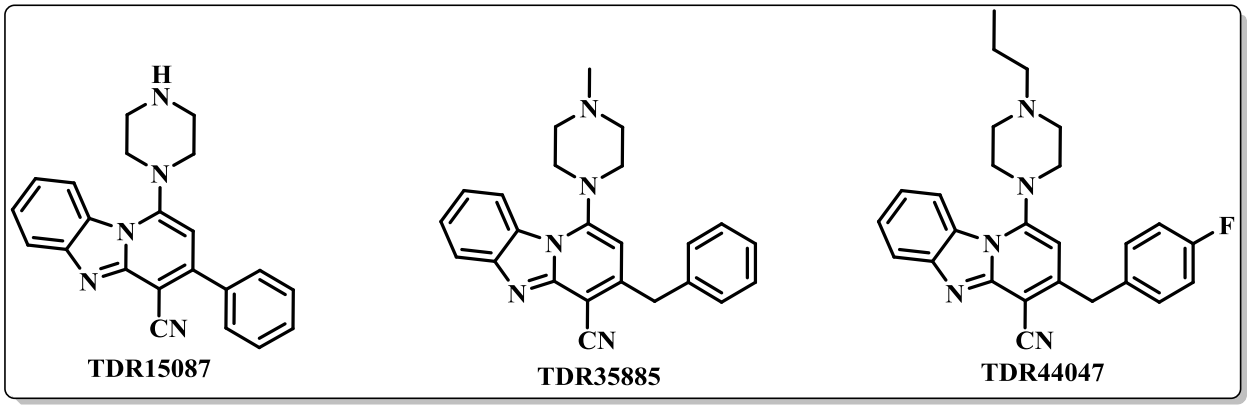

Fig. 2.5: Structures of PBI screening hits with potent antiplasmodial activity.

However, all three hits were proven to be inactive in the standard *in vivo P. berghei* mouse model up to high doses of 4 × 100 mg/kg ip, most likely attributable to a combination of poor solubility and metabolic stability.[107] In an attempt to identify compounds that would retain activity in the *P. berghei* model, Ndakala *et al.*, embarked on SAR optimization around the PBI core focusing on 3-aryl derivatives with alkylamino side chains (**Fig. 2.6**). Several analogues possessing submicromolar activity against the K1 strain of *P. falciparum* were identified, the most active being **4c** with an IC_{50} of 0.047 μM (**Fig. 2.6**). The lead compound **4c** and its mono-desethyl metabolite **4h** also showed a good combination of *in vitro* antiplasmodial activity and favorable selectivity index (SI) when tested for cytotoxicity against the mammalian L6 cell line.

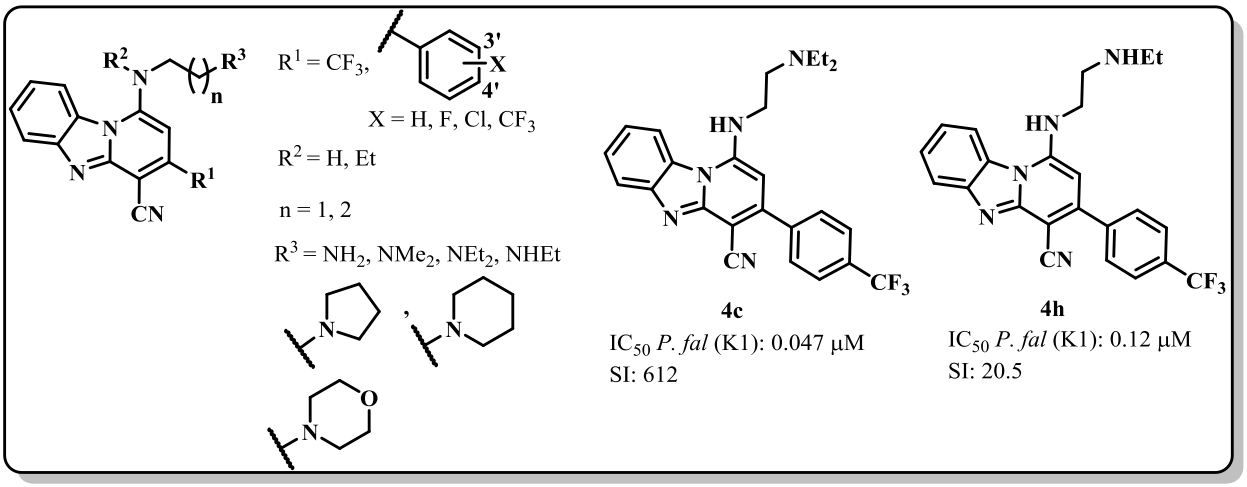

Fig. 2.6: SAR optimization around the PBI core and structures of lead compounds **4c** and **4h**.

Determination of the *in vitro* microsomal metabolic stability in human, rat and mouse liver microsomes (HLM, RLM and MLM) indicated that compound **4c** had a short degradation half-life (13.7 min in HLM, 24.8 min in RLM and 24.1 min in MLM) as compared to the relatively moderate half-life of **4h** (136.8 min in HLM, 284.4 min in RLM and 321.2 min in MLM). This information was vital during *in vivo* efficacy determination as it was evident that the metabolite **4h** contributes significantly to the activity of **4c**.

Hydrochloride salts of the most active compounds **4c**, **4h**, **4j** and **4i** were prepared for single-dose oral efficacy studies in the *P. berghei* mouse model (**Table 2.1**). These showed significant efficacy at a dose of 25 mg/kg (70.33% reduction in parasitemia on day 5 for **4c**), which was not significantly improved at a higher dose of 50 mg/kg (78.22% reduction in parasitemia on day 5 for **4c**).[107] This observation presumably arose from saturation of systemic exposure owing to solubility-limited absorption. Single- and multi-dose *in vivo* efficacy studies of the orally administered salt of **4h** against *P. berghei* also indicated that the activity plateaus with doses above 25 mg/kg (50.24%, 71.22% and 79.79% reduction in parasitemia on days 3, 4 and 5 at 50 mg/kg dose), and the scenario is replicated following subcutaneous administration. Preliminary systemic exposure studies following oral and subcutaneous administration of a **4h** salt also indicated saturation occurring at doses above 25 mg/kg orally or 50 mg/kg subcutaneously. It was, therefore, concluded that solubility-limited absorption resulted in limited bioavailability of these compounds, leading to limited systemic exposure and efficacy with increasing dose.[107]

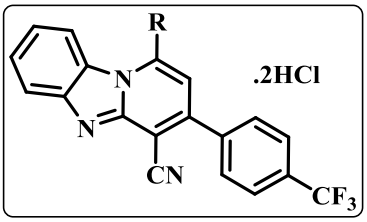

Cpd	R	Dose (mg/kg)	% reduction in parasitemia				MSD (days)
			Day 2	Day 3	Day 4	Day 5	
4c	$-NH(CH_2)_2N(Et)_2$	1×50	5.15	29.76	59.97	78.22	8
4c	$-NH(CH_2)_2N(Et)_2$	1×25	13.07	24.38	51.13	70.33	8
4h	$-NH(CH_2)_2NHEt$	1×50	30.78	50.24	71.22	79.79	12.7
4h	$-NH(CH_2)_2NHEt$	1×25	23.51	55.45	62.25	68.92	13.3
4j	$-NH(CH_2)_2N$ 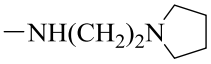	1×50	14.04	47.92	73.01	88.53	8.7
4j	$-NH(CH_2)_2N$ 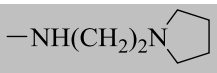	1×25	14.75	43.20	63.73	63.72	7.7
4i	$-NH(CH_2)_2N$ 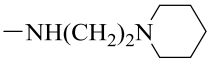	1×50	23.38	9.30	0.00	0.00	5
4i	$-NH(CH_2)_2N$ 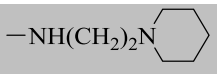	1×25	28.44	28.07	38.72	46.41	12.7
CQ		1×10	99.99				9
Control							5

Table 2.1: Oral efficacy of dihydrochloride salts of selected PBI compounds in the *P. berghei* mouse model.[107] CQ - chloroquine

2.5 RATIONALE

The findings by Ndakala *et al.*, as illustrated above, were crucial because there was no prior published literature related to the antimalarial activity of PBI analogs.[107] A novel series of PBIs was identified with good *in vitro* antiplasmodial activity against *P. falciparum* and oral efficacy in the *P. berghei* mouse model. Pharmacokinetic pitfalls, however, curtailed the *in vivo* activity of these compounds, most notably low bioavailability presumably resulting from solubility-limited absorption. Oral absorption was found to be saturated at relatively low doses, presumably owing to poor dissolution or solubility.

This, therefore, called for further optimization of the lead PBI to identify analogs with improved pharmacokinetic profiles. This was hypothesized to be achievable through improving solubility while maintaining or improving antiplasmodial activity and metabolic stability.

In this research project, PBI analogs bearing cyclic amine substituents suitably functionalized with polar, hydrogen-bonding groups were synthesized in an effort to improve aqueous solubility while maintaining or improving antiplasmodial activity and metabolic stability.

2.6 DESIGN, SYNTHETIC PROCEDURES AND CHARACTERIZATION OF PYRIDO[1,2-*a*]BENZIMIDAZOLE ANALOGUES WITH CYCLIC AND FUNCTIONALIZED AMINE SUBSTITUTIONS.

2.6.1 Introduction

Design of the analogues to be synthesized in this research project was based upon previous SAR optimization around the PBI core carried out by Ndakala *et al*. As such, cyclic and polar group-functionalized amine substitutions were carried out at position C1 of the scaffold (**Fig. 2.7**). In the previous study, substitutions at this position were mainly based on aliphatic straight chain diamines and a few unsubstituted alicyclic amines.[107] Left-hand side (LHS) substitution was not carried out in the previous study. The 4-trifluoromethylphenyl (C3) and cyano (C4) substitutions were fixed as these were determined to confer good activity and selectivity from the previous study.

Cyclic and functionalized amines (**Fig. 2.8**) offered an attractive choice for substitution because they explore a new chemical space for introduction of polar substituents.

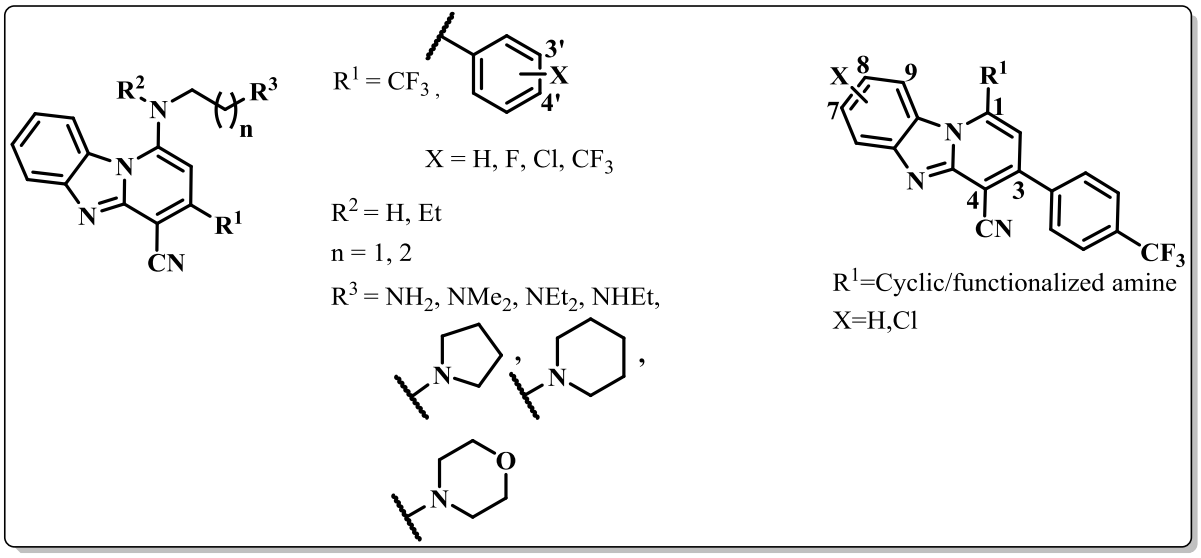

Fig. 2.7: SAR optimization of the PBI core from previous study (left) and current project (right).

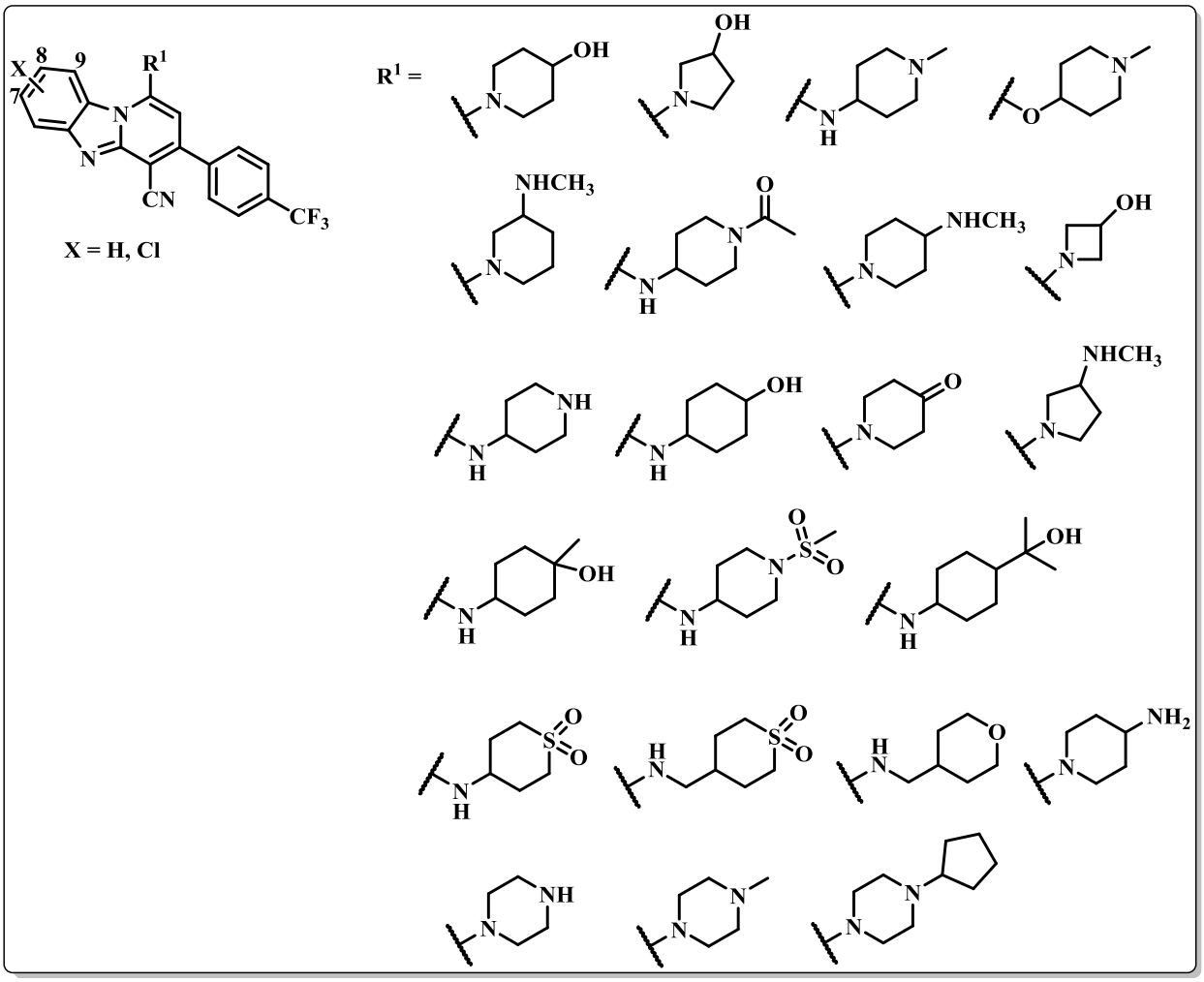

Fig. 2.8: Cyclic and functionalized amine substituents utilized in the current SAR.

2.6.2 Synthesis of LHS-unsubstituted analogues

Left-hand side unsubstituted compounds were synthesized via the three step reaction shown in **Scheme 1** below.[107]

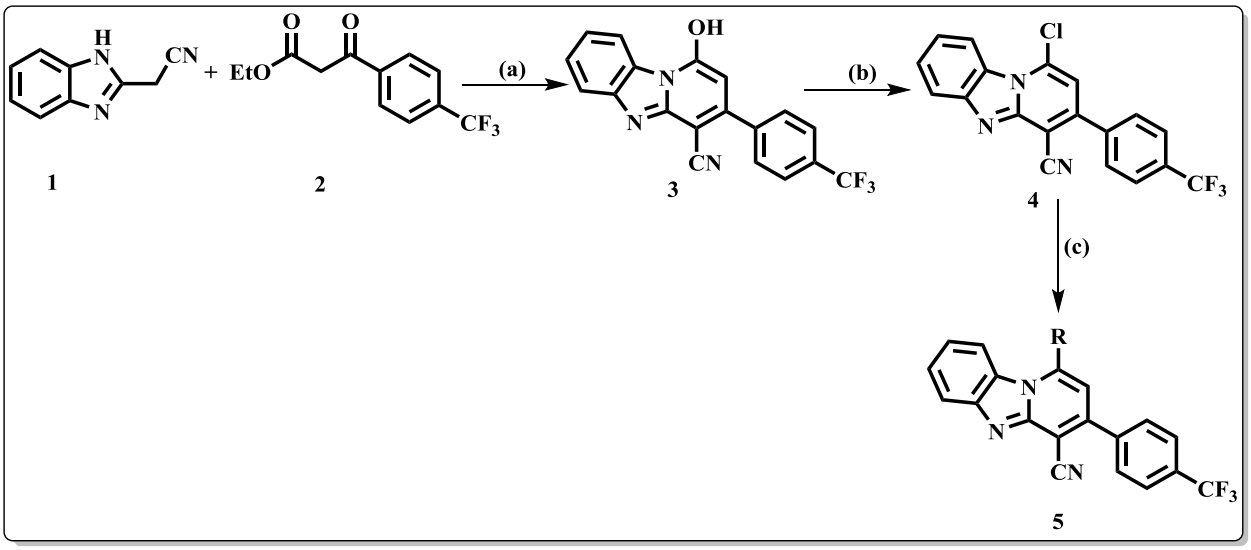

Scheme 1: Reagents and conditions: (a) NH_4OAc, 150 ºC, 1h; (b) $POCl_3$, 130 ºC, 2h; (c) Amine, Et_3N, THF, 80 ºC, microwave irradiation, 20 min.

2.6.2.1 Synthesis of hydroxy intermediate 3

Compound **3** was synthesized via a condensation reaction by heating a mixture of 2-benzimidazole acetonitrile, ethyl (4-trifluoromethylbenzoyl) acetate and NH_4OAc.

This first step in the proposed mechanism of this reaction **(Scheme 2)** is abstraction of one of the relatively acidic methylene protons of the starting material, 2-benzimidazole acetonitrile, by NH_4OAc to afford a carbanion intermediate. This nucleophilic intermediate then attacks the β-ketoester chemoselectively at C3 resulting in the corresponding open-chain intermediate. Protonation of this alkoxide intermediate results in a secondary alcohol intermediate, which then cyclizes.

Protonation of the secondary alcohol group then occurs, forming the better water leaving group which is lost in a subsequent elimination reaction to form the first C-C double bond of the newly formed ring. Finally, aromatization provides the driving force for loss of the acidic α-hydrogen resulting in intermediate **3**.

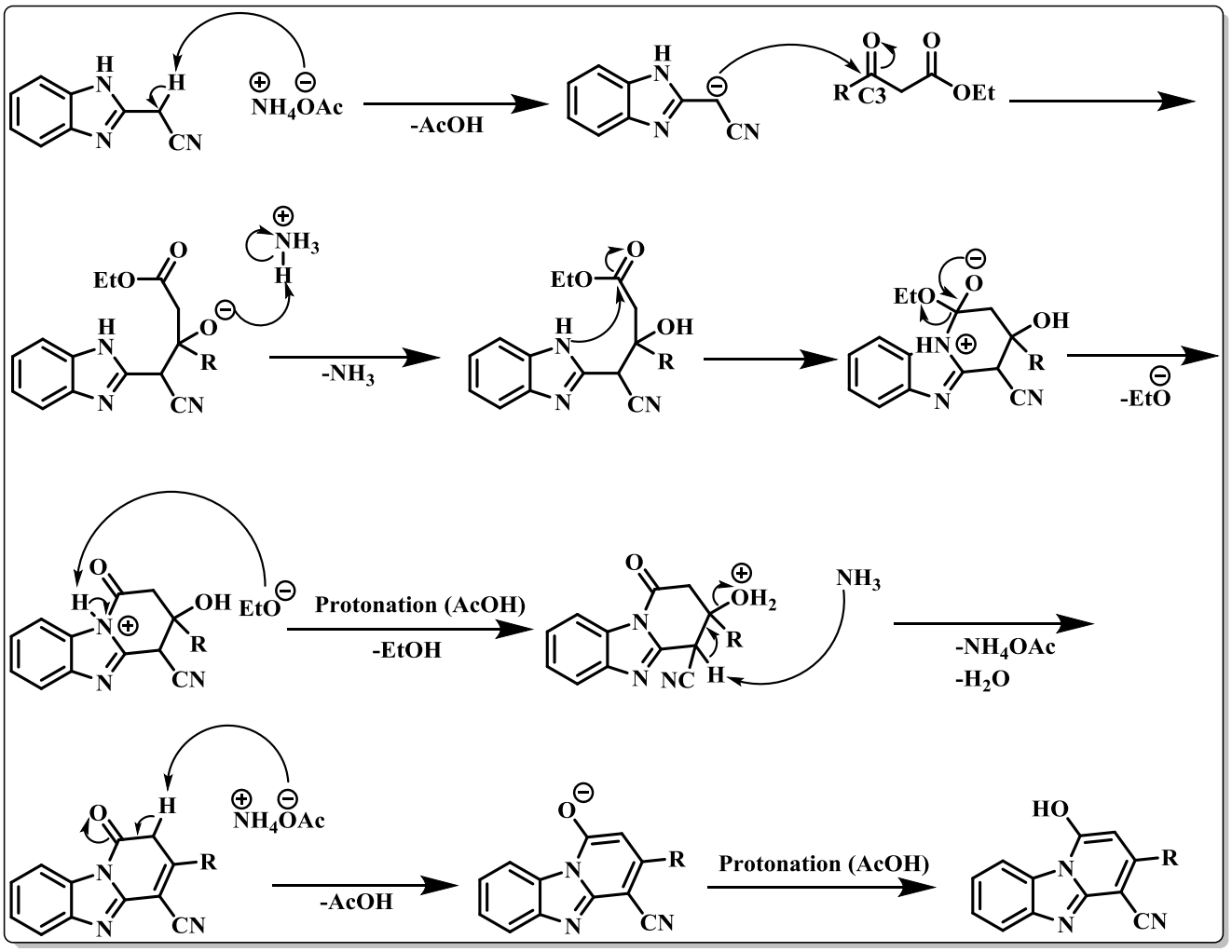

Scheme 2: Proposed mechanism for formation of hydroxy intermediate **3**.

2.6.2.2 Synthesis of chloro intermediate 4

Compound **4** was synthesized by refluxing a mixture of compound **3** and $POCl_3$.

This reaction is initiated via a nucleophilic attack by one of the hydroxyl lone pairs of compound **3** on the electrophilic phosphorus center of $POCl_3$ with release of a chloride anion (**Scheme 3**). The chloride anion then undergoes an aromatic nucleophilic substitution reaction with the activated alcohol group which is the better leaving group. This yields the chlorinated intermediate **4** with hydrochloric acid and phosphenic chloride as side products.

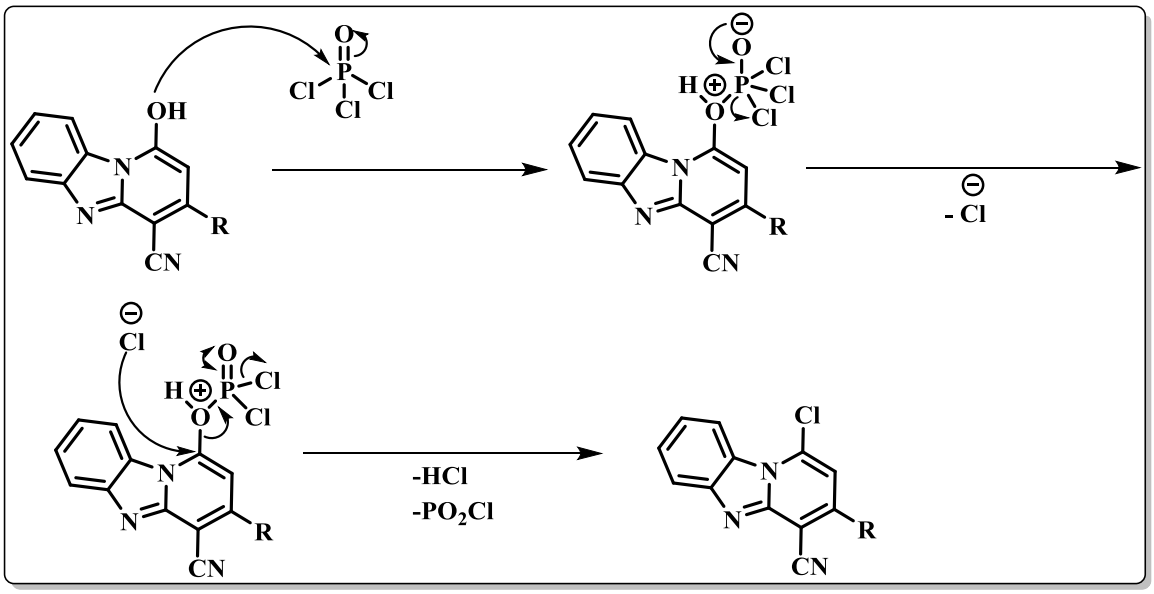

Scheme 3: Proposed mechanism of chlorination of compound **3** to afford intermediate **4**.

2.6.2.3 Synthesis of final target compounds 5a-u

Synthesis of final compounds **5i-u** is described by considering compound **5r** as an example:

Compound **4** was added to a stirred mixture of 4-aminomethyltetrahydropyran and triethylamine in THF and the mixture was irradiated under microwave.

Formation of these final compounds occurs via aromatic nucleophilic substitution of the chloro substituent of **4** by an appropriate amine (**Scheme 4**). This yields the aminated derivative and hydrogen chloride as a side product. Triethylamine is added as the base in this reaction, and plays the additional role of mopping up the hydrogen chloride produced. This is a requirement for the amination reaction to proceed to completion.

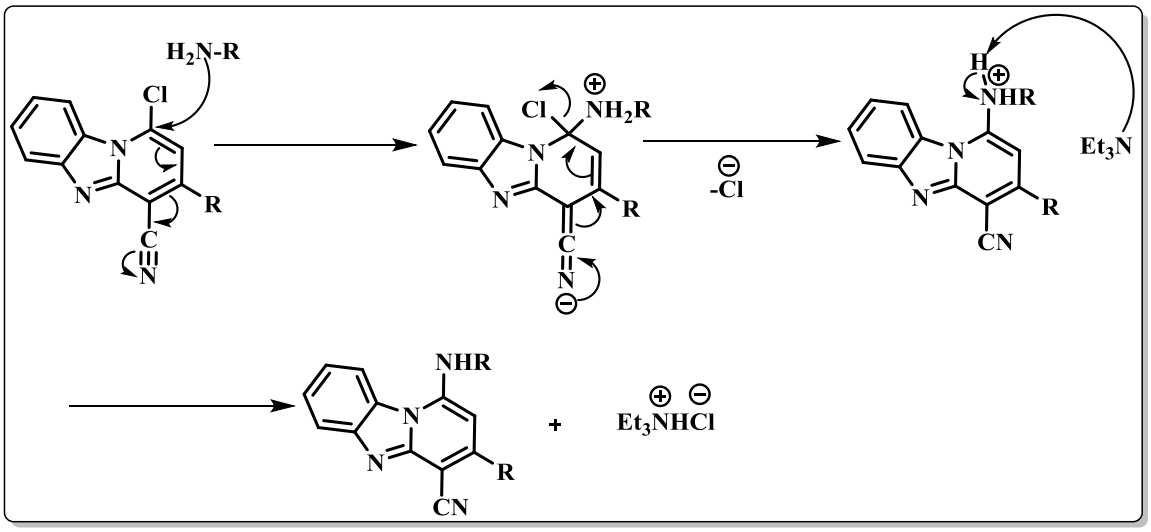

Scheme 4: Mechanism of amination of compound **4** to yield final compounds.

2.6.3 Synthesis of LHS-substituted target compounds 5v-6a

Benzimidazole starting materials with C5, C6 and/or C7-substitution patterns were not commercially available. Therefore, to synthesize pyridobenzimidazole analogues with substitution on the left-hand side of the molecule, appropriately substituted 2-benzimidazole acetonitrile intermediates had to be synthesized as illustrated in **Scheme 5** below.

The first step involves a cyclocondensation reaction between the appropriately substituted benzenediamine **(i)** and ethyl cyanoacetate **(ii)** to afford the substituted 2-benzimidazole acetonitrile intermediate **1a**. This is then reacted with ethyl (4-trifluoromethylbenzoyl) acetate **2** in a second cyclocondensation reaction to yield the hydroxy intermediate **3a**. Chlorination of **3a** with $POCl_3$ affords **4a** which is aminated in a similar fashion as the unsubstituted intermediate above to yield the final compounds **5**.

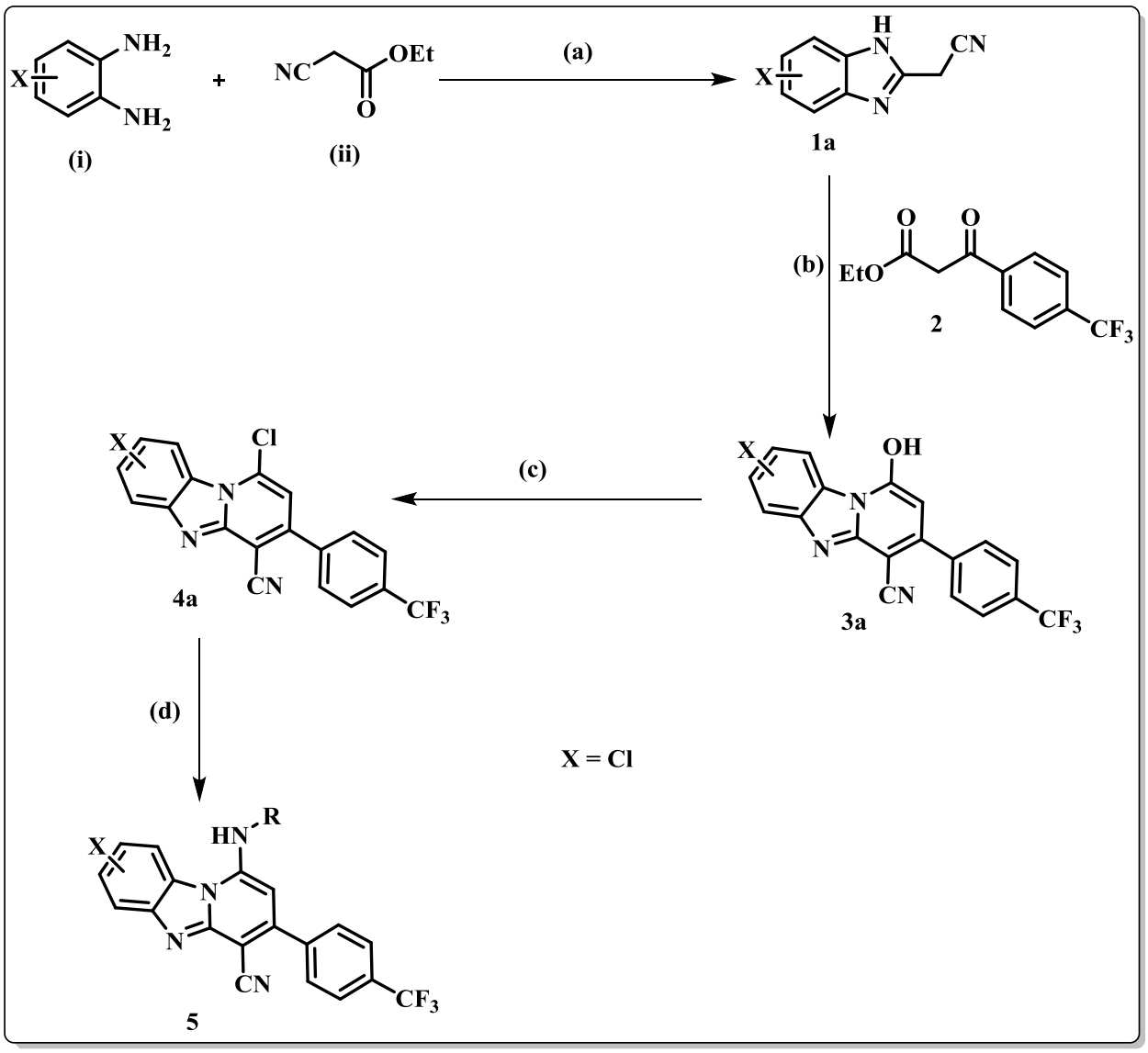

Scheme 5: Reagents and conditions: (a) DMF, 160 ºC, 24h; (b) NH_4OAc, 150 ºC, 1h; (c) $POCl_3$, 130 ºC, 2h; (d) Amine, Et_3N, THF, 80 ºC, microwave irradiation, 20 min.

The first step in the cyclocondensation reaction above is nucleophilic attack of the electrophilic carbonyl carbon of ethyl cyanoacetate by the benzenediamine, resulting in a tetrahedral intermediate. This stabilizes by proton transfer to form the hemi-aminal as shown in **Scheme 6**. Expulsion of the ethoxide ion leads to formation of the keto intermediate, which undergoes a second nucleophilic attack to give the secondary alcohol intermediate. An elimination step with aromatization as the driving force then follows, forming the substituted 2-benzimidazole acetonitrile product.

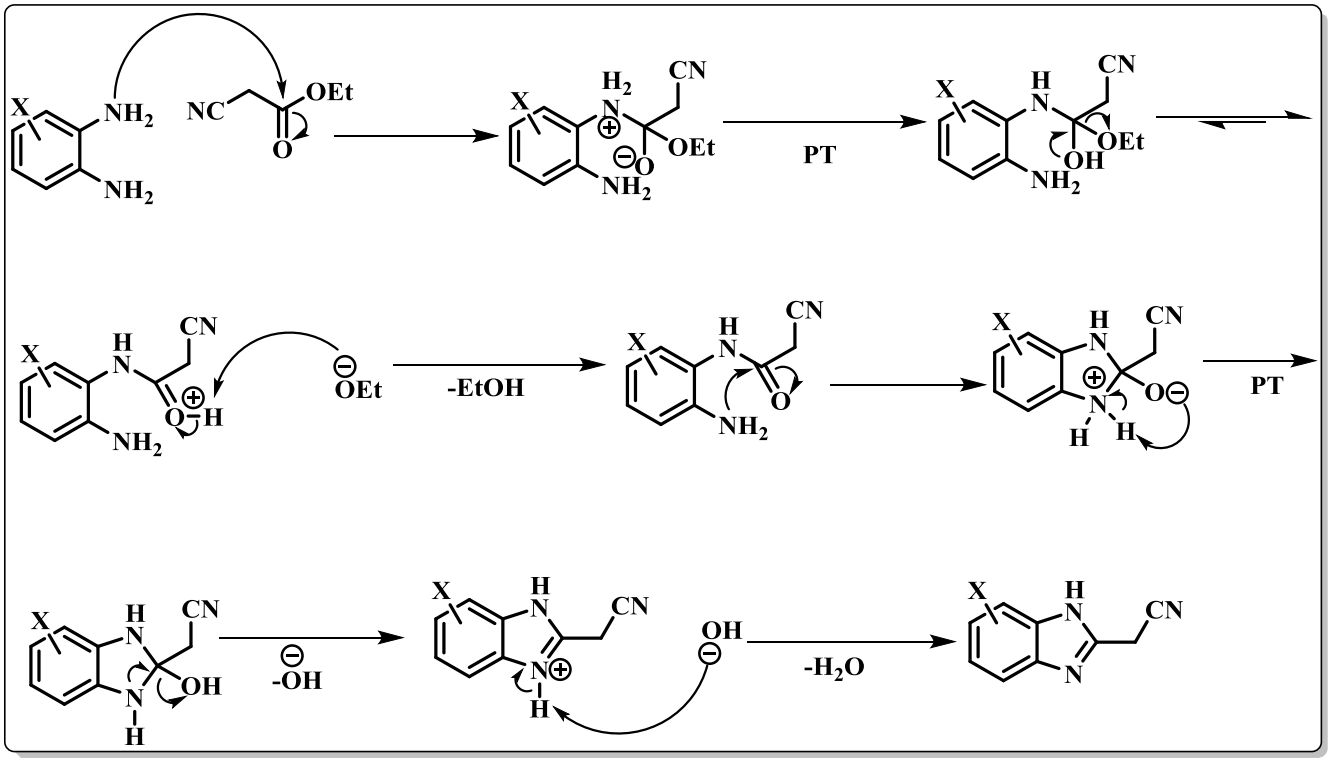

Scheme 6: Proposed mechanism for synthesis of substituted 2-benzimidazole acetonitrile analogues.

The isolated percentage yields of final compounds, molecular ion (*m/z*) peaks on liquid chromatography coupled to mass spectrometer (LC-MS) and melting points are summarized in **Table 2.2** below.

Table 2.2: Yield, MS peaks and melting points of final compounds.

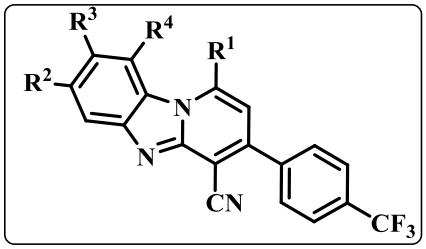

Code	R^1	R^2	R^3	R^4	Yield (%)	MW	MS peak	MP (°C)
FJC-2 (5a)	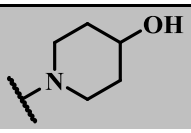	H	H	H	55	436.44	437.1	307-309

Code	R^1	R^2	R^3	R^4	Yield (%)	MW	MS peak	MP (°C)
FJC-3 (5b)	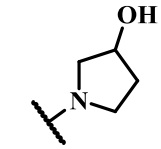	H	H	H	46	422.41	423.1	260-262
FJC-4 (5c)	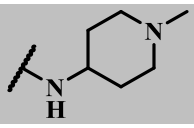	H	H	H	51	449.48	450.2	215-217
FJC-5 (5d)	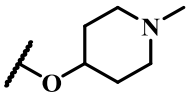	H	H	H	10	450.47	451.2	304-306
FJC-6 (5e)	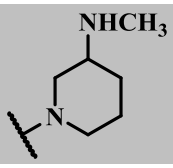	H	H	H	21	449.48	450.2	215-216
FJC-7 (5f)	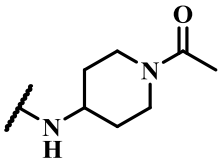	H	H	H	48	477.49	478.2	253-255
FJC-8 (5g)	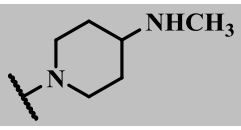	H	H	H	17	449.48	450.2	247-249
FJC-9 (5h)	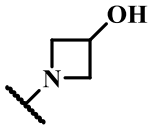	H	H	H	57	408.38	409.1	289-290
FJC-10 (5i)	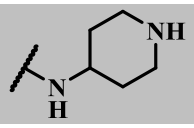	H	H	H	83	435.45	436.1	>270
FJC-11 (5j)	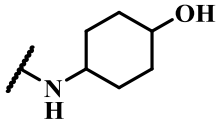	H	H	H	16	450.47	451.2	244-246
FJC-12 (5k)	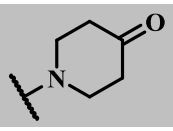	H	H	H	21	434.42	435.1	>270
FJC-13 (5l)	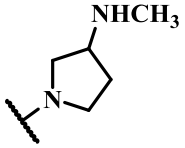	H	H	H	70	435.45	436.2	225-228
FJC-14 (5m)	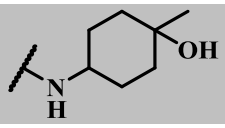	H	H	H	27	464.49	465.2	>270

Code	R^1	R^2	R^3	R^4	Yield (%)	MW	MS peak	MP (°C)
FJC-15 (5n)	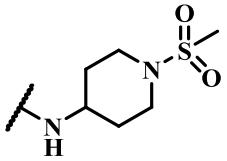	H	H	H	56	513.54	514.1	>270
FJC-17 (5o)	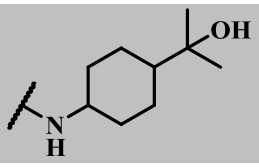	H	H	H	66	492.55	493.2	277-280
FJC-18 (5p)	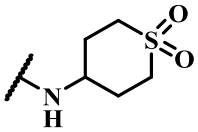	H	H	H	35	484.50	485.1	>270
FJC-19 (5q)	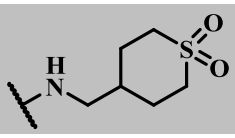	H	H	H	30	498.52	499.1	>270
FJC-20 (5r)	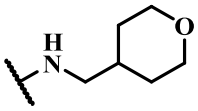	H	H	H	61	450.47	451.2	227-229
FJC-21 (5s)	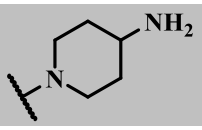	H	H	H	85	435.45	436.2	233-235
FJC-22 (5t)	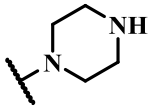	H	H	H	52	421.43	422.1	>270
FJC-23 (5u)	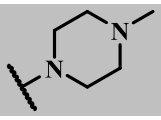	H	H	H	70	435.45	436.1	232-234
FJC-24 (5v)	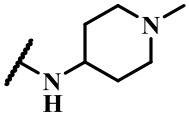	Cl	Cl	H	61	518.37	518.1	264-266
FJC-25 (5w)	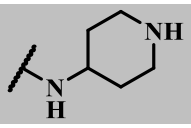	Cl	H	Cl	8	504.34	504.0	262-263
FJC-26 (5x)	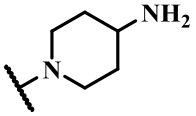	Cl	H	Cl	32	504.34	504.0	247-248
FJC-27 (5y)	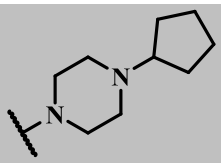	Cl	H	Cl	39	558.43	558.1	209-211

Code	R^1	R^2	R^3	R^4	Yield (%)	MW	MS peak	MP (°C)
FJC-28 (5z)	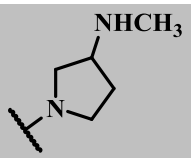	H	H	Cl	58	469.90	470.1	>270
FJC-29 (6a)	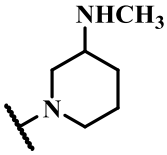	H	H	Cl	74	483.92	484.1	>270

2.7 SPECTROSCOPIC ANALYSIS OF KEY INTERMEDIATES AND FINAL TARGET COMPOUNDS.

All the compounds synthesized were characterized primarily by proton NMR (^{1}H-NMR) and Carbon-13 NMR (^{13}C-NMR). To aid in assigning protons, correlation spectroscopy (COSY) analysis was also done.

2.7.1 Hydroxy intermediate 3

Characteristic features of the ^{1}H-NMR spectrum of compound **3 (Fig. 2.9)** are the appearance of a broad singlet at δ 13.85 ppm integrating for one proton corresponding to the OH proton and a singlet at δ 6.12 ppm corresponding to the H^2 proton. There are also two doublets at δ 7.93 ppm and 7.88 ppm corresponding to the four aromatic protons $H^{12,13}$ and $H^{11,14}$ on the phenyl side group respectively, as well as a triplet at δ 7.43 ppm corresponding to the aromatic H^8 proton. A third doublet at δ 8.63 ppm corresponds to the H^9 proton. The close proximity of signals corresponding to H6 (doublet) and H7 (triplet) makes the two to merge into a multiplet integrating for two protons in the aromatic section.

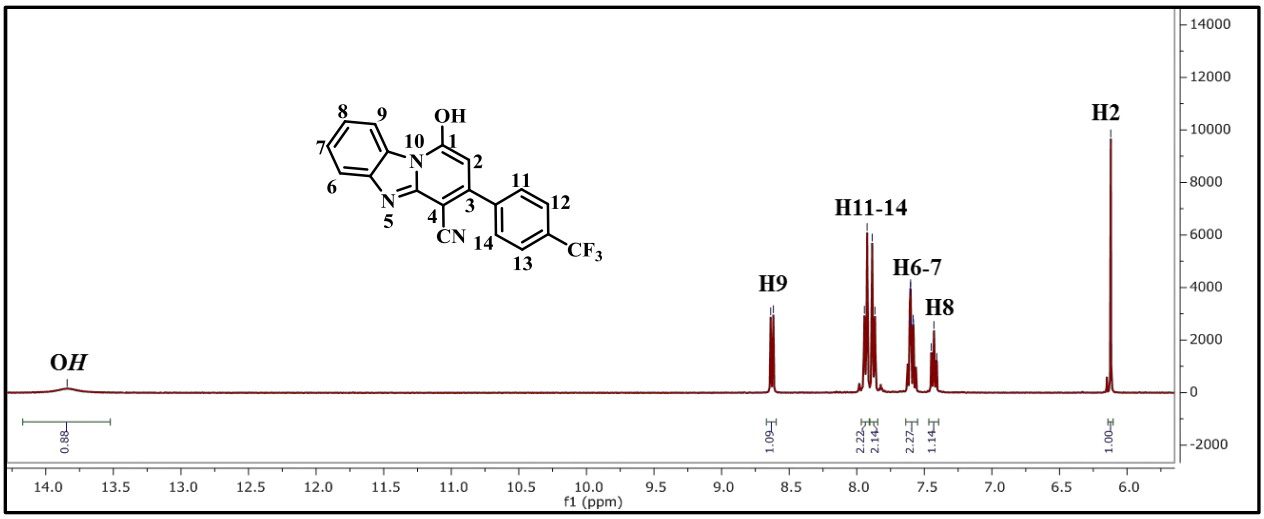

Fig. 2.9: ^{1}H-NMR spectrum of hydroxy intermediate **3**.

The ^{13}C-NMR spectrum of compound **3 (Fig. 2.10)** indicates that the expected 19 carbon atoms are present. The chemical shift corresponding to C4 of the PBI core appears at the most upfield position (δ 68.5 ppm) due to the combined shielding effect of the pyridyl ring π electrons and cyano group electrons. On the other hand, C1 (δ 158.6 ppm) is the most downfield signal due to the electronegative effect of the hydroxyl group. The relatively low value of this shift (<180 ppm) also indicates that the enol tautomer of compound **3** is the predominant product under these reaction conditions.[108] The LC-MS spectrum gave a pseudo-molecular ion peak of *m/z* 354.1 (t_R = 4.58 min), corresponding to $[M+H]^+$ for this compound.

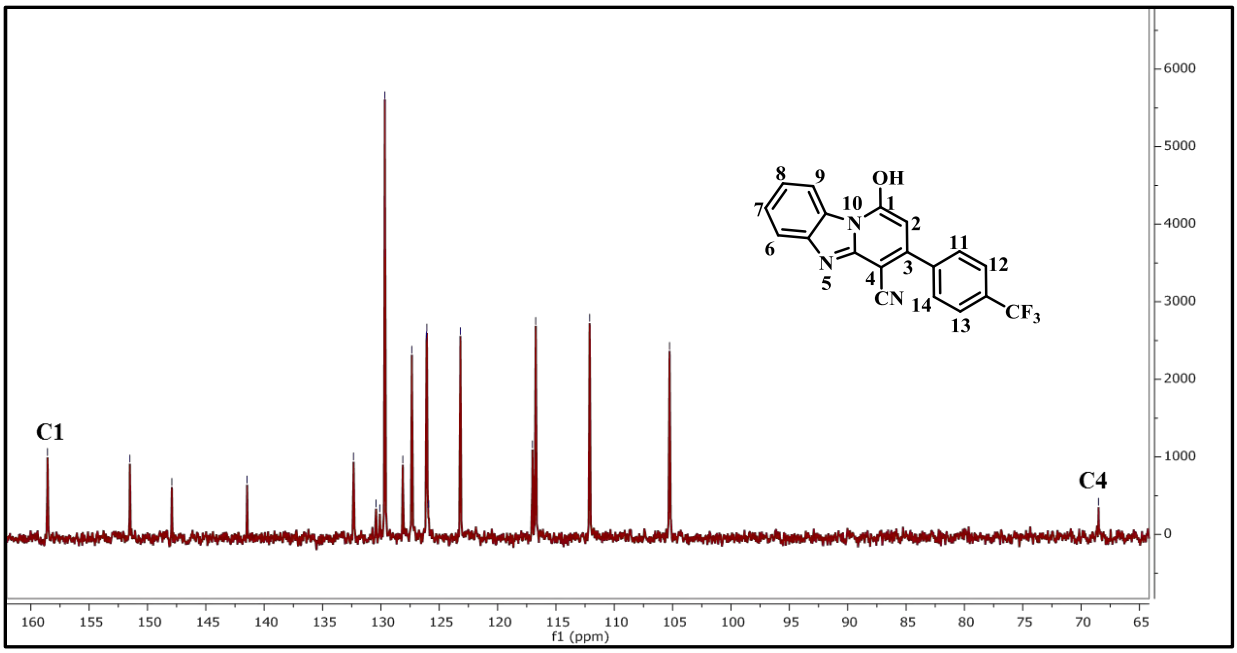

Fig. 2.10: ^{13}C-NMR spectrum of hydroxy intermediate **3**.

2.7.2 Chloro intermediate 4

The ^{1}H-NMR spectrum of compound **4 (Fig. 2.11)** is characterized by disappearance of the broad singlet corresponding to the OH proton observed in compound **3** due to replacement of the hydroxyl group by the chloro substituent. A downfield shift of the singlet of H^{2} proton (δ 7.69 ppm in **4** compared to δ 6.12 ppm in **3**) due to the deshielding effect of the chloro substituent at C-1 is observed as well. There is also a multiplet at δ 8.03 ppm corresponding to the aromatic H^{6} proton and the four phenyl side group protons $H^{11\text{-}14}$. Two triplets are observed at δ 7.70 ppm and 7.54 ppm, each integrating for one proton. These correspond to the aromatic protons H^{7} and H^{8} respectively.

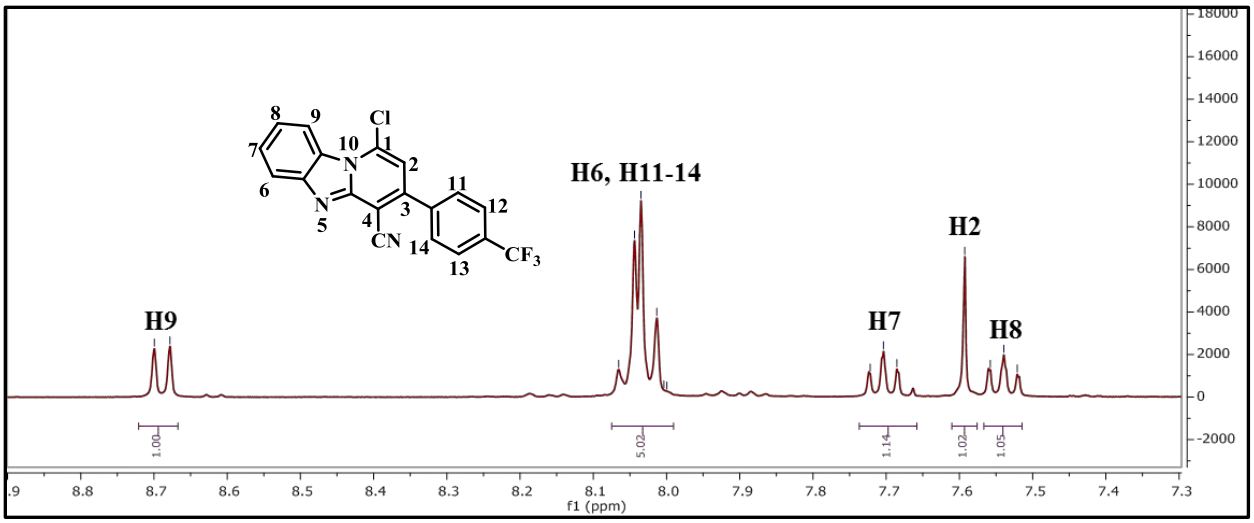

Fig. 2.11: ^{1}H-NMR spectrum of chloro intermediate **4**.

The ^{13}C-NMR spectrum of compound **4** (**Fig. 2.12**) confirms the presence of 19 carbon atoms as expected. The most upfield shift, corresponding to C4, now appears at δ 97.6 ppm. This is a slight downfield shift as compared to the equivalent signal for compound **3**, presumably due to the strong electron-withdrawing effect of the chloro substituent which partially deshields C4. Carbon 1 still appears as the most downfield position, at δ 148.3 ppm. The LC-MS spectrum gave a pseudo-molecular ion peak of *m/z* 372.1 (t_R = 4.63 min), corresponding to $[M+H]^+$ for this compound.

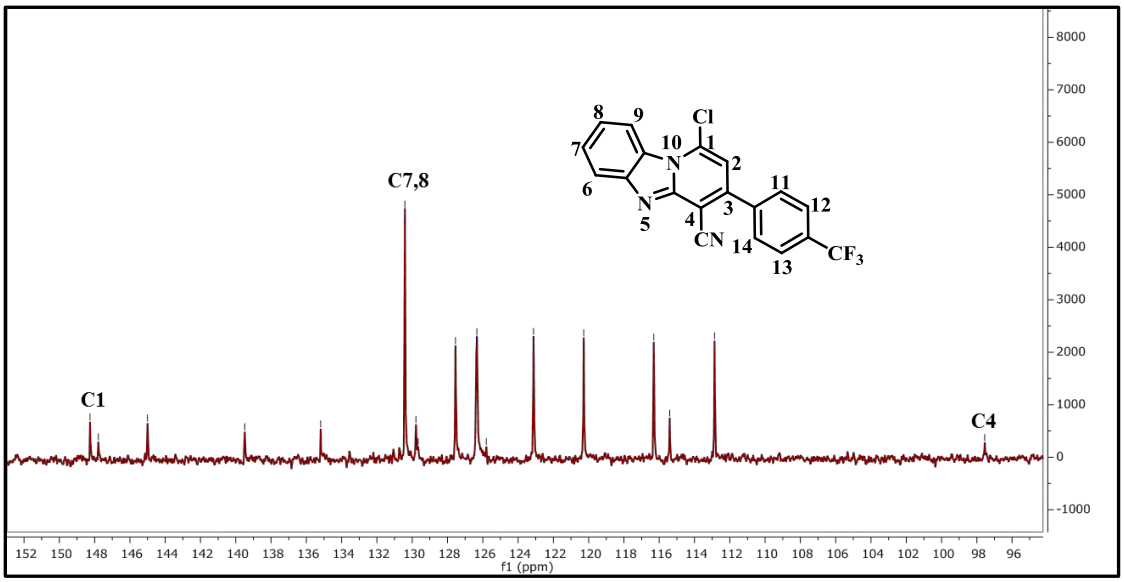

Fig. 2.12: ^{13}C-NMR spectrum of chloro intermediate **4**.

2.7.3: Final target compounds FJC-2 to FJC-29 (5a-6a)

The characteristic ^{1}H-NMR spectra of final target compounds **5a**-**6a** can be described by considering the spectrum of compound **FJC-20** (**5r)** as an example.

The aromatic section of the spectrum of **5r** remains generally unchanged as there is no substitution on the PBI core. Therefore, the spectra of chloro intermediate **4** and final target compound **5r** are fairly comparable in this section. There are two characteristic doublets at δ 8.50 and δ 7.86 ppm corresponding to the H^{9} and H^{6} protons respectively (**Fig. 2.13**). There is also a singlet at δ 7.96 ppm which integrates for four protons. This corresponds to the four aromatic protons $H^{11\text{-}14}$. Two triplets, each integrating for one proton, are observed at δ 7.58 and 7.41. These correspond to the aromatic H^{7} and H^{8} protons on the PBI core.

An upfield shift of the H^{2} singlet from δ 7.69 ppm in the ^{1}H-NMR spectrum of compound **4** to δ 6.35 ppm in the **5r** spectrum indicates the absence of the deshielding effect of the chloro substituent. This is due to its replacement by the amine side group in **5r**.

Confirmation of the amination step is indicated by appearance of a singlet at δ 7.68 ppm, corresponding to the NH proton (**Fig. 2.13**). This is further supported by appearance of a doublet at δ 3.50 ppm, which corresponds to the two methylene bridge protons H^{15}.

Since substitution is carried out using alicyclic amine groups, extra chemical shifts appear upfield of shifts corresponding to the PBI core protons. In the case of **5r**, there is appearance of multiplets at δ 3.89, 3.35, 3.27, 2.14, 1.75 and 1.35 ppm, which represent the tetrahydropyranyl chair protons $H^{16\text{-}20}$, labeled as axial (a) or equatorial (e). This confirms substitution of the chloro substituent by the appropriate cyclic amine side chain.

Two distinct singlets are also observed at δ 3.33 and δ 2.09 ppm. The former signal corresponds to water present in DMSO-*d*, while the latter is due to acetone, incorporated into the **5r** crystal during recrystallization.

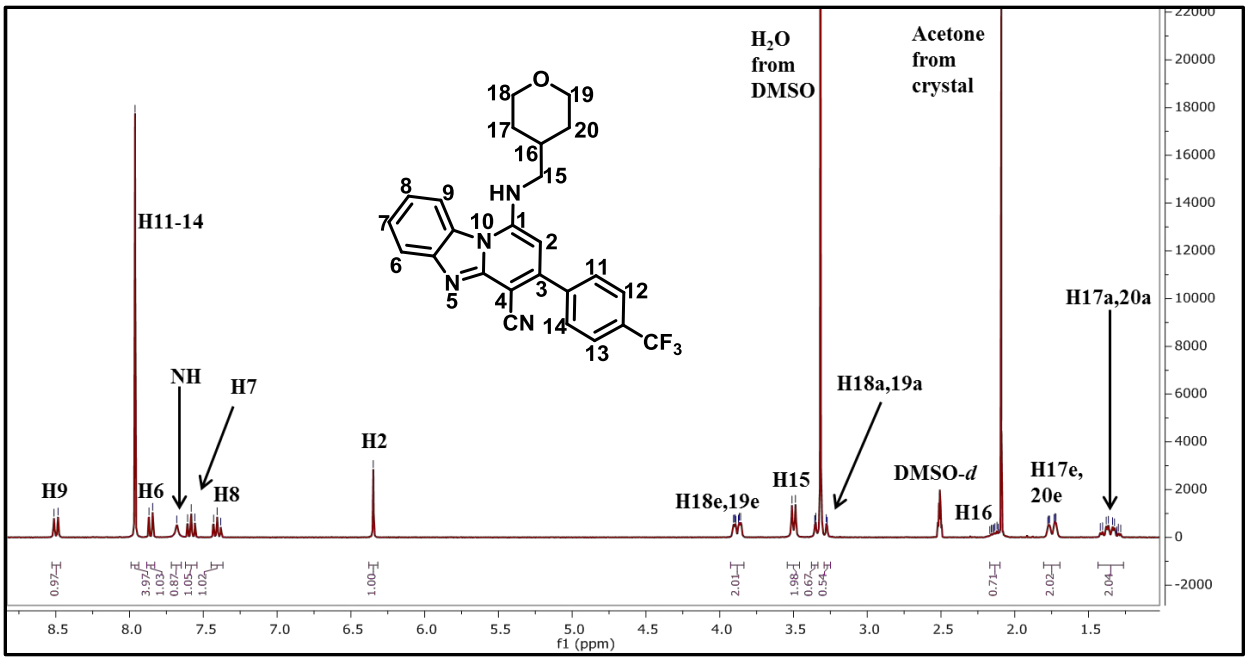

Fig. 2.13: ^{1}H-NMR spectrum of final target compound **FJC-20** (**5r**).

The ^{13}C-NMR spectrum of **5r** (**Fig. 2.14**) shows that the expected 25 carbon atoms present in the compound‟s structure are accounted for. The most downfield shift, at δ 150.60 ppm, corresponds to C1 of the PBI core structure due to its attachment to the nitrogen atom of the amine –NH bridge. The most upfield signals occur at δ 34.33 and 31.33 ppm, corresponding to tetrahydropyranyl ring carbons C17 and C20 respectively.

A signal at δ 30.86 ppm, corresponding to the methyl groups of acetone, is also observed. For purposes of clarity, the signal due to the carbonyl carbon of acetone (occurring at δ 206.86 ppm), has been omitted from the spectrum below.

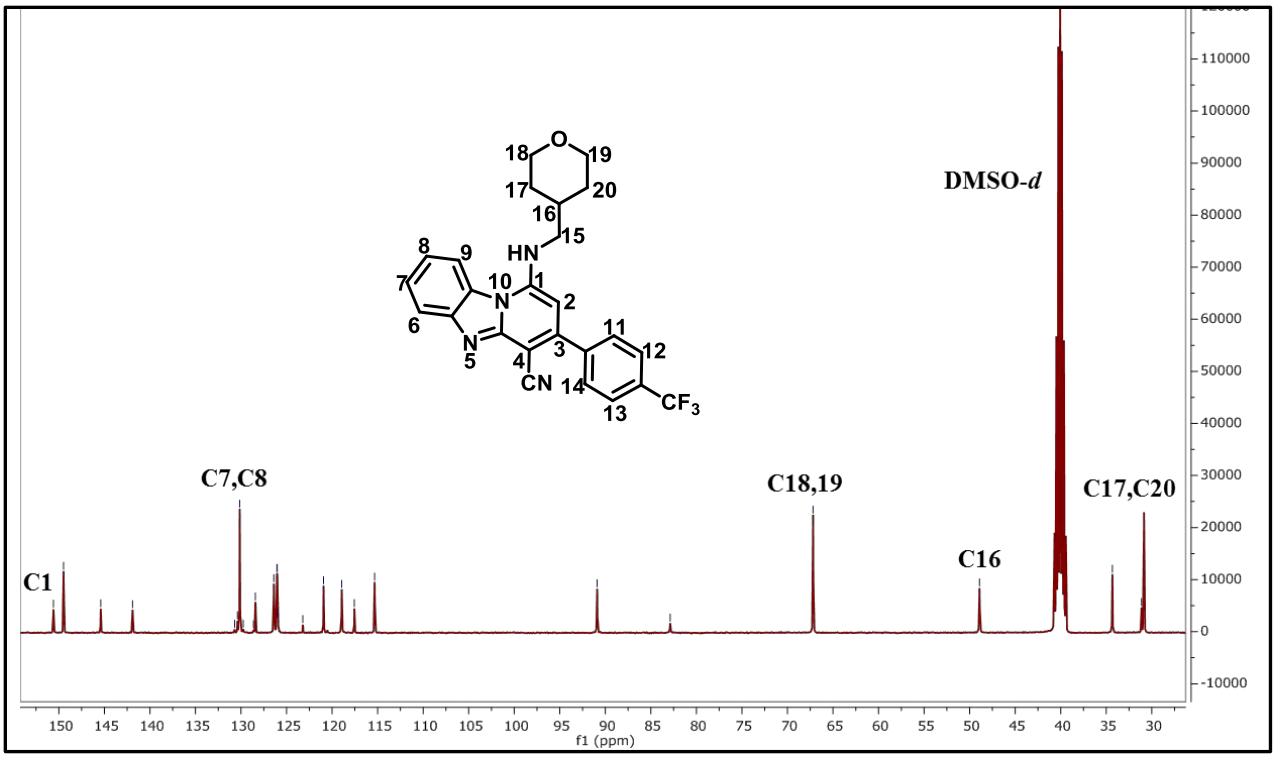

Fig. 2.14: ^{13}C-NMR spectrum of target compound **5r**.

2.8 PHARMACOLOGICAL AND SOLUBILITY EVALUATION OF FINAL TARGET COMPOUNDS.

Pharmacological and solubility evaluation of target compounds was carried out according to the screening cascade shown in **Fig. 2.15**. All the target compounds synthesized were screened for *in vitro* beta-hematin inhibition and *in vitro* antiplasmodial activity against the chloroquine-sensitive NF54 strain of *P. falciparum*. Selected compounds were also tested for activity against the gametocyte and liver stage forms of *P. falciparum* and *P. berghei* respectively. Potent compounds from the antiplasmodial assay were further screened for cytotoxicity against the mammalian Chinese Hamster Ovarian (CHO) cell line and for *in vitro* metabolic stability in mouse liver microsomes.

The apparent solubility of the analogues was determined using the turbidimetric assay.

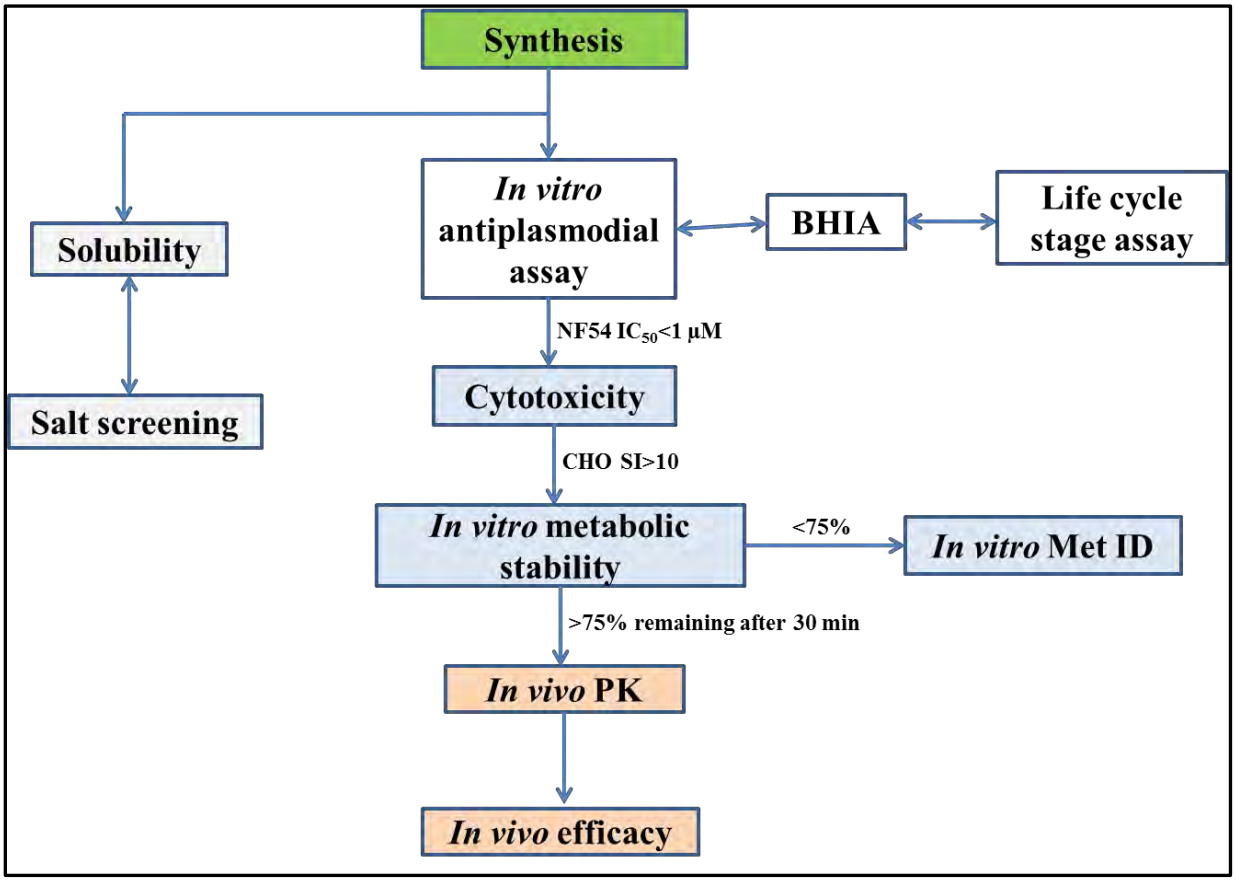

Fig. 2.15: Screening cascade for PBI analogues.

Biological activity and apparent solubility data of the compounds are summarized in **Table 2.3** below.

Table 2.3: Pharmacological activity and solubility of PBI analogues.

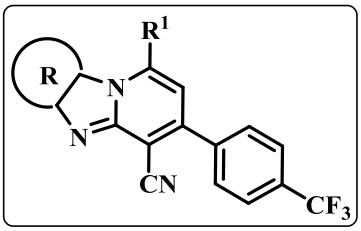

Code	R	R[1]	IC$_{50}$ (µM) BHIA[a]	NF54	CHO[b]	Early gametocyte	SI[c]	Met Stab[d] (%)	Solubility (µM)
FJC-2 (5a)		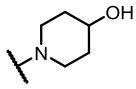	>35000	>23					5-10
FJC-3 (5b)		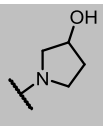	4242.93	8.48					5-10
FJC-4 (5c)		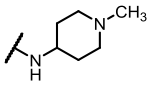	47.62	0.44	5.98 ± 2.75	3.49	14	63.1 ± 13.3	20-40
FJC-5 (5d)		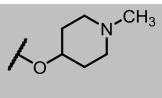	40.76	0.70	4.07 ± 0.21	2.84	6		10-20
FJC-6 (5e)		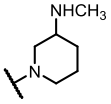	175.47	1.38		4.58			>100
FJC-7 (5f)	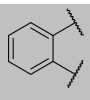	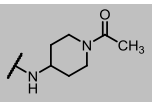	79.25	4.42					5-10
FJC-8 (5g)		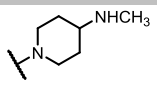	87.23	0.84	6.31 ± 1.24	1.15	8		>100
FJC-9 (5h)		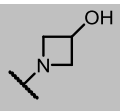	>70000	21.32					<5

Code	R	R^1	IC50 (µM) BHIA[a]	NF54	CHO[b]	Early gametocyte	SIc	Met Stab[d] (%)	Solubility (µM)
FJC-10 (5i)		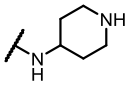	16.9	0.36	16.5 ± 1.7		46	64.7 ± 14.2	10-20
FJC-11 (5j)		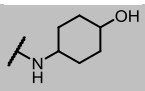	76.53	>10					5-10
FJC-12 (5k)		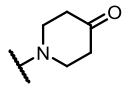	>20000	>9.58					<5
FJC-13 (5l)		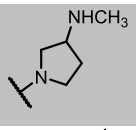	120.96	1.14					20-40
FJC-14 (5m)		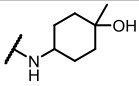	66.48	6.45					<5
FJC-15 (5n)		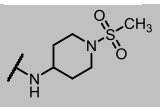	131.22	5.02					5-10
FJC-17 (5o)		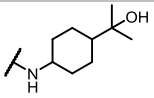	9878	4.96					5-10
FJC-18 (5p)		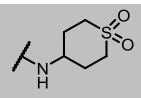	276.03	7.81					<5
FJC-19 (5q)		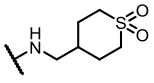	192.21	>10					<5
FJC-20 (5r)		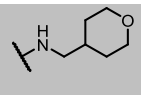	>26000	>10					<5
FJC-21 (5s)		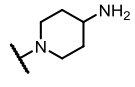	80.21	0.95	15.8 ± 1.5		17	92.3 ± 8.3	20-40
FJC-22 (5t)		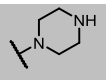	169.45	4.18					20-40

Code	R	R^1	IC50 (µM)				SI[c]	Met Stab[d] (%)	Solubility (µM)
			BHIA[a]	NF54	CHO[b]	Early gametocyte			
FJC-23 (5u)		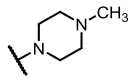	285.12	9.18					10-20
FJC-24 (5v)	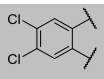	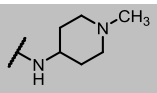	27.81	0.69	4.19 ± 2.6		6		5-10
FJC-25 (5w)		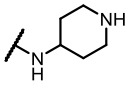	7.85	0.27	5.90 ± 1.4		22	100.4 ± 6.1	1-5
FJC-26 (5x)	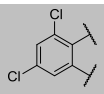	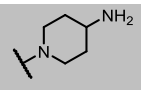	18.33	0.41	2.98 ± 0.2		7		5-10
FJC-27 (5y)	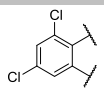	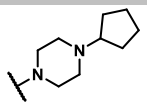	111.69	1.79					1-5
FJC-28 (5z)	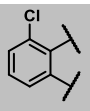	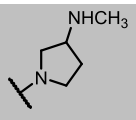	39.13	1.72					10-20
FJC-29 (6a)	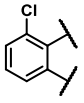	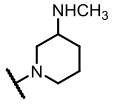	41.49	1.51					40-80
Chloroquine			43.57	0.006					
Amodiaquine			17.46	0.009					
4h[e]			40.51	0.11					10-20
Podophyllotoxin					0.021				
Propranolol								29.1 ± 1.0	
Midazolam								0.1 ± 0.0	
MMV 390048								97.2 ± 4.3	

[a]Beta hematin inhibition activity. [b]Cytotoxicity determined using mammalian Chinese Hamster Ovarian cell line. [c]Selectivity Index. [d]Metabolic stability determined as % remaining unchanged after 30 min incubation in mouse liver microsomes. [e]Lead compound **4h** from previous study.

2.8.1 *In vitro* antiplasmodial and beta-hematin inhibition activity

For the LHS-unsubstituted analogues, piperidinyl compounds **5c**, **d**, **g**, **i** and **s** showed the most potent antiplasmodial activity (IC_{50} 0.36-0.95 µM). Replacing the piperidine substituent with a

pyrrolidine ring gives compounds with moderate activity, as is the case for compounds **5b** (IC_{50} 8.48 μM) and **5l** (IC_{50} 1.14 μM). The same observation is made with the piperazinyl compounds **5t** and **5u** (IC_{50} values of 4.175 μM and 9.175 μM respectively). Compound **5h**, bearing a hydroxyazetidine substituent, was found to be inactive in both assays. The piperidine side chain, therefore, is hypothesized to offer optimal target-ligand interaction for this group of compounds.

The cyclic amine side groups were linked to C1 of the PBI ring either directly or via a linker. Most compounds synthesized possess a –NH linker between the PBI scaffold and the cyclic amine substituent. Antiplasmodial activity was, however, found to be maintained in the case of an ether linker. Compound **5d**, which contains an ether linkage between the primary PBI scaffold and the piperidinyl side chain, was found to be active (NF54 IC_{50} 0.70 μM).

Compounds bearing a piperidinyl or cyclohexyl substitution without a second basic center, or where the basicity of the second nitrogen atom is reduced, showed only moderate *in vitro* antiplasmodial activity (IC_{50} range 4.42-7.81 μM). This can be observed for compounds **5f**, **m**, **n**, **o** and **p**. This could imply that presence of a second nitrogen atom, in addition to the linker, is vital for antiplasmodial activity.

Substitution with highly polar groups e.g. hydroxyl and keto functions in place of the second basic group was found to be detrimental to the activity of these compounds, as shown by compounds **5a**, **j** and **k** (NF54 IC_{50} > 9.58 μM for all three). Extension of the chain linking the PBI core to the cycloalkyl amino substituent also gives compounds with poor activity as illustrated by **5q** and **5r** (NF54 IC_{50} > 10 μM for both compounds). These observations suggest that optimal target-ligand interaction is interfered with by both introduction of highly polar functions and extension of the PBI-amine linker chain length.

LHS-substituted analogues were synthesized to investigate the effect of chloro substituents on *in vitro* antiplasmodial and beta-hematin inhibition activity, as well as cytotoxicity and microsomal metabolic stability. Mono- and dichloro-substituted analogues of the most potent compounds **5c**, **5e**, **5i**, **5l** and **5s** were synthesized. One LHS analogue, **5y**, was synthesized with a bulky cyclopentylpiperazinyl substituent at C1. This was done to investigate the effect of the bulky cyclic amine on *in vitro* activity and solubility.

Generally, LHS-substituted analogues displayed similar or improved antiplasmodial and beta-hematin inhibition potency compared to their parent unsubstituted analogues. The monochloro-substituted analogues **6a** and **5z** both showed improved beta-hematin inhibition potency (IC_{50} 41.49 μM and 39.13 μM respectively) compared to their unsubstituted parent compounds **5e** and **5l** (IC_{50} 175.47 μM and 120.96 μM respectively). This observation implies that monochloro-substitution on the left side of the PBI ring possibly improves the compounds‟ interaction with beta hematin and also inhibition potency, as reported for chloroquine analogues.[109] Both sets of analogues show comparable moderate antiplasmodial activity (NF54 IC_{50} range 1.14 μM – 1.72 μM). Monochloro-substitution, therefore, does not significantly affect *in vitro* antiplasmodial activity.

In the case of dichloro-substituted LHS analogues, compound **5v** (BHIA IC_{50} 27.81 μM) was found to show more potent beta-hematin inhibition activity compared to its unsubstituted analogue **5c** (BHIA IC_{50} 47.62 μM). The antiplasmodial activity of **5v** (IC_{50} 0.69 μM) was comparable to that of **5c** (IC_{50} 0.44 μM). Both **5w** and **5x** showed improved *in vitro* activity compared to their unsubstituted analogues **5i** and **5s**. Compound **5w** (BHIA IC_{50} 7.85 μM, NF54 IC_{50} 0.27 μM) was found to possess an almost 2-fold increase in both beta-hematin and antiplasmodial potency as compared to **5i** (BHIA IC_{50} 16.9 μM, NF54 IC_{50} 0.36 μM). There was an even greater increase in *in vitro* potency in the case of **5x**, with a 4-fold increase in beta-hematin inhibition potency (IC_{50} 18.33 μM), accompanied by a 2-fold increase in antiplasmodial activity (IC_{50} 0.41 μM) in comparison to the parent unsubstituted compound **5s** (BHIA IC_{50} 80.21 μM, NF54 IC_{50} 0.95 μM). These drastic improvements in *in vitro* potency are thought to arise from improved ligand-target interaction after substitution with the lipophilic, electron-withdrawing chloro groups.

Compound **5y** with a bulky cyclopentylpiperazine substituent was found to possess slightly lower antiplasmodial activity (IC_{50} 1.79 μM) compared to other LHS - substituted analogs bearing two chloro groups. It also showed significantly lower beta-hematin inhibition potency (IC_{50} 111.69 μM). The bulky amine group, therefore, appears to be detrimental to both antiplasmodial and beta-hematin inhibition potency.

The PBI group of compounds are speculated to exert their antiplasmodial activity, at least partly, via inhibition of heme detoxification by *Plasmodium* parasites. This is based upon their structural

similarity to quinoline antimalarials e.g. chloroquine, which are known to act via the mechanism above. Presence of the hydrophobic, planar structure and basic amine side group are two vital structural features also found in quinoline antimalarials.[109] This observation formed the basis for testing PBI analogues for *in vitro* beta-hematin inhibition activity. A number of compounds synthesized in this research project were found to possess similar or higher beta-hematin inhibition potency compared to chloroquine. For instance, compound **5w** (BHIA IC_{50} 7.85 μM), is more potent than the standards chloroquine (IC_{50} 43.57 μM) and amodiaquine (IC_{50} 17.46 μM)**.** The analogue **5w** also displays higher beta-hematin inhibition activity than the lead compound **4h** from previous study (IC_{50} 40.51 μM).

A cut-off IC_{50} value of <100 μM was taken to indicate good beta-hematin inhibition activity for these compounds. In general, compounds possessing potent beta-hematin inhibition activity also showed good antiplasmodial activity. Examples include analogues **5c** (BHIA IC_{50} 47.62 μM, NF54 IC_{50} 0.44 μM), **5d** (BHIA IC_{50} 40.76 μM, NF54 IC_{50} 0.70 μM) and **5i** (BHIA IC_{50} 16.9 μM, NF54 IC_{50} 0.36 μM). However, there is no direct correlation between these activities. This observation may suggest that these compounds exert their antiplasmodial effect via a different or additional mechanism aside from the speculated inhibition of heme detoxification by *Plasmodium* parasites.[109]

A plot of Log IC_{50} against Log BHIA for the 18 most potent compounds (NF54 IC_{50} < 10 μM) illustrates this relationship, as depicted in **Fig. 2.16**. Although a general trend can be observed in the logarithmic comparison of beta-hematin inhibition to *in vitro* antiplasmodial potency, no direct relationship between the two can be established from this graph.

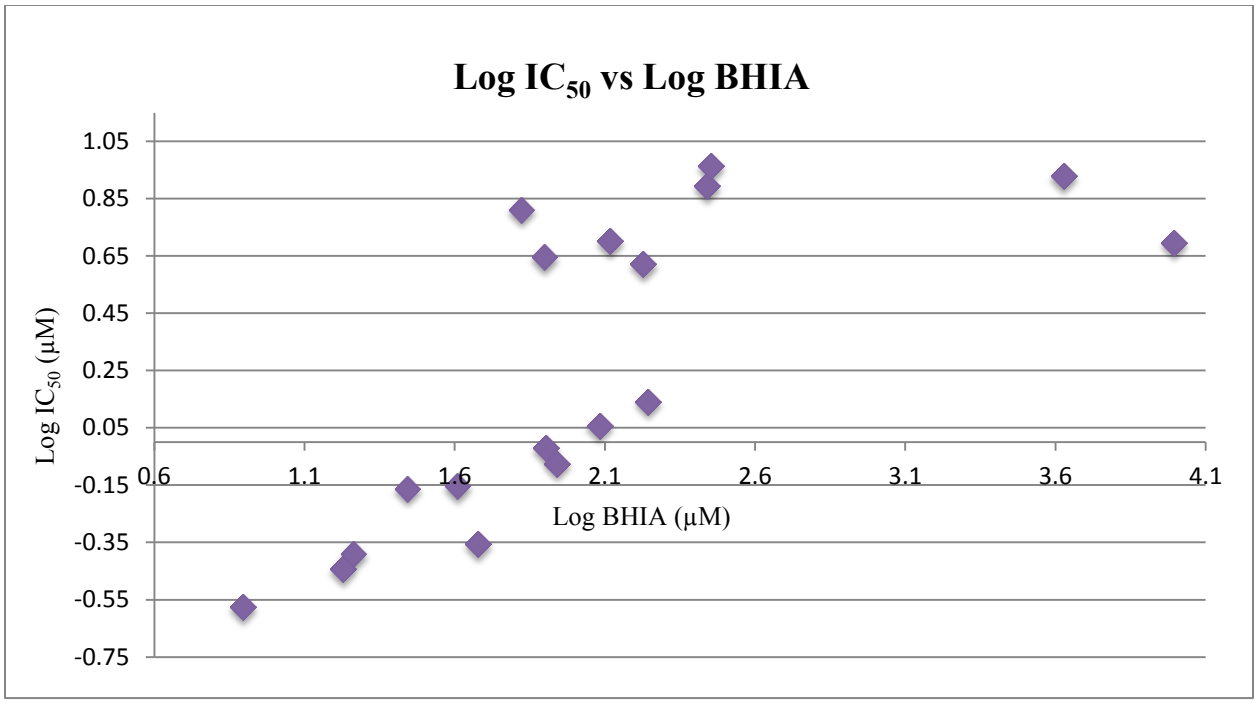

Fig. 2.16: Comparison of Log IC_{50} and Log BHIA for the most potent compounds.

All the analogues synthesized in this project showed lower antiplasmodial potency compared to the lead compound **4h** from previous study. Compound **4h** (NF54 IC_{50} 0.11 µM) was twice as active as the most active compound **5w** (IC_{50} 0.27 µM) from this study.

2.8.2 Cytotoxicity and microsomal metabolic stability in MLM

Compounds which displayed potent antiplasmodial activity with IC_{50} values less than 1 µM were tested for cytotoxicity against the mammalian CHO cell line. Furthermore, those showing a selectivity index of 10 or higher from this assay were tested for microsomal metabolic stability in mouse liver microsomes. Single point metabolic stability was determined by measuring the percentage concentration of the compound remaining unchanged after 30 minutes of incubation in mouse liver microsomes. A value of 75% or higher is taken as the indicator for stability in this assay.

For the LHS-unsubstituted compounds, analogues **5c**, **5d**, **5g**, **5i** and **5s** were screened for cytotoxicity in the CHO assay. Compounds **5d** and **5g** displayed high levels of cytotoxicity with selectivity indices below 10 (SI 6 and 8 respectively), while the rest had acceptable selectivity indices of 14 (**5c**), 46 (**5i**) and 17 (**5s**). An *in vitro* metabolic stability assay on the three non-

cytotoxic analogues in MLM indicated that **5c** and **5i** possessed only moderate stability (63% and 65% remaining unchanged respectively). Analogue **5s** (92% remaining unchanged) was found to be metabolically stable in this assay.

Of the five LHS-substituted analogues synthesized, three (**5v**, **5w** and **5x**) had antiplasmodial potency below 1 μM, and were therefore screened for cytotoxicity. All three were found to display higher cytotoxicity against CHO cells compared to the unsubstituted parent compounds **5c**, **5i** and **5s**. This resulted in a consistent reduction in the selectivity indices of these compounds, with a 2-fold or greater reduction observed for each compound pair. Selectivity indices for these compounds were found to be 6 (**5v**), 22 (**5w**) and 7 (**5x**), as shown in **Fig. 2.17**. Therefore, in spite of the minimal sample size, this consistent observation is sufficient to validate a conclusion for this series of compounds. Left-hand side di-substitution with lipophilic electron-withdrawing groups appears to favor both beta-hematin inhibition and *in vitro* antiplasmodial activity, but is detrimental to the cytotoxicity profile.

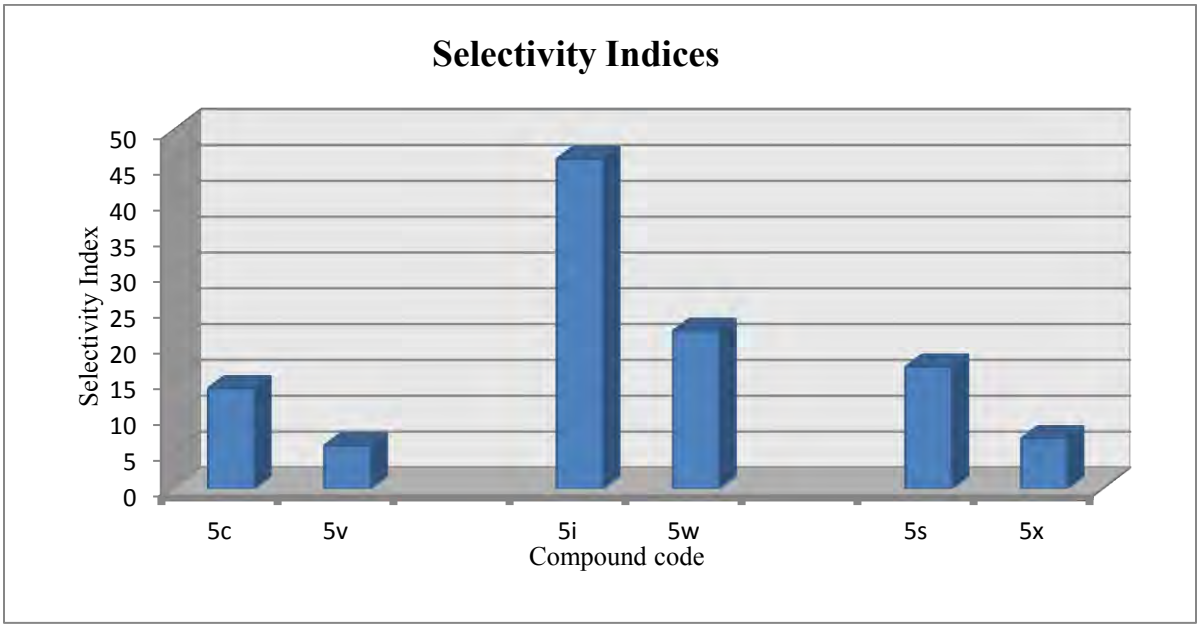

Fig. 2.17: Comparison of selectivity indices of parent compounds and their LHS- substituted analogues.

The LHS-analogue **5w**, the only one of the three with selectivity index >10, was screened for metabolic stability against mouse liver microsomes. It showed a markedly improved profile, with most of the compound remaining unchanged after 30 min incubation (100.4% ± 6.1). Therefore,

in comparison to the parent compound **5i** (64.7% ± 14.2), chloro di-substitution has afforded a more metabolically stable derivative in spite of the increased cytotoxicity.

2.8.3 Metabolite identification

As illustrated on the screening cascade in **Fig. 2.19**, metabolite identification was indicated for compounds found to be metabolically unstable in the *in vitro* MLM assay. This was done to identify metabolic hotspots which may be fixed as part of a lead optimization campaign. Analogues **5c** and **5i** were, therefore, subjected to metabolite identification. This was done by incubating the compounds for 60 min in MLM followed by identification of ensuing metabolites by LC-MS/MS.

The diagnostic ions and resulting fragment ions after incubation of compounds **5c** (**FJC-4**) and **5i** (**FJC-10**) are summarized in **Table 2.4** below.

Table 2.4: Diagnostic ions and metabolites identified.

Diagnostic ions	Parent/ Metabolite	RT[a] (min)	$[M+H]^+$ (m/z)	Relative amount (%)	Biotransformation	Diagnostic ions (*m/z*)		Tentative Identity
						A	B	
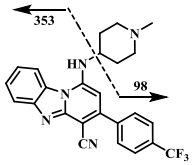	Parent	7.0	450	82	-	353	98	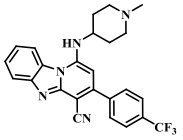
	M1 (5i)	6.9	436	4	-14 N-demeth.	353	84	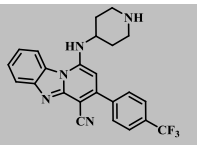
	M2	7.1	466	10	+16 +O	353	114	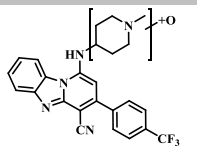
	M3	7.3	480	4	+30 +2O-2H	367	114	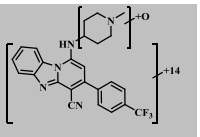

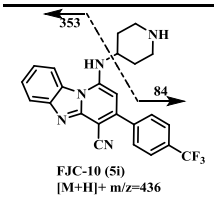 FJC-10 (5i) [M+H]+ m/z=436	Parent	6.95	436	90	-	353	84	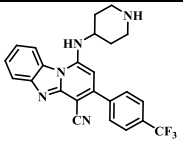
	M1	7.25	466	3	+30 +2O-2H	367	100	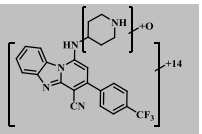
	M2	7.40	452	3	+16 +O	353	100	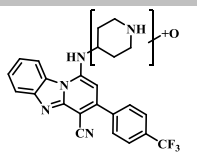
	M3	7.60	450	4	+14 +O-2H	353	98	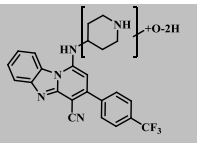

[a]Retention time.

From the LC-MS/MS data, it was determined that **5c** was metabolized to one major mono-oxidation metabolite (**M2**), one *N*-demethylation product (**M1**) and one metabolite (**M3**) having a mass shift of M+30 compared to the parent compound. The fragmentation pattern indicates that oxidation occurs on the piperidine ring in **M1**, as indicated in **Fig. 2.18**. The N-desethyl metabolite **M1** is actually the active compound **5i**. This implies that in an *in vivo* setting, some of the activity attributed to **5c** could actually arise from the analog **5i** after metabolism of the parent compound. The metabolite **M3** arises as a result of oxidation on both the piperidine ring and PBI core.

Formation of metabolites was NADPH- and liver-microsomes dependent. This confirms that the biotransformations are mediated by CYP450 enzymes in the microsome fractions. Metabolite **M3** was detected in non-NADPH incubations, meaning its formation is also mediated by non-CYP450 enzymes.

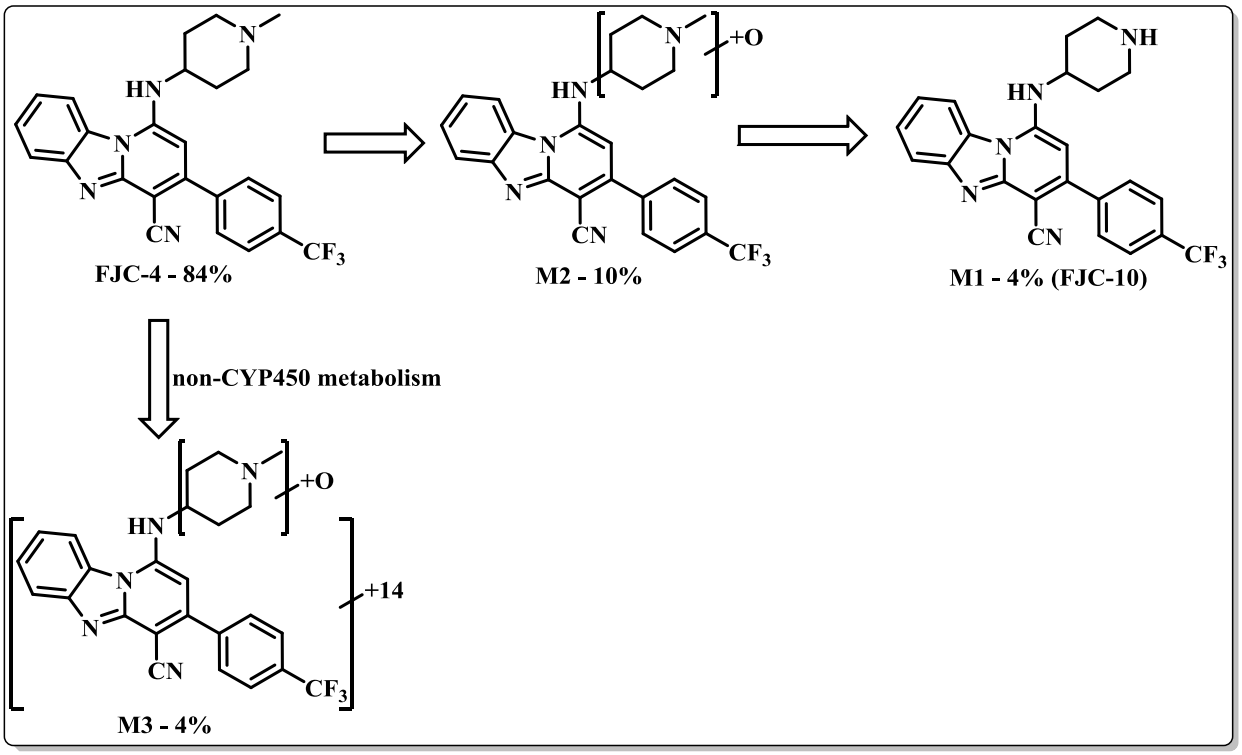

Fig. 2.18: Proposed metabolic pathway for **FJC-4** in mouse liver microsomes.

The analogue **5i**, on the other hand, was metabolized to one mono-oxidation metabolite (**M2**), one keto derivative (**M3**) and one metabolite (**M1**) having a mass shift of M+30 compared to the parent compound. Fragmentation patterns also indicate that oxidation occurred on the piperidine ring in **M2** and **M3**, and on both the piperidine ring and PBI core in **M1** (**Fig. 2.19**).

As was the scenario for compound **5c**, formation of metabolites was NADPH- and liver-microsomes dependent, a pointer for metabolism by CYP450 enzymes. Metabolite **M1** was detected in non-NADPH incubations. This implies that its formation is also mediated by non-CYP450 enzymes.

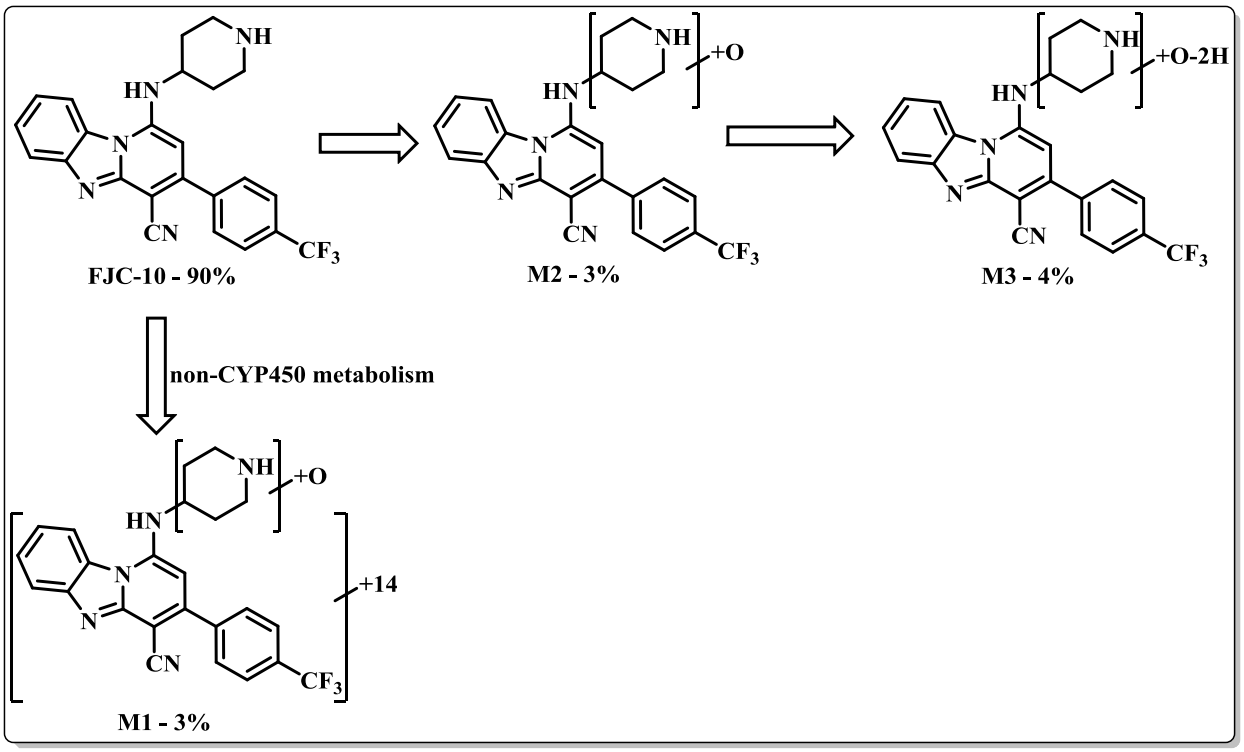

Fig. 2.19: Proposed metabolic pathway of **FJC-10** in mouse liver microsomes.

2.8.4 Metabolic stability in HLM

Analogues **5c**, **5i** and **5s** were tested for *in vitro* metabolic stability in human liver microsomes. All were found to be stable, with ≥ 75% remaining unchanged after 30 minutes of incubation. The values obtained for the three compounds were 75% (**5c**), 99% (**5i**) and 91% (**5s**) respectively.

2.8.5 Gametocidal activity

Novel antimalarials possessing activity against gametocytes are of interest in research due to their transmission blocking potential.[110] This would be achieved by preventing transmission of gametocytes to mosquitoes by infected individuals, which bridges the mosquito-human parasite life cycle. Few antimalarial drugs in current clinical use possess anti-gametocyte activity, giving this area of exploration even more significance.[45,51-53,110] Dual-acting antimalarials, with activity against both the blood-stage and gametocyte forms of the parasite, would have the potential advantage of blocking transmission in addition to potentially achieving clinical cure.

Initial screening of compounds **5c**, **5d**, **5e** and **5g** against early stage gametocytes of the chloroquine-sensitive NF54 strain of *P. falciparum* indicated that these possess only moderate

gametocidal activity (IC_{50} 1.15-4.58 μM). These four compounds were selected for initial screening as they show good *in vitro* antiplasmodial activity (**Table 2.3**).

Compounds **5i**, **5l** and **5s** were then selected for a dual point gametocidal activity testing against gametocytes of the NF54 strain of *P. falciparum* owing to their potent activity in the initial gametocyte screen. They were screened against early and late stage gametocytes using the luciferase reporter assay and the ATP assay.[110] The results are presented in **Table 2.5** below.

Table 2.5: Dual point gametocidal activity of compounds **5i**, **l** and **s**.

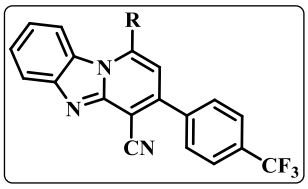

Code	R	Gametocyte activity (IC_{50}, μM)			
		Luciferase assay		ATP assay	
		Early stage	Late stage	Early stage	Late stage
FJC-10 (5i)	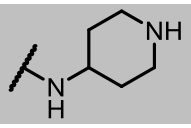	8.964	5.599	NS*	1.162
FJC-13 (5l)	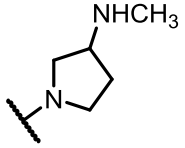	NS	NS	NS	4.085
FJC-21 (5s)	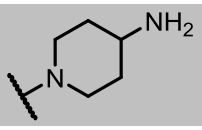	NS	NS	NS	1.634
Methylene blue		0.195	0.143	-	0.9
Artemisinin		0.043	0.011	-	0.015

*NS – Compound not selected for dose-response determination on a particular platform based on initial screening results.

All three compounds displayed only moderate gametocidal activity, as determined by the ATP assay. Compound **5l**, a pyrrolidine-based analog, was also found to show much less activity (IC_{50} 4.085 μM) compared to the piperidines **5i** and **5s** (IC_{50} 1.162 and 1.634 μM respectively).

The analog **5i** showed significant stage specificity, with an almost two-fold reduction in the half-maximal inhibitory concentration from early to late stage gametocytes as determined by the

luciferase assay (IC_{50} 8.964 μM to 5.599 μM). This change could be attributed to the biological target(s) of **5i** being predominantly expressed by the late stage forms of gametocytes.

2.8.6 Liver stage activity

Novel antimalarial agents possessing dual activity against both blood and liver stage forms of *Plasmodium* form an important research segment.[111,112] These agents would potentially achieve radical cure of malaria by clearing both forms of the parasite, thereby preventing recrudescence. They could also potentially prevent development of clinical malaria by clearance of liver schizont forms of the parasite during the exoerythrocytic stage of infection.

Additionally, recent drug discovery efforts have been directed at identifying agents with activity against hypnozoite forms of *P. vivax* and *P. ovale*. These would prevent relapses associated with the two parasite species.[111,113,114]

Compounds **5c**, **d**, **g**, **i** and **j** were screened for activity against liver forms of the parasite. From this initial screening, only compound **5i** (**FJC-10**) was found to demonstrate a favorable infection control profile coupled with good cell confluency. Determination of the *in vitro* inhibitory potency of **5i** showed that the compound has a moderate IC_{50} of 3.31 μM against *Plasmodium berghei* liver stage forms.

2.9 SOLUBILITY

Apparent solubility of all compounds synthesized was determined using the turbidimetric solubility assay.[84] Hydrocortisone and Reserpine were used as the respective positive and negative controls for this determination.

2.9.1 General procedure

The assay involved initial dissolution of the test compounds in DMSO to obtain 10 mM stock solutions. Serial dilutions were then prepared on 96-well plates from a concentration range of 0.25 mM to 10 mM, with a blank well of 0 mM included as a reference. This was done in triplicate for all the samples on the pre-dilution plate. From each pre-dilution solution, secondary dilutions of the samples in DMSO and 0.01 M pH 7.4 phosphate-buffered saline (PBS) were then prepared on a second 96-well plate, the turbidimetric assay plate. This plate set up was also done in triplicate. All samples were assayed at a concentration range of 0-200 μM.

The assay plate was then incubated for 2 hours, after which absorbance of the solutions was determined at 620 nm. This value is chosen because few organic compounds are known to absorb UV radiation at the specified wavelength. Any observed absorbance, therefore, is expected to be due to particles which crash out of solution beyond the solubility limit of the particular sample.

By plotting the corrected absorbance versus concentration curves, the apparent solubility of the compounds was determined. This is indicated by the point in the PBS curve at which the plot shows a definite deviation from the baseline and a concomitant increase in corrected absorbance values due to presence of particles in solution as a result of the sample compound‟s insolubility.

As expected, hydrocortisone was expressly soluble in the entire concentration range of the assay while Reserpine showed only moderate solubility (5-10 μM) as illustrated in **Fig. 2.20** and **2.21** below. These findings validated the sample results for this solubility assay.

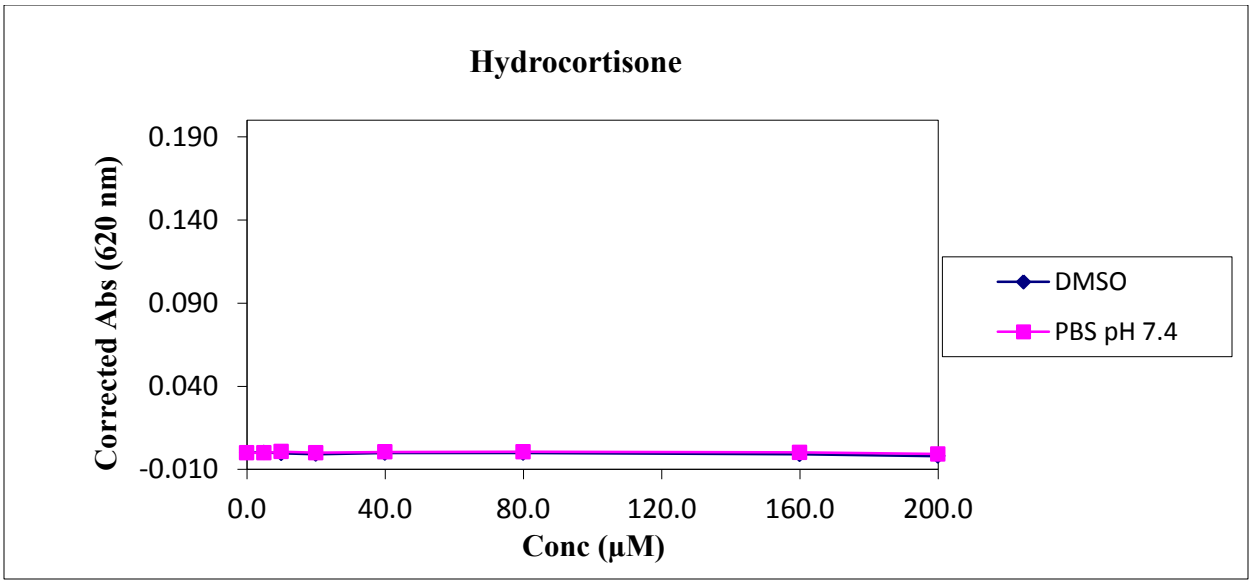

Fig. 2.20: Corrected absorbance versus concentration curve for hydrocortisone.

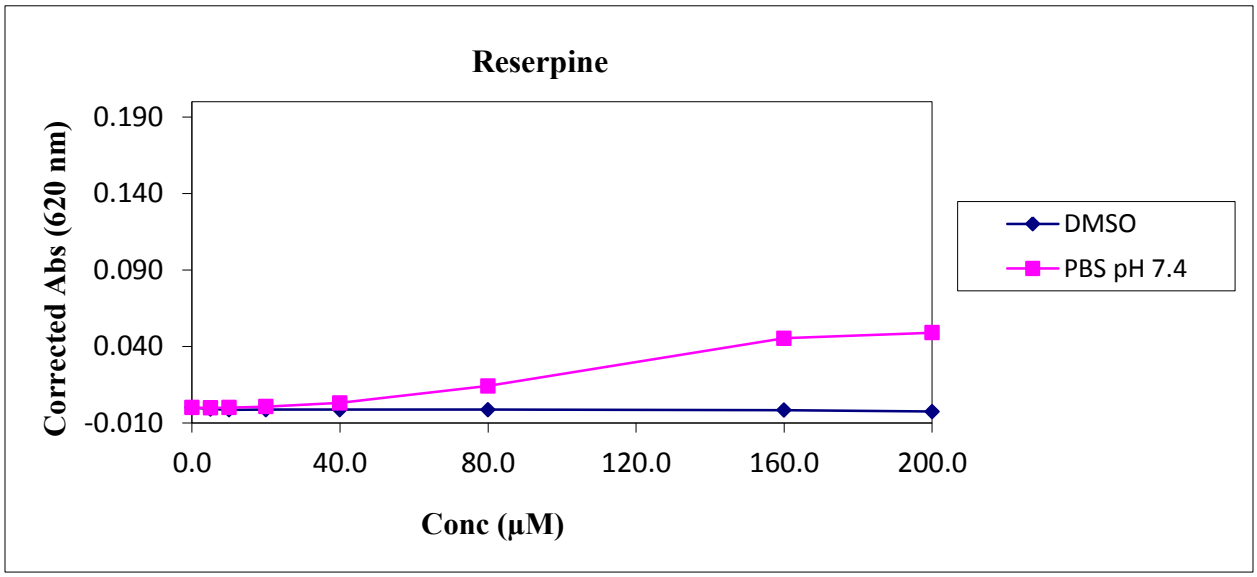

Fig. 2.21: Corrected absorbance versus concentration curve for reserpine.

2.9.2 Solubility of LHS-unsubstituted analogues 5a-u

Solubility values as determined for the samples **5a-u** are presented in **Table 2.3**.

The general classification of turbidimetric solubility ranges for organic compounds analyzed by this method is as follows[83,115]:

- ✓ Solubility < 1 μM – Highly insoluble
- ✓ Solubility of 1-100 μM – Moderately soluble
- ✓ Solubility >100 μM – Highly soluble

From this assay, therefore, all but two of the compounds were found to have moderate solubility in PBS at physiological pH. The lead compound **4h** from previous study was found to have a moderate turbidimetric solubility value of 10-20 μM in this assay.

In spite of substitution with polar solubilizing groups, mainly hydroxyl and keto functions, most compounds only showed solubility in the low moderate range as exemplified by compounds **5a**, **b**, **h, k** and **m** among others (< 5-10 μM). Compounds **5p**, **q** and **r** containing sulfonyl and tetrahydropyranyl substitutions also showed very low aqueous solubility (< 5 μM). This phenomenon may be explained on the basis of formation of new intermolecular hydrogen bonds between the polar groups, augmenting even tighter crystal packing and thus reducing aqueous solubility.[93] This is a common downside associated with attempts to improve aqueous solubility by introduction of polar, hydrogen-bonding groups.

A slight improvement in solubility was observed for compounds with amino substitution in place of the more polar groups. Compounds **5c**, **l**, **s** and **t** were all comparatively more soluble (20-40 μM) than the analogues discussed above. Their solubilities were comparable to that of **4h**. This can be attributed to more favorable hydrogen-bonding interactions between the analogues and water, therefore augmenting their solubilization.

Piperidinyl compounds **5e** and **5g** were found to show the highest aqueous solubility (> 100 μM) and can be classified as being highly soluble. The two analogues both contain an aminomethyl substitution on the piperidine ring, at position 3 in **5e** and 4 in **5g**. This structural feature is thought to offer optimal interaction with water, presumably by hydrogen bond formation. The two compounds, therefore, showed the best solubility in this series.

The single crystal x-ray diffraction (XRD) structure of **5c** indicates that the aminopiperidine substituent provides a suitable site for hydrogen bonding with water molecules. Even though this phenomenon was only observed in the **5c** hemihydrate crystal, it is still a plausible possibility in aqueous solutions of **5c** and other piperidine containing analogues. This could account for the improved solubility of analogues **5e** and **5g**. Details of the x-ray crystal structure are discussed in the next chapter.

2.9.3 Solubility of LHS-substituted compounds 5v-6a

Chloro-substituted analogues **5v**, **w**, **x** and **y** were found to possess low apparent solubilities of between 1-10 μM while **5z** showed a slight improvement with solubility of 10-20 μM. The most soluble of these analogues, **6a**, had a moderate solubility range of 40-80 μM.

It is observed that LHS-substituted analogues **5v**, **w** and **x** all showed lower solubility as compared to their unsubstituted parent compounds **5c**, **i** and **s**. The same is true of **5z** and **6a**, which showed significant reductions of apparent solubility in comparison to compounds **5l** and **5e**, from which they were derived. This is hypothesized to occur because of increased lipophilicity of the LHS-substituted compounds as a result of the additional chloro groups. In the case of compound **5y**, the bulky lipophilic cyclopentylpiperazine substituent is thought to additionally contribute to its extremely low solubility.

2.9.4 Comparison of tPSA and CLogP of new compounds to 4h

The predicted topological polar surface area (tPSA) and calculated Log P (CLog P) values of analogues synthesized in this research project were compared to the lead compound **4h** from previous study (**Table 2.6**). This was done to determine the influence of these parameters on aqueous solubility. Although tPSA is commonly used as a predictor of trans-membrane permeability and absorption characteristics,[116] in this instance the parameter is only used to predict relative polarity of the new compounds in comparison to **4h**. CLog P is used to compare the relative lipophilicities.

Table 2.6: Comparison of tPSA and CLogP for PBI analogues.

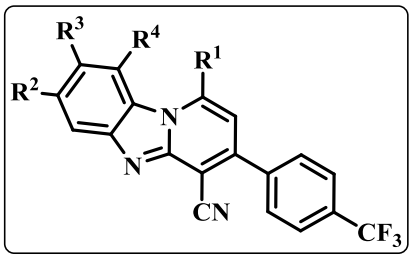

Code	R^1	R^2	R^3	R^4	tPSA ($Å^2$)[a]	CLog P[b]
4h	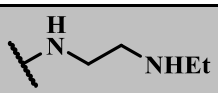	H	H	H	63.45	5.82
FJC-2 (5a)	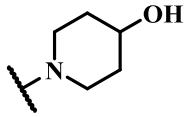	H	H	H	62.86	4.48
FJC-3 (5b)	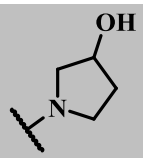	H	H	H	62.86	4.68
FJC-4 (5c)	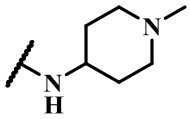	H	H	H	54.66	5.73
FJC-5 (5d)	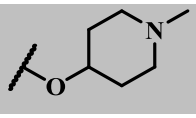	H	H	H	51.86	5.61
FJC-6 (5e)	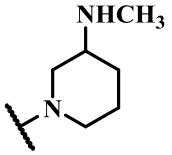	H	H	H	54.66	5.60
FJC-7 (5f)	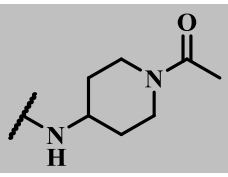	H	H	H	71.73	4.33
FJC-8 (5g)	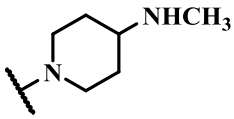	H	H	H	54.66	4.73
FJC-9 (5h)	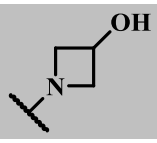	H	H	H	62.86	4.87

Code	R^1	R^2	R^3	R^4	tPSA (Å^2)[a]	CLog P[b]
FJC-10 (5i)	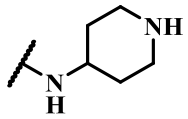	H	H	H	62.86	5.29
FJC-11 (5j)	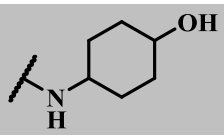	H	H	H	71.65	5.62
FJC-12 (5k)	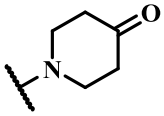	H	H	H	68.49	5.22
FJC-13 (5l)	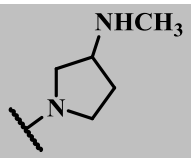	H	H	H	54.66	5.04
FJC-14 (5m)	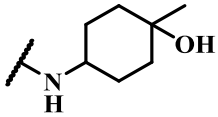	H	H	H	71.65	6.14
FJC-15 (5n)	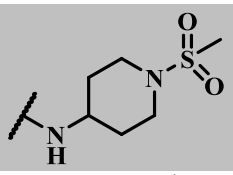	H	H	H	85.56	4.88
FJC-17 (5o)	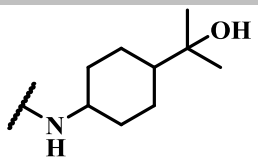	H	H	H	71.65	6.94
FJC-18 (5p)	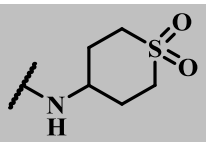	H	H	H	85.56	5.02
FJC-19 (5q)	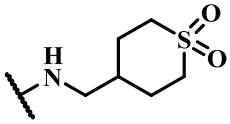	H	H	H	85.56	4.54
FJC-20 (5r)	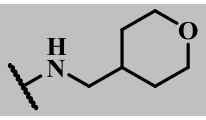	H	H	H	60.65	5.92
FJC-21 (5s)	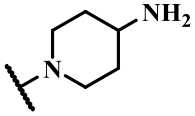	H	H	H	68.65	4.58
FJC-22 (5t)	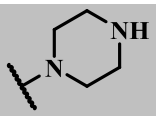	H	H	H	54.66	5.17

Code	R^1	R^2	R^3	R^4	tPSA ($Å^2$)[a]	CLog P[b]
FJC-23 (5u)	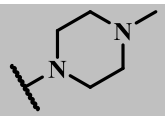	H	H	H	45.87	5.75
FJC-24 (5v)	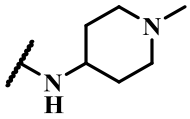	Cl	Cl	H	54.66	7.04
FJC-25 (5w)	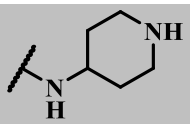	Cl	H	Cl	63.45	6.71
FJC-26 (5x)	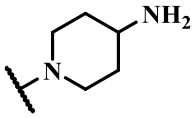	Cl	H	Cl	68.65	6.01
FJC-27 (5y)	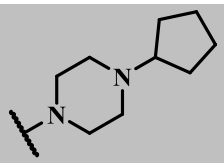	Cl	H	Cl	45.87	8.44
FJC-28 (5z)	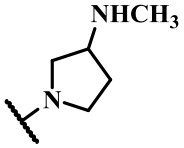	H	H	Cl	54.66	5.76
FJC-29 (6a)	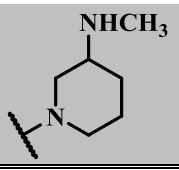	H	H	Cl	54.66	6.32

[a]Topological polar surface area, calculated using ChemBioDraw Ultra suite 14.0

[b]Calculated Log P, determined using ChemBioDraw Ultra suite 14.0

Most of the compounds synthesized had a comparable or lower tPSA value than compound **4h** (63.45 $Å^2$). This can be taken to imply similar or lower polarity as compared to the lead compound.

2.9.4.1 Effect of polarity and lipophilicity on antiplasmodial activity

Among the LHS-unsubstituted analogues, compounds with the most potent *in vitro* antiplasmodial activity were found to have similar or lower tPSA compared to **4h** (63.45 $Å^2$). Examples include **5c**, **5d**, **5e**, **5g**, **5i** and **5l** (tPSA 51.86-62.86 $Å^2$). A similar observation is made for the most active LHS-substituted compounds **5x**, **5w**, **5y**, **5z** and **6a** (tPSA 45.87-63.45 $Å^2$). Compounds **5s** and **5x**, with a slightly higher polar surface area value of 68.65 $Å^2$, were also found to be active. On the other hand, some of the most inactive compounds also had comparable or lower polarity to that of **4h**, such as compounds **5b**, **5c**, **5h** and **5r** (tPSA 54.66-62.86 $Å^2$). It is

therefore logical to conclude that similar or lower tPSA to **4h** seems to favor activity of the new PBI analogues, but some inactive compounds also show polar similarity to **4h**. Antiplasmodial activity seems to rely more on presence or absence of the second basic center than simply on polarity of the new compounds.

A clearer picture emerges in the case of highly polar analogues compared to **4h**. These were all found to have reduced antiplasmodial activity, or to be inactive. Compounds **5f**, **5j**, **5m** and **5o** (tPSA 71.65-71.73 $Å^2$) were only moderately active to inactive in the *in vitro* antiplasmodial assay. The same can be said concerning compounds **5n**, **5p** and **5q** (tPSA 85.56 $Å^2$). A drastic increase in polarity of these compounds compared to the previous lead compound **4h**, therefore, appears to be detrimental to antiplasmodial activity.

Changes in lipophilicity did not seem to impact greatly upon antiplasmodial activity. Compound **4h** was projected to have a CLogP of 5.82. Various active analogues had higher lipophilicity compared to this, for instance **5v**, **5w**, **5x** and **5y** (CLog P 6.01-8.44). Compounds with comparable lipophilicity to **4h** such as **5c**, **5d** and **5e** (CLog P 5.60-5.73) as well as those with lower values for instance **5g**, **5l** and **5s** (CLog P 4.73-5.04) were all found to possess potent antiplasmodial activity. In the same breadth, inactive compounds also had a range of lipophilicity values that were higher, similar to or lower than that of **4h**. The *in vitro* antiplasmodial activity of these compounds, therefore, seemed to be affected more by other factors than by changes in lipophilicity.

2.9.4.2 Effect of polarity and lipophilicity on solubility

The lead compound **4h** from previous optimization studies was found to have moderate apparent solubility of 10-20 µM by the turbidimetric assay.

As was observed in the case of antiplasmodial activity, most compounds with similar or improved solubility compared to **4h** were also found to be those with comparable or lower tPSA than the analogue **4h**. Compounds **5c**, **5l** and **5t** (apparent solubility 20-40 µM) all have a tPSA of 54.66 $Å^2$, much lower than **4h** (63.45 $Å^2$). The two compounds **5e** and **5g** which showed high apparent solubility of > 100 µM were both predicted to have a tPSA of 54.66 $Å^2$. Analogue **5s**, with a slightly higher polarity of 68.65 $Å^2$, was also found to show moderate solubility in the range of 20-40 µM. A drastic increase in polarity of the new compounds was found to lower

their apparent solubilities, as exemplified by compounds **5m**, **5o**, **5p** and **5q** among others. These were all determined to have low apparent solubility in the range of < 5-10 μM, with high tPSA values of 71.65-85.56 $Å^2$. As alluded to earlier, formation of new intermolecular hydrogen bonds between the novel polar groups in these compounds is a possible mechanism that would account for their poor aqueous solubility. The analogues all contain strong hydrogen bond donor and acceptor functions such as hydroxyl, keto and sulfonyl groups.

Increased lipophilicity led to a reduction in solubility, as expected. This is best illustrated by considering the apparent solubilities of LHS-substituted analogues in comparison to their unsubstituted parent compounds. All the chloro-substituted analogues, with increased lipophilicity, had reduced solubility. Unsubstituted compounds **5c**, **5i** and **5s** (CLog P 4.58-5.73) had an average solubility range of 20-40 μM while the chloro-substituted compounds **5v**, **5w** and **5x** (CLog P 6.01-7.04) showed an average solubility range of only 5-10 μM. Unsubstituted compounds with higher CLog P than **4h** (CLog P 5.82) also generally showed reduced apparent solubility, as illustrated by compounds **5o** and **5m** (CLog P 6.94 and 6.14) among others. This was an expected observation since increased lipophilicity generally reduces aqueous solubility in organic molecules.

2.10 C0NCLUSIONS

PBI analogues with cyclic and functionalized amine substituents were successfully synthesized, characterized and tested for both pharmacological and physicochemical properties.

Various analogues possessing potent beta-hematin inhibition and antiplasmodial activity were identified. None of the analogues synthesized was, however, found to show superior antiplasmodial activity relative to the lead compound **4h** from a previous study. This could imply that the straight-chain aliphatic diamine substituent in **4h** generally offers more favorable ligand-target interaction than cyclic amine substituents for this group of compounds. On a brighter note, a number of analogues with similar or superior beta-hematin inhibition potency compared to **4h**, chloroquine and amodiaquine were identified. This could indicate the potential of cyclic amine-substituted PBIs to be applied in other disease areas such as schistosomiasis where hemoglobin degradation is speculated to be a druggable target.

Compounds with moderate to high microsomal metabolic stability were identified. In particular, chloro-substitution on the left hand side of the molecule was found to afford high microsomal metabolic stability.

Cytotoxicity emerged as a major stumbling block for this class of compounds. For the LHS-unsubstituted analogues, two out of the five highly potent compounds could not be progressed in the screening cascade due to a low selectivity index (< 10). For the LHS-substituted compounds, two out of the three highly active analogues were found to be cytotoxic and could not be tested for microsomal metabolic stability. More SAR optimization therefore needs to be carried out around the molecule to improve the selectivity index.

The primary strategy employed in an attempt to improve aqueous solubility of PBI analogues in this research project was introduction of polar and hydrogen-bonding groups on the cyclic amine side groups. This functionalization approach was found to be partly successful, and partly counterproductive. Introduction of highly polar hydrogen bond donor and acceptor functions e.g. hydroxyl, keto and sulfonyl groups reduced the apparent solubility of resulting molecules. This was attributed to formation of new intermolecular hydrogen bonds, further augmenting crystal packing and reducing aqueous solubility. Introduction of amino-group based substituents, on the

other hand, led to improved aqueous solubility. This is hypothesized to be a result of optimal hydrogen bonding interactions between the PBI molecules and water molecules, thereby enhancing their solubilization.

Generally, increased polarity was found to be detrimental to both antiplasmodial activity and apparent solubility. Increased lipophilicity led to reduced apparent solubility, as anticipated. This information was deduced by comparing the tPSA and CLog P values of newly synthesized analogues with those of the lead PBI compound **4h** from previous study.

REFERENCES

92. Enumula, S.; Pangal, A.; Gazge, M.; Shaikh, J. A.; Ahmed, K. Diverse pharmacological aspects of benzimidazole derivatives – A review. *Res. J. Chem. Sci.*, **2014**, *4*, 78-88.

93. Graham Solomons, T. W. Organic Chemistry. 11th Ed., **2013**.

94. Bansal, Y.; Silakari, O. The therapeutic journey of benzimidazoles: A review. *Bioorg. Med. Chem.*, **2012**, *20*, 6208-6236.

95. Keller, P.; Muller, C.; Engelhardt, I. et al. An antifungal benzimidazole derivative inhibits ergosterol biosynthesis and reveals novel sterols. *Antimicrob. Agents Chemother.*, **2015**, *59*, 6296-6307.

96. Takeshita, H.; Watanabe, J.; Kimura, Y. et al. Novel pyridobenzimidazole derivatives exhibiting antifungal activity by the inhibition of β-1,6-glucan synthesis. *Bioorg. Med. Chem. Lett.*, **2010**, *20*, 3893-3896.

97. Ansari, K. F.; Lal, C. Synthesis, physicochemical properties and antimicrobial activity of some new benzimidazole derivatives. *Eur. J. Med. Chem.*, **2009**, *44*, 4028-4033.

98. Chandrasekera, N. S.; Alling, T.; Bailey, M. A. et al. Identification of phenoxyalkylbenzimidazoles with antitubercular activity. *J. Med. Chem.*, **2015**, *58*, 7273-7285.

99. Pieroni, M.; Tipparaju, S. K.; Lun, S. et al. Pyrido [1, 2*a*] benzimidazole-based agents active against tuberculosis (TB), multidrug-resistant (MDR) TB and extensively drug-resistant (XDR) TB. *Chem. Med. Chem.*, **2011**, *6*, 334-342.

100. Pan, T.; He, X.; Chen, B. et al. Development of benzimidazole derivatives to inhibit HIV-1 replication through protecting APOBEC3G protein. *Eur. J. Med. Chem.*, **2015**, *95*, 500-513.

101. Hayashi, S.; Hirao, A.; Nakamura, H. et al. Discovery of 1-[1-(1-Methylcyclooctyl)-4-piperidinyl]-2-[(3R)-3-piperidinyl]-1*H*-benzimidazole: Integrated drug design and structure-activity relationships for orally potent, metabolically stable and potential-risk reduced novel non-peptide nociceptin/orphanin FQ receptor agonist as antianxiety drug. *Chem. Biol. Drug Des.*, **2009**, *74*, 369-381.

102. Keri, R. S.; Hiremathad, A.; Budagumpi, S.; Nagaraja, B. M. Comprehensive review in current developments of benzimidazole-based medicinal chemistry. *Chem. Biol. Drug Des.*, **2015**, *86*, 19-65.

103. Musonda, C. C.; Whitlock, G. A.; Witty, M. J.; Brun, R.; Kaiser, M. Chloroquine-astemizole hybrids with potent *in vitro* and *in vivo* antiplasmodial activity. *Bioorg. Med. Chem. Lett.*, **2009**, *19*, 481-484.

104. Keurulainen, L.; Vahermo, M.; Puente-Felipe, M. et al. A developability-focused optimization approach allows identification of *in vivo* fast-acting antimalarials: *N*-[3-[(Benzimidazol-2-yl)amino]propyl]amides. *J. Med. Chem.*, **2015**, *58*, 4573-4580.

105. Camacho, J.; Barazarte, A.; Gamboa, N. et al. Synthesis and biological evaluation of benzimidazole-5-carbohydrazide derivatives as antimalarial, cytotoxic and antitubercular agents. *Bioorg. Med. Chem.*, **2011**, *19*, 2023-2029.

106. Saify, Z. S.; Azim, M. K.; Ahmad, W. et al. New benzimidazole derivatives as antiplasmodial agents and plasmepsin inhibitors: Synthesis and analysis of structure-activity relationships. *Bioorg. Med. Chem. Lett.*, **2012**, *22*, 1282-1286.

107. Ndakala, A. J.; Gessner, R. K.; Gitari, P. W.; October, N.; White, K. L.; Hudson, A.; Fakorede, F.; Shackleford, D. M.; Kaiser, M.; Yeates, C.; Charman, S. A.; Chibale, K. Antimalarial pyrido [1, 2-*a*] benzimidazoles. *J. Med. Chem.*, **2011**, *54*, 4581-4589.

108. More O'Ferrall, R. A.; Murray, B. A. ^{1}H and ^{13}C NMR spectra of α-heterocyclic ketones and assignment of keto, enol and enaminone tautomeric structures. *J. Chem. Soc. Perkin Trans.*, **1994**, *2*, 2461-2470.

109. Egan, T. J.; Hunter, R.; Kaschula, C. H.; Marques, H. M.; Misplon, A.; Walden, J. Structure-function relationships in aminoquinolines: Effect of amino and chloro groups on quinoline-hematin complex formation, inhibition of β-hematin formation and antiplasmodial activity. *J. Med. Chem.*, **2000**, *43*, 283-291.

110. Lucantoni, L.; Duffy, S.; Adjalley, S. H.; Fidock, D. A.; Avery, V. M. Identification of MMV Malaria Box inhibitors of *Plasmodium falciparum* early stage gametocytes using a

luciferase-based high throughput assay. *Antimicrob. Agents Chemother.*, **2013**, *57*, 6050-6062.

111. Smith, P. W.; Diagana, T. T.; Yeung, B. K. S. Progressing the global antimalarial portfolio: Finding drugs which target multiple *Plasmodium* life stages. *Parasitology*, **2014**, *141*, 66-76.

112. Meister, S.; Plouffe, D. M.; Kuhen, K. L. et al. Imaging of *Plasmodium* liver stages to drive next-generation antimalarial drug discovery. *Science*, **2011**, *334*, 1372-1377.

113. Cogswell, F. B. The hypnozoite and relapse in primate malaria. *Clin. Microbiol. Rev.*, **1992**, *5*, 26-35.

114. Wells, T. N. C.; Burrows, J. N.; Baird, J. K. Targeting the hypnozoite reservoir of *Plasmodium vivax*: The hidden obstacle to malaria elimination. *Trends Parasitol.*, **2010**, *26*, 145-151.

115. Lipinski, C. A. Drug-like properties and the causes of poor solubility and poor permeability. *J. Pharmacol. Toxicol.*, **2000**, *44*, 235-249.

116. Fernandes, J.; Gattass, C. R. Topological surface area defines substrate transport by multidrug resistance associated protein 1 (MRP1/ABCC1). *J. Med. Chem.*, **2009**, *52*, 1214-1218.

CHAPTER 3: SINGLE CRYSTAL X-RAY STRUCTURE ANALYSIS AND SALT SCREENING OF FJC-4.

3.1 INTRODUCTION

This chapter describes the single crystal x-ray diffraction (XRD) analysis of **FJC-4** (**5c**) as well as salt screening attempts on the compound. The analogue **5c** was chosen for further structural and salt screening studies as it possesses a favorable *in vitro* antiplasmodial activity profile, coupled with a good selectivity index and moderate metabolic stability. Initially, analogue **FJC-21** (**5s**) was selected along with **5c** for XRD analysis, but attempts to obtain single crystals of **5s** were unsuccessful.

Elucidation of the single crystal structure of **5c** was projected to provide useful information relating the structural features of the compound to its solubility characteristics. Properties such as polymorphism, molecular conformation, planarity, π-stacking interactions, crystal packing characteristics and hydrogen bonding patterns all influence the intrinsic solubility profile of a compound.[117] Understanding the single crystal structure, together with powder x-ray diffraction (PXRD) patterns, could also be useful in selection of suitable co-formers to employ in co-crystal screening.[118] Co-crystal formation was, however, not carried out in this research project.

Single crystals of **5c** were grown by slow evaporation using a range of solvents selected by considering their polarity and pharmaceutical acceptability. These included acetone, methanol, ethanol, acetonitrile, ethyl acetate, 2-butanone (methyl ethyl ketone) and n-propanol. Crystals of appreciable size and shape were only obtained from acetone and acetonitrile. These were the ones used in XRD and thermal analysis.

Salt screening of **5c** was conducted using a range of acidic salt formers, as the compound is a weak base (predicted pKa 9.13 by ChemBioDraw Ultra 14.0). Out of the eight acids attempted, five formed salts with **5c**. Kinetic solubility of the salt forms, as well as the free base form of the compound, was then determined.

3.2 INITIAL ANALYSIS OF FJC-4 CRYSTAL STRUCTURE

The first batch of crystals was obtained from slow evaporation of a solution of **5c** in acetone. These were characterized first by thermal analysis and then by XRD analysis. Thermal analytical methods used were hot-stage microscopy (thermomicroscopy), thermogravimetric analysis (TGA) and differential scanning calorimetry (DSC).

3.2.1 Thermomicroscopy

Thermomicroscopic analysis of a single crystal of **5c** was done to determine whether the crystals obtained were solvated or non-solvated. An appropriately-sized single crystal of **5c** was submerged in silicone oil and heated between 23 and 270 °C, as summarized in **Fig. 3.1**. It was found that the crystal was solvated, with desolvation observed between approximately 132 and 163 °C. The physical appearance of the crystal was drastically altered upon completion of the desolvation phase. Onset of melting was observed at ~232 °C, and the crystal darkened significantly beyond 250 °C. This was taken as a possible marker of decomposition.

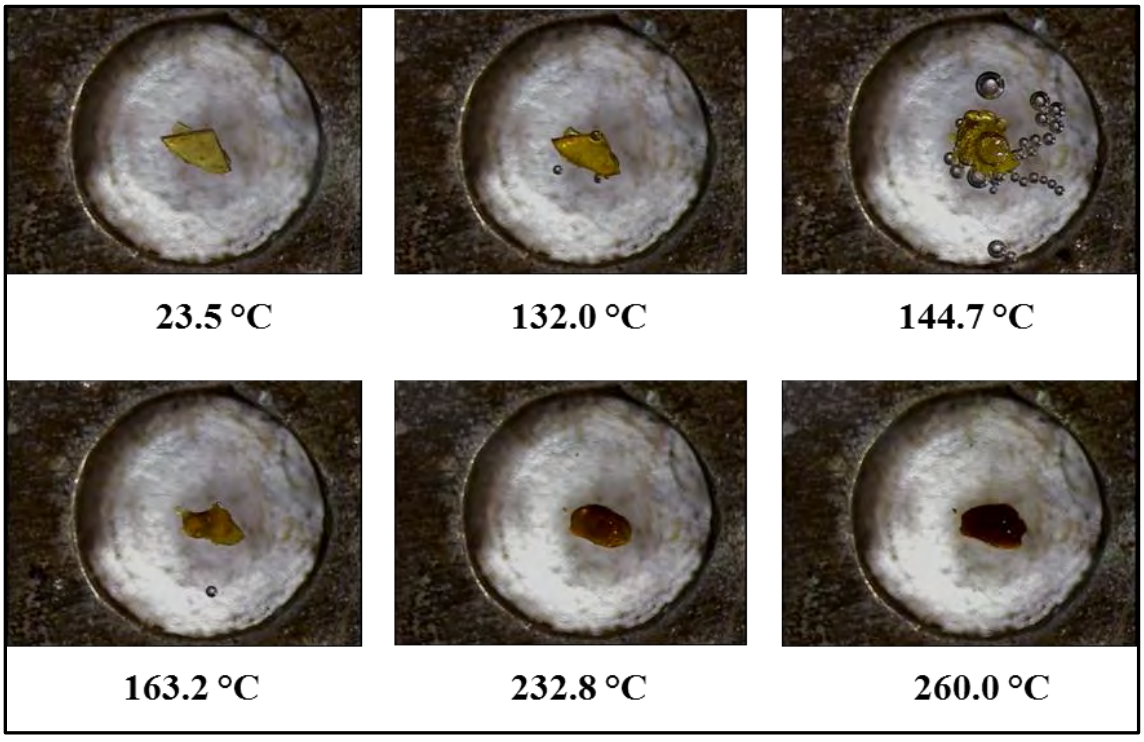

Fig. 3.1: Summarized thermomicroscopic changes of the **5c** crystal recrystallized from acetone.

Since the crystals were grown in acetone, solvation was speculated to be due to inclusion of acetone and/or water molecules in the crystal. The high desolvation temperature suggested tight

bonding associations between the **5c** molecules and solvent molecules. The desolvation onset of ~132 °C is much higher than the boiling points of both acetone (56 °C) and water (100 °C), further suggesting formation of a solvate as opposed to a simple clathrate structure.[119,120]

3.2.2 Thermogravimetric analysis

The TGA traces obtained by heating a single crystal of **5c** showed desolvation mass losses of 10.39%, 9.59% and 10.19% respectively (**Fig. 3.2**). This gives an average mass loss of **10.06 ± 0.24%** due to solvent loss. Theoretical values for percentage mass loss corresponding to various stoichiometric ratios of **5c** to water or acetone or both solvents were compared to the experimental value. It was found that the experimental value obtained strongly suggests a solvated **5c** crystal containing both water and acetone in the ratio 1:1. This solvate corresponds to a theoretical desolvation mass loss of **10.05%**.

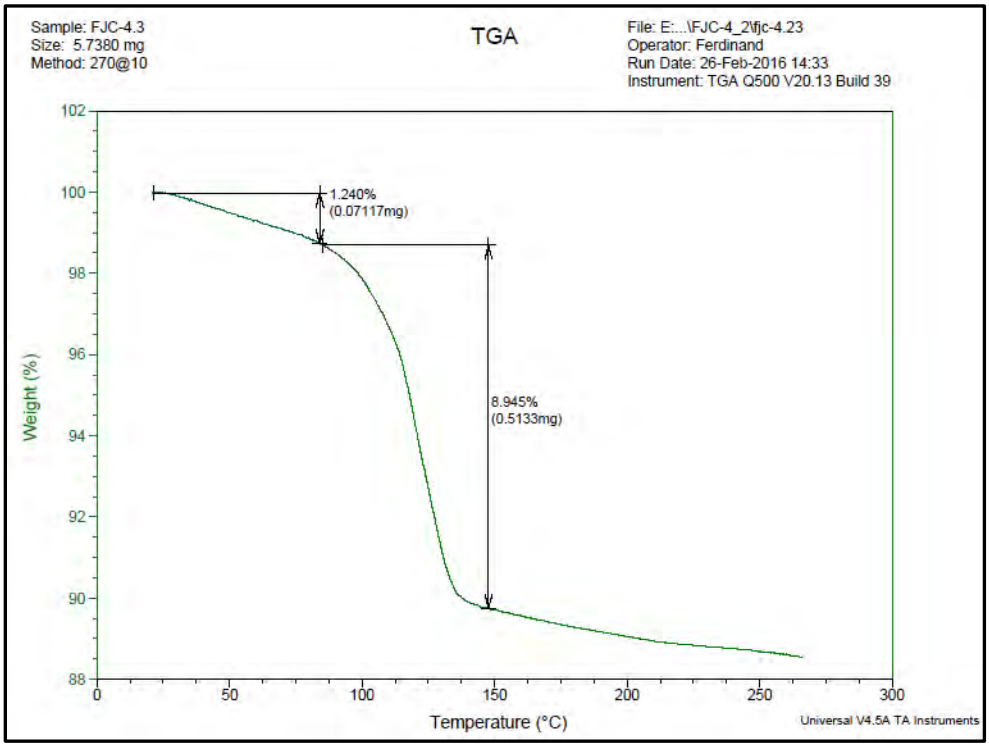

Fig. 3.2: Representative TGA trace of **5c** crystal from acetone.

It was observed from the TGA traces that loss of mass commenced much earlier than expected, and at a lower temperature than expected from thermomicroscopic data. A lower initial loss of mass was followed by a more definite desolvation phase. This could be attributed to initial loss of surface solvent, followed by loss of solvent molecules incorporated into the crystal.

3.2.3 DSC analysis

The DSC trace of **5c** crystals shows two distinct endotherms (**Fig. 3.3**).

The first, peaking at approximately 113 °C, denotes absorption of heat required for desolvation. This endotherm has an early onset of about 62.5 °C, and is complete at an approximate temperature of 150 °C. The broad nature of the endotherm, therefore, indicates desolvation occurring over a wide temperature range and requirement of significant energy input to break the solvent and **5c** molecule association. This is a further pointer of strong binding of solvent molecules in the crystal architecture.

The second endotherm, corresponding to melting of **5c**, peaks at approximately 220 °C. This is a sharp endotherm with an onset of about 212 °C and completion at ~225 °C. No energy changes associated with decomposition were observed on the DSC trace within the temperature range of analysis.

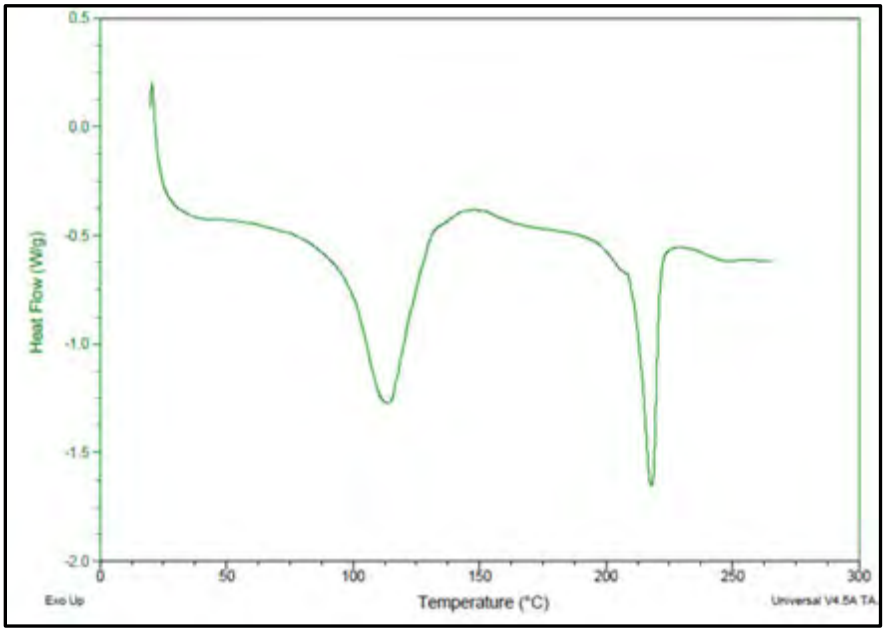

Fig. 3.3: DSC trace of **5c** crystals from acetone.

3.2.4 Single crystal XRD analysis

Crystal data, collection procedures and refinement results for the **5c** solvate crystal obtained from acetone are summarized in **Table 3.1** below.

Table 3.1: Crystal data for **5c** crystal obtained from acetone.

Parameter	**Value**
Empirical formula	$C_{25}H_{22}F_3N_5$ (unknown solvent ratio)
Formula weight (g/mol)	449.48 (+ unknown solvent weight)
Temperature (K)	173(2)
Wavelength (Å)	0.71073
Crystal system	Monoclinic
Space group	I2/a
Cell parameters (Å, °)	a=36.097(3) b=6.8165(6) c=23.851(2)
	α=90 β=117.81(2) γ=90
Cell volume ($Å^3$)	5191(1)
Crystal size (mm)	0.130 × 0.160 × 0.270
Θ min (°)	2.38
Θ max (°)	26.24
Reflections used	6986

High residual electron density, coupled with a number of unresolved electron density peaks, made it impossible to fully elucidate the solvate structure and bonding pattern. Determination of the complete asymmetric unit (ASU) from this structure was also unsuccessful.

From the partial crystal structure obtained, however, it was possible to confirm the atom connectivity expected in **5c** (ORTEP diagram **Fig. 3.4**). Presence of the planar pyridobenzimidazole core linked to the piperidine side group (chair conformer) was also confirmed. Bond angles, bond lengths and hydrogen-bonding patterns were, however, not determined from this structure. These are considered in the next section where complete refinement of the **5c** crystal structure was successful.

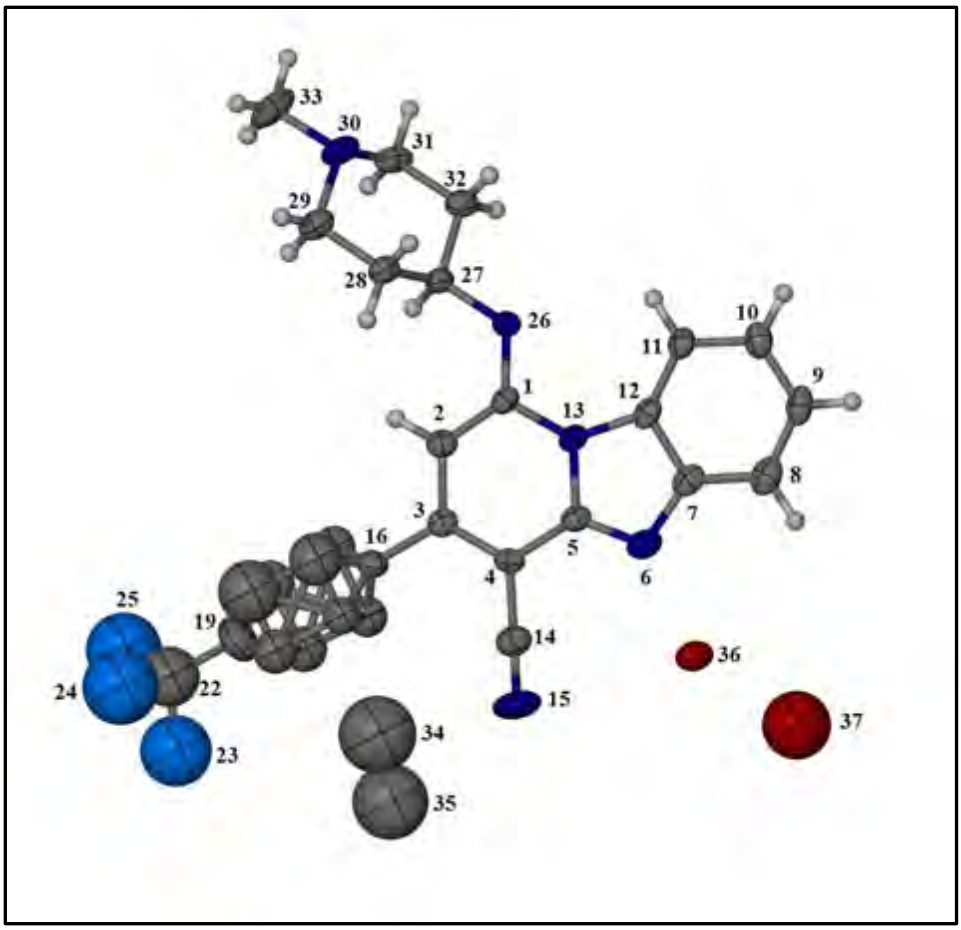

Fig. 3.4: Incompletely refined ASU of **5c** solvate crystal obtained from acetone. Note the multiple equivalent positions of atoms C17-C18 and C20-C21. Hydrogen atoms are also absent on C17-C18 and C20-C21 as well as the bridge nitrogen atom N26. Extra electron densities labeled as atoms 34-37 are possibly from solvent molecules.

3.3 CONCLUSIVE ANALYSIS OF FJC-4 SINGLE CRYSTAL STRUCTURE

A follow-up attempt to solve the complete crystal structure of **5c** was done using single crystals obtained by slow evaporation of a solution of **5c** in acetonitrile. Thermal studies and XRD analysis are outlined in the following sections.

3.3.1 Thermomicroscopy

A single crystal of **5c** was studied for physical changes and desolvation on the hot-stage microscope at a temperature range of approximately 28-290 °C, as summarized in **Figure 3.5**. Initial heating produced no observable change in the crystal‟s appearance. At approximately 166 °C, apparent development of linear cracks was observed throughout the crystal body, after which desolvation commenced at about 214 °C. Loss of solvent continued until ~235 °C when all solvent was lost. As observed previously, physical crystal appearance was also drastically altered after desolvation was complete. Onset of melting was recorded at ~239 °C, and significant darkening of the crystal occurred beyond 250 °C, possibly attributable to decomposition.

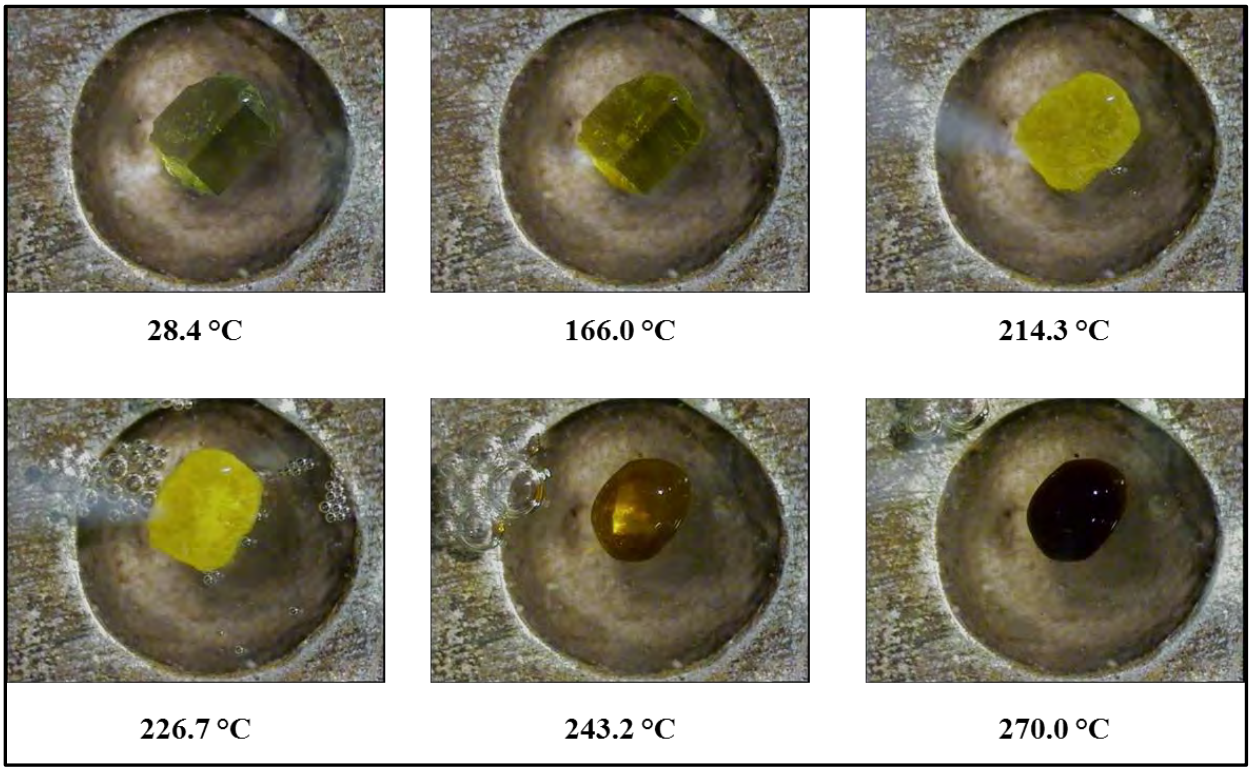

Fig. 3.5: Summarized thermomicroscopic changes of **5c** crystal obtained from acetonitrile.

The high temperature required for onset of desolvation (~214 °C) was suggestive of a tightly associated solvate between molecules of **5c** and those of the solvent. Since the crystals were obtained from slow evaporation of a **5c** solution in acetonitrile, the two likely candidates responsible for solvation were taken to be water and acetonitrile itself. These both have much lower boiling points (100 °C and 82 °C respectively) compared to the desolvation onset temperature.

3.3.2 Thermogravimetric analysis

The TGA traces of **5c** crystals presently under study showed desolvation mass losses of 1.93% and 2.03% respectively (**Fig. 3.6**). This represents an experimental mean mass loss of **1.98 ± 0.05%**. The value closely relates to the theoretical mass loss expected for a **5c**-hemihydrate (**5c**:water ratio of 1:0.5), which was calculated to be **1.97%**. This finding was a major indicator of the current crystal being a hemihydrate of **5c**.

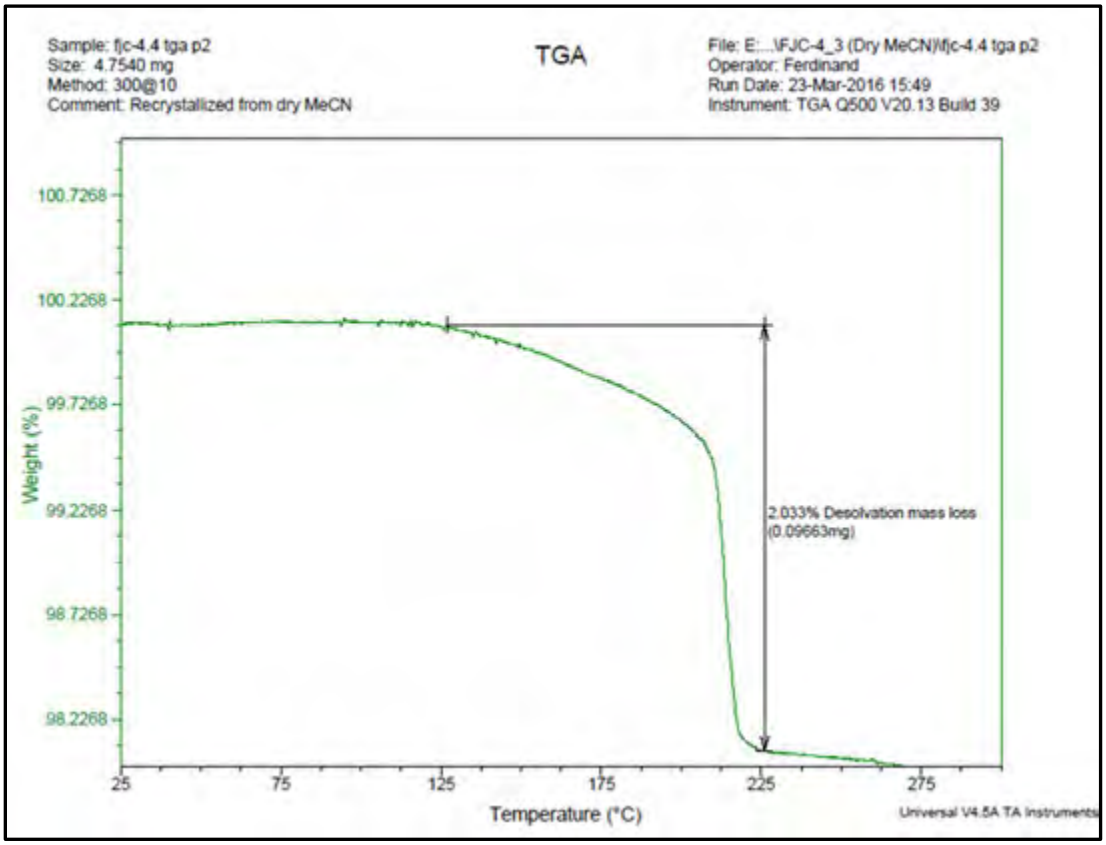

Fig. 3.6: Representative TGA trace of **5c** crystals from MeCN.

3.3.3 DSC analysis

The DSC trace of these **5c** crystals also displayed two distinct endotherms, as shown in **Fig. 3.7**.

The first of these, with onset at ~210 °C, corresponds to energy absorption in order to facilitate desolvation. This endotherm peaks at approximately 215 °C and the trace returns to the baseline at about 218 °C. In contrast to the first endotherm obtained with the previous batch of crystals, this occurs at a much higher temperature, indicating a higher energy requirement for dehydration. The current endotherm also occurs over a narrower temperature range.

The second endotherm, peaking at ~230 °C, corresponds to melting of the anhydrous crystal. This occurs over a wider range and also involves a higher energy change. No energy change characteristic of decomposition was observed in the DSC trace within the temperature range of analysis.

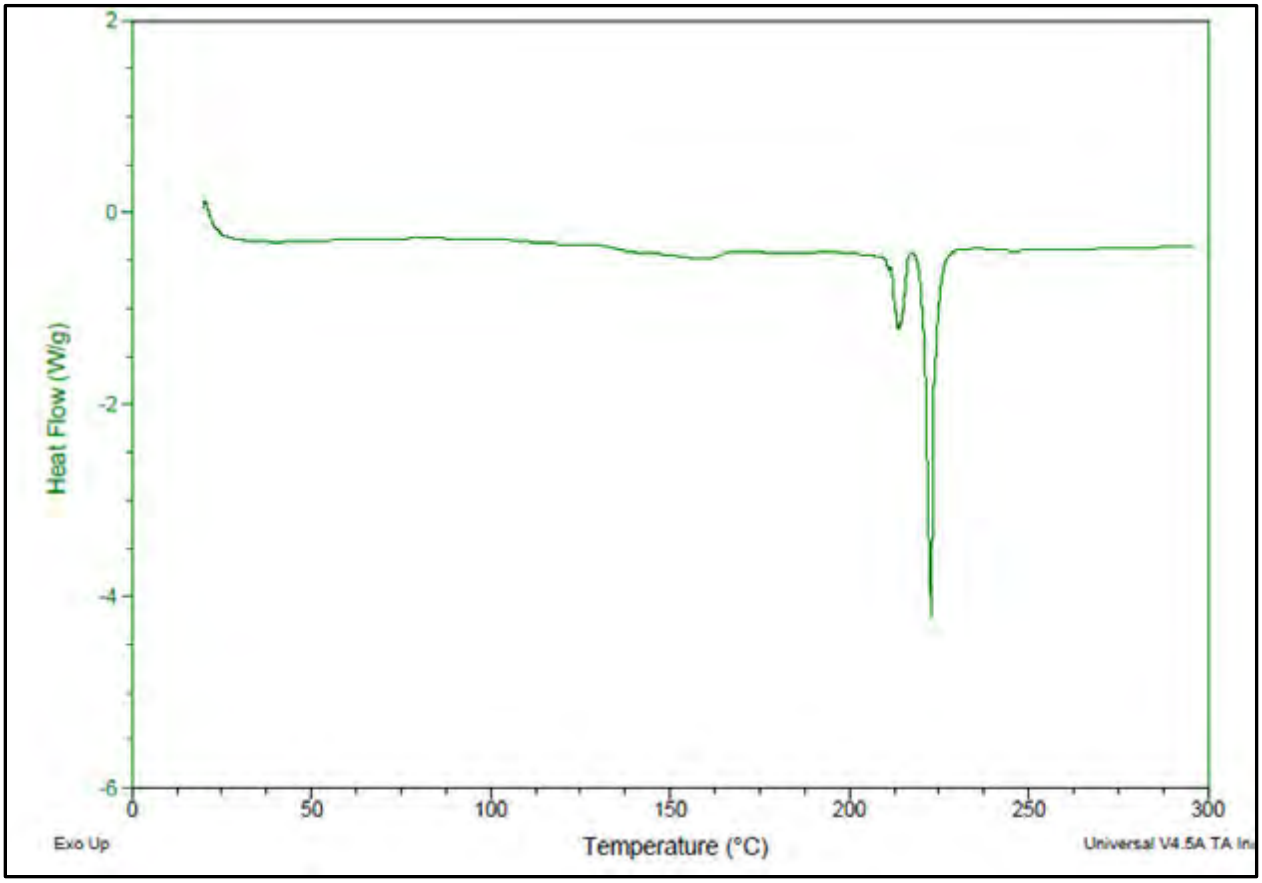

Fig. 3.7: DSC trace of **5c** crystals from MeCN.

3.3.4 Single crystal XRD analysis

Crystal data, intensity data-collection procedures and refinement results for the **5c** hemihydrate crystal are summarized in **Table 3.2** below.

Table 3.2: Crystal data and refinement results of **5c** hemihydrate form.

Parameter	**Value**
Empirical formula	$C_{25}H_{22}F_3N_5.0.5\ H_2O$
Formula weight (g/mol)	458.48
Temperature (K)	173(2)
Wavelength (Å)	0.71073
Crystal system	Monoclinic
Space group	$P2_1/c$
Cell parameters (Å,°)	a=9.6742(8) b=39.402(3) c=11.744(1)
	α=90 β=92.582(2) γ=90
Cell volume ($Å^3$)	4472.2(6)
Z	8
Crystal size (mm)	0.290 × 0.200 × 0.160
Θ range (°)	2.35-27.70
Reflections collected/unique	86427/9947
R1/wR2 for all data	0.0660/0.1175
Goodness of fit	1.027
$\Delta\rho_{min}$, $\Delta\rho_{max}$ ($eÅ^{-3}$)	-0.536, 0.779

3.3.4.1 General comments

As illustrated by the ORTEP diagram in **Fig. 3.8** below, the crystal structure is a hemihydrate (one half water molecule for each **5c** molecule). The ASU consists of two molecules of **5c** (denoted A and B) that are hydrogen bonded to one water molecule. The water molecule acts as the hydrogen-bond donor through H34A and H34B, with the piperidine ring nitrogen N30A and PBI core nitrogen N6B being the hydrogen bond acceptors via their respective lone pairs.

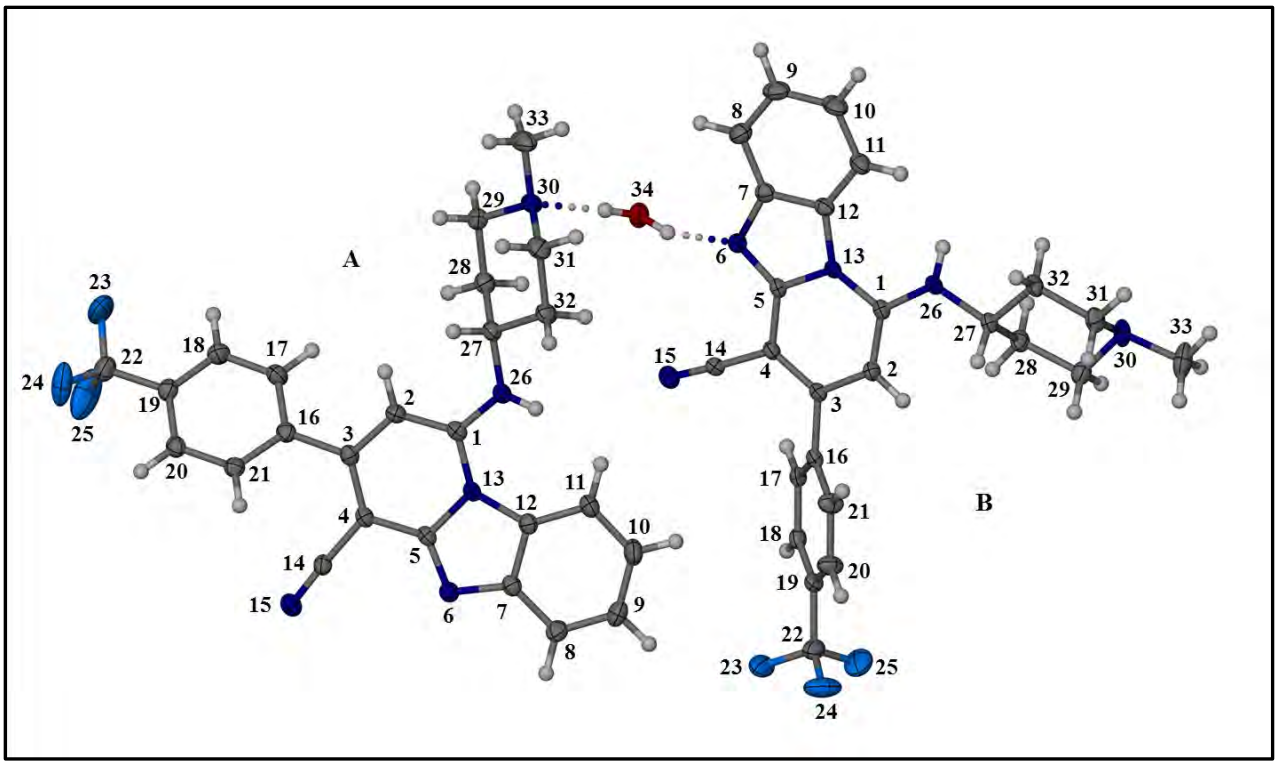

Fig. 3.8: Asymmetric unit of **5c** hemihydrate.

Both molecules of **5c** occur in their neutral state in the hemihydrate crystal.

The cyano substituent at C4 (labeled as C14-N15) is linear and coplanar to the PBI core as expected. The piperidine side group on C1 is in the chair conformation as anticipated. Substituted bonds on the piperidine ring (N26-C27 and N30-C33) both occur in the equatorial position, also in accordance with expectation. The phenyl ring substituent at C3 is non-coplanar with the PBI core.

3.3.4.2 Intra- and intermolecular geometry

The ORTEP diagram (**Fig. 3.9**) shows an ASU dimer of **5c** hemihydrate. Individual ASU fragments are labeled I and II.

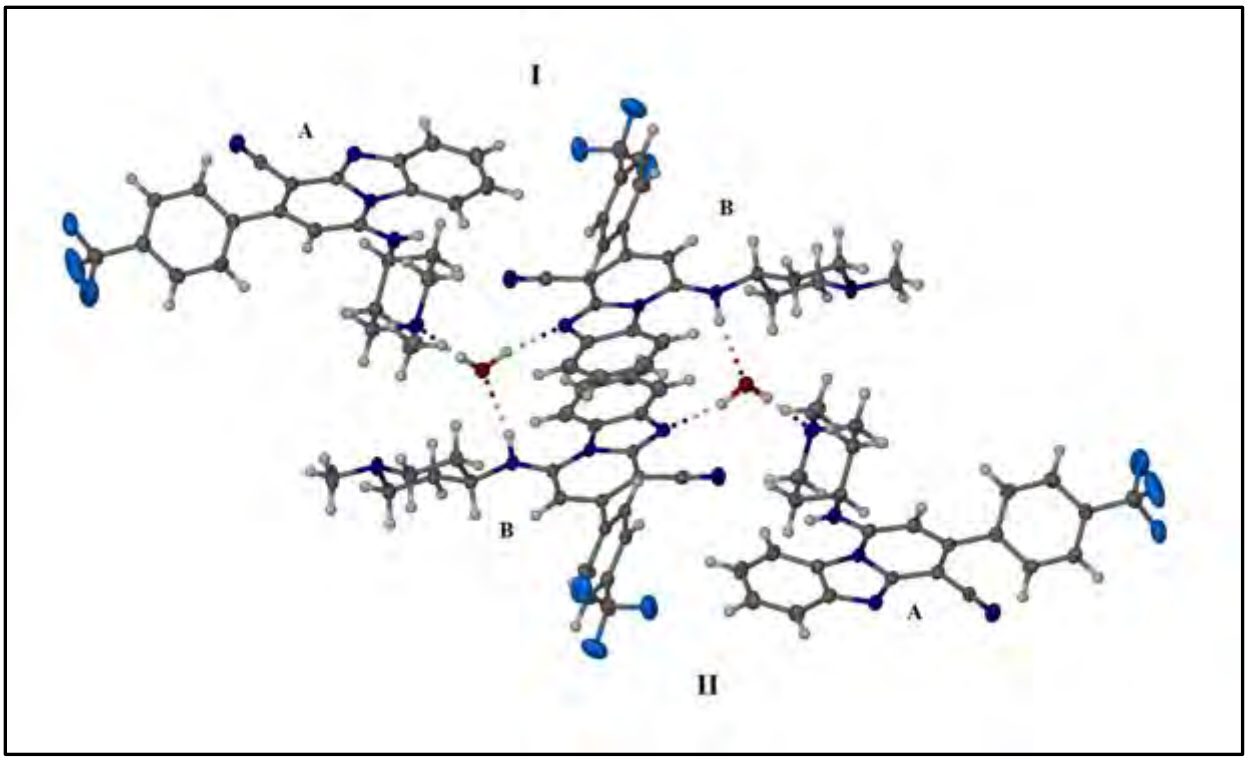

Fig. 3.9: Centrosymmetric ASU dimer of **5c** hemihydrate.

The two ASU fragments are linked by two hydrogen bonds comprising the bridge nitrogen N26B acting as donor through H26B and the oxygen of water (O34) as acceptor. This results in a centrosymmetric dimer architecture that comprises the building block of the **5c** hemihydrate crystal. It was interesting to note that the basic nitrogen N26A does not participate in hydrogen bonding either as a donor or acceptor.

The tricyclic pyridobenzimidazole (PBI) ring is planar to within a range of -0.034(1)-0.083(2) Å for the deviations of the atoms from the *least squares* plane. Considerable π-π stacking[121] is observed between individual rings of adjacent PBI systems, as summarized by the *centroid-to-centroid* distances in **Table 3.3** below.

Basing on the specific ring systems involved in π-stacking, parallel displaced and parallel staggered orientations are found to be involved in the interactions.[122,123]

These extensive π-π stacking interactions are hypothesized to account, at least partly, for the poor aqueous solubility exhibited by PBI analogues. Stacking interactions interfere with adequate solubilization in water, reducing aqueous solubility.

Table 3.3: *Centroid-to-centroid* distances of π-stacked ring systems in **5c** hemihydrate.

Ring systems	ARU	Distance (Å)
C1A,C2A,C3A,C4A,C5A,N13A and C7A,C8A,C9A, C10A, C11A,C12A	x, 3/2 - y, ½ + z	3.526(1)
C5B,C7B,C12B,N1B,N6B and similar ring	1 – x, 1 – y, 1 – z	3.476(9)
C1B,C2B,C3B,C4B,C5B,N13B and C7B,C8B,C9B,C10B,C11B,C12B	1 – x, 1 – y, 1 – z	3.789(1)
C7B,C8B,C9B,C10B,C11B,C12B and C5B,C7B,C12B,N6B,N13B	1 – x, 1 – y, 1 – z	3.601(1)

A close examination of the corresponding torsion angles in molecules A and B of the ASU shows that they adopt different values. The planar PBI core structure is found to be non-coplanar with both the piperidine ring at C1 and phenyl substituent at C3 to varying degrees between the A and B fragments in the ASU (**Table 3.4**).

Table 3.4: Torsion angles between individual ring systems in **5c** hemihydrate ASU.

Angle	Torsion angle in ASU fragment (°)	
	A	B
C2-C1-N26-C27	7.6(2)	3.4(2)
C1-N26-C27-C28	-82.4(2)	72.2(2)
C2-C3-C16-C21	37.7(2)	47.7(2)

As mentioned earlier, the basic bridge nitrogen N26A does not participate in hydrogen bonding, presumably due to unfavorable conformational properties. Strong hydrogen bonds[124] between the individual ASU fragments and water are responsible for maintaining the hemihydrate architecture, as summarized in **Table 3.5** below. Relatively weaker C-F···H bonds and intramolecular C-H···N bonds are also observed.[124-126]

Table 3.5: Hydrogen bonds for **5c** hemihydrate form (Å,°), where D = Donor and A = Acceptor

D-H···A	d(D-H)	d(H···A)	d(D···A)	<(D-H···A)
N26B-H26B···O34	0.89(2)	2.06(2)	2.896(2)	157(2)
O34-H34A···N30A	0.91(2)	2.01(2)	2.922(2)	177(3)
O34-H34B···N6B	0.92(3)	1.98(3)	2.870(2)	163(2)
C9A-H9A···F23B	0.95	2.49	3.334(2)	147
C11A-H11A···N15B	0.95	2.40	3.279(2)	154
C11B-H11B···N26B (intra)	0.95	2.59	3.081(2)	113
C20B-H20B···F25B (intra)	0.95	2.39	2.718(2)	100

d = distance (Å), < = angle (°). Symmetry codes 1 – x, 1 – y, 1 – z.

3.3.4.3 Packing characteristics

The packing diagram of **5c** hemihydrate molecules within a single unit cell is shown in **Fig. 3.10** below. Water molecules are depicted as space-filling models for clarity.

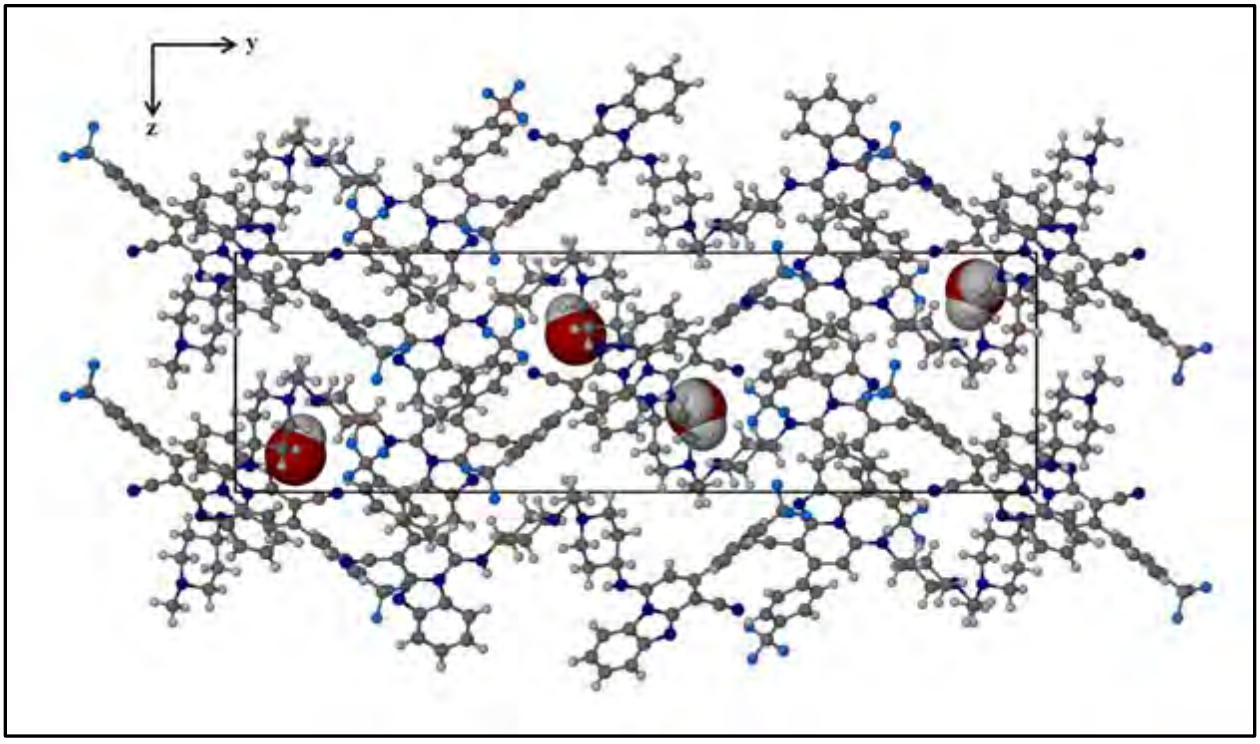

Fig. 3.10: Packing diagram of **5c** hemihydrate crystal viewed parallel to the *a*-axis.

From the packing diagram, it was observed that water molecules are held in isolated sites within the crystal, completely surrounded by molecules of **5c**. This explains the high temperature of onset of dehydration observed during thermomicroscopy studies (~214 °C). The water molecules are tightly held in place and hydrogen bonded to surrounding **5c** molecules, requiring a high amount of energy to be dislodged.

3.4 SALT SCREENING

Salts of **5c** were obtained by screening the free-base compound for salt formation with various acidic counterions. Initial screening involved small-scale trials which were then scaled up after confirmation of salt formation.[80,81]

3.4.1 Introduction

Salt formation is a well-known method employed in improving aqueous solubility of poorly soluble drugs.[66,80-83,127] This culminates in improved oral bioavailability of such molecules. Pharmaceutical salts are widely used in formulations presently in the market, to improve both solubility and stability of API molecules. Salt screening, preparation and characterization are usually combined with solubility and physical stability studies to select a suitable salt form for manufacture. The most appropriate salt form is one that presents an improved solubility profile as well as superior physical characteristics and stability in comparison to the free base/acid form of the drug.[66,80,81]

3.4.2 General procedure

Salt screening of **5c** was performed by the acid addition method at room temperature. Approximately 2-3 mg of **5c** was dissolved in dichloromethane (DCM) and 0.5-1 equivalents of acid were added with stirring. The salts were formed as DCM-insoluble precipitates which were then filtered, triturated in diethyl ether and dried.[82] The procedure was scaled up after confirmation and isolation of a salt form.

Kinetic solubility studies of salts obtained as above, along with the **5c** free base form for comparison, were then carried out.

Since emphasis was primarily upon improving solubility, physical studies of the salts were not conducted. Parameters such as water content, hygroscopicity, stress stability and photostability were not determined due to the scope of this research project.

3.4.3 Results and discussion

A total of eight acids, selected based on pharmaceutical acceptability, were used in the screening exercise for salt formation with **5c**. Salts were obtained with hydrochloric acid, sulfuric acid, hydrobromic acid, nitric acid and succinic acid. No observable salt formation was detected with acetic acid, phosphoric acid and methanesulfonic acid.

The salts, along with the free base compound, were scaled up and assessed for kinetic solubility in phosphate-buffered saline (pH 7.4) with 2% DMSO. Analysis of samples was performed by HPLC-DAD. The results are summarized in **Table 3.6** below.

Table 3.6: Kinetic solubility of **FJC-4** (**5c**) and its salts at pH 7.4.

Name	Structure	MW	Solubility (µM)
FJC-4 (Free base)	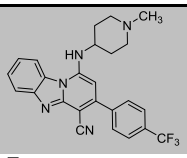	449.48	108.2
FJC-4.2HCl	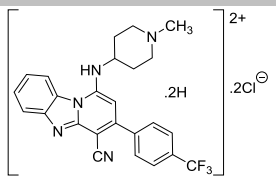	522.40	65.1
FJC-4.2HBr	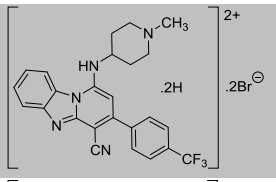	611.30	56.2
FJC-4.Sulfate	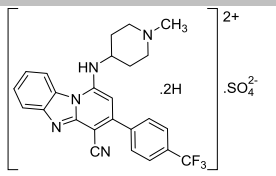	547.44	125.2
FJC-4.Nitrate	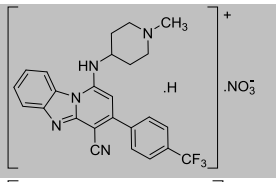	512.49	<5
FJC-4.Succinate	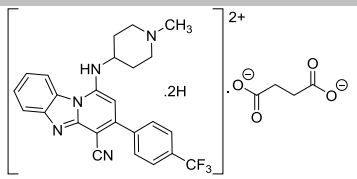	567.57	140.4

The solubility classification in this assay was as follows[83]:

- ✓ Solubility ≥ 150 μM – Highly soluble
- ✓ Solubility 50-150 μM – Moderately soluble
- ✓ Solubility 5-49 μM – Low
- ✓ Solubility <5 μM – Very low

The free base form of the compound was found to possess moderate aqueous solubility at physiological pH. Excluding the nitrate, all salts were also shown to possess solubility in the moderate range at the specified pH.

Improved aqueous solubility in comparison to the free base was observed with the sulfate and succinate salts. However, both still lay within the moderate range. Improved solubility is hypothesized to arise from better interaction between water and the ionized molecules of **5c**.

The dihydrochloride and dihydrobromide salts both exhibited reduced solubility at pH 7.4, with the nitrate showing extremely low solubility. This observation can be attributed to common ion effects in solution arising from the acidic counterions used in salt synthesis.[82,127] Also, the pH used in this analysis (7.4) may be unfavorable to solubilization of the salts.

3.5 CONCLUSIONS

The thermal properties and single crystal structure of the **5c** hemihydrate crystal were determined. The crystal structure enabled molecular conformational characteristics of the compound to be ascertained, especially torsion angles, π-π stacking interactions and hydrogen bonding.

Salt screening of **5c** against eight potential acidic salt formers yielded five salts, two of which displayed a superior kinetic solubility profile than the free base at physiological pH.

REFERENCES

117. Santos, O.; Freitas, J.; Cazedey, E. et al. Structure, solubility and stability of Orbifloxacin crystal forms: Hemihydrate versus anhydrate. *Molecules*, **2016**, *21*, 328-347.

118. El-Gizawy, S.; Osman, M.; Arafa, M. et al. Aerosil as a novel co-crystal co-former for improving the dissolution rate of hydrochlorothiazide. *Int. J. Pharm.*, **2015**, *478*, 773-778.

119. Martin, A. A simplified van der Waals-Platteeuw model of clathrate hydrates with multiple occupancy of cavities. *J. Phys. Chem. B*, **2010**, *114*, 9602-9607.

120. Skieneh, J.; Najafabadi, B. K.; Horne, S. et al. crystallization of Esomeprazole Magnesium water/butanol solvate. *Molecules*, **2016**, *21*, 544-554.

121. McGaughey, G.; Gagne, M.; Rappe, A. π-Stacking interactions. *J. Biol. Chem.*, **1998**, *273*, 15458-15463.

122. Gazit, E. A possible role for π-stacking in the self-assembly of amyloid fibrils. *FASEB J.*, **2002**, *16*, 77-83.

123. Zhang, Y.; Liang, H. Synthesis and structural characterization of the sodium salt of a new sulfonate-containing water-soluble *N*-donor ligand – Self-assembly in the solid state by π-π stacking interactions. *Molecules*, **2006**, *11*, 163-168.

124. Jeffrey, G. A. and Saenger, W. Hydrogen bonding in biological structures. Springer-Verlag (Berlin), **1991**, 18-20.

125. Perrin, C.; Nielson, J. "Strong" hydrogen bonds in chemistry and biology. *Annu. Rev. Phys. Chem.*, **1997**, *48*, 511-544.

126. Sarkhel, S.; Desiraju, G. N-H···O, O-H···O and C-H···O hydrogen bonds in protein-ligand complexes: Strong and weak interactions in molecular recognition. *Proteins*, **2003**, *54*, 247-259.

127. Elder, D.; Holm, R.; De Diego, H. Use of pharmaceutical salts and co-crystals to address the issue of poor solubility. *Int. J. Pharm.*, **2013**, *453*, 88-100.

CHAPTER 4: SUMMARY AND FUTURE PROSPECTS

4.1 General Summary and Conclusions

Pyrido[1,2-*a*]benzimidazole analogues with cyclic and functionalized amine side chain substituents were synthesized. Compounds bearing left-hand side substitutions with lipophilic, electron-withdrawing chloro groups were also synthesized. Established organic synthetic routes were employed to achieve the above. All compounds synthesized were characterized by ^{1}H-NMR, ^{13}C-NMR and LC-MS as well as melting point determination.

The *in vitro* antiplasmodial and beta-hematin inhibition activities as well as cytotoxicity and microsomal metabolic stability of the analogues were determined. Apparent solubility of all the compounds was determined by the turbidimetric solubility assay. Salt screening and subsequent kinetic solubility studies were also carried out on one of the analogues.

From the *in vitro* activity determinations, the following conclusions were drawn:

- ✓ Analogues containing an aminopiperidine substituent showed the most potent antiplasmodial and beta-hematin inhibition activity.
- ✓ Replacement of the amine linker with an ether linker between the PBI core and piperidine ring maintained activity.
- ✓ Compounds containing aminopyrrolidine and piperazine substituents showed moderate antiplasmodial and beta-hematin inhibition activity.
- ✓ Inclusion of polar functions on the amine side group was detrimental to both antiplasmodial and beta-hematin inhibition potency.
- ✓ Extension of the chain linking the PBI core to the amine side group also led to reduced activity.
- ✓ Left-hand side dichloro substitution resulted in tremendous improvement in both antiplasmodial and beta-hematin inhibition activity, as well as microsomal metabolic stability. The substituted compounds were, however, more cytotoxic.
- ✓ Generally, analogues with potent beta-hematin inhibition activity also showed good antiplasmodial activity. The two potencies were, however, not directly related.
- ✓ All the compounds selected for gametocidal and liver stage activity testing were found to be moderately active in the two assays.

From the solubility studies carried out, it was concluded that:

- ✓ All but two of the analogues displayed low to moderate solubility in the turbidimetric assay.
- ✓ Aminopiperidine- and aminopyrrolidine-substituted compounds showed the most significant improvement in solubility compared to the lead compound **4h** from previous study.
- ✓ Presence of highly polar functions on the amine side group led to reduced solubility.
- ✓ Left-hand side dichloro substitution also reduced apparent solubility.
- ✓ In the salt screening exercise, five salts of **5c** were obtained, two of which displayed improved solubility over the free base as determined by the kinetic solubility assay.

4.2 Future Outlook and Recommendations

Further attempts to improve the aqueous solubility of PBIs, especially by increasing dihedral angles as well as co-crystal formation and cyclodextrin inclusion complexation should be prioritized. These approaches were not employed in this research project. Exploration of the SAR around the PBI core to eliminate cytotoxicity arising from left-hand side dichloro substitution should also be considered. The analogue **FJC-25** (**5w**) would provide an appropriate lead for such studies. Additionally, it may be useful to test the frontrunner compounds from this research project for activity against chloroquine-resistant strains of *P. falciparum* to investigate their applicability in that area. Selected frontrunner compounds from the current study (and their salts) may need to be studied for *in vivo* PK and efficacy in the *P. berghei* mouse model. This is based on the moderate activity displayed by analogue **5c** (83% reduction in parasitemia, 16 MSD at 4 × 50 mg/kg po dose).

The single crystal XRD structure of **5c** hemihydrate provided useful information on the planar nature of the tricyclic PBI core, and the resulting π-stacking interactions. This data can be used in future design of PBI analogues with substitution patterns aimed primarily at reducing planarity of the core as a means to achieving improved solubility (**Fig. 4.1**). Reduced planarity of the PBI core would reduce stacking interactions, resulting in improved solubility. This substituent design

strategy can be employed in addition to other strategies already attempted to improve solubility while maintaining or improving activity and metabolic stability.

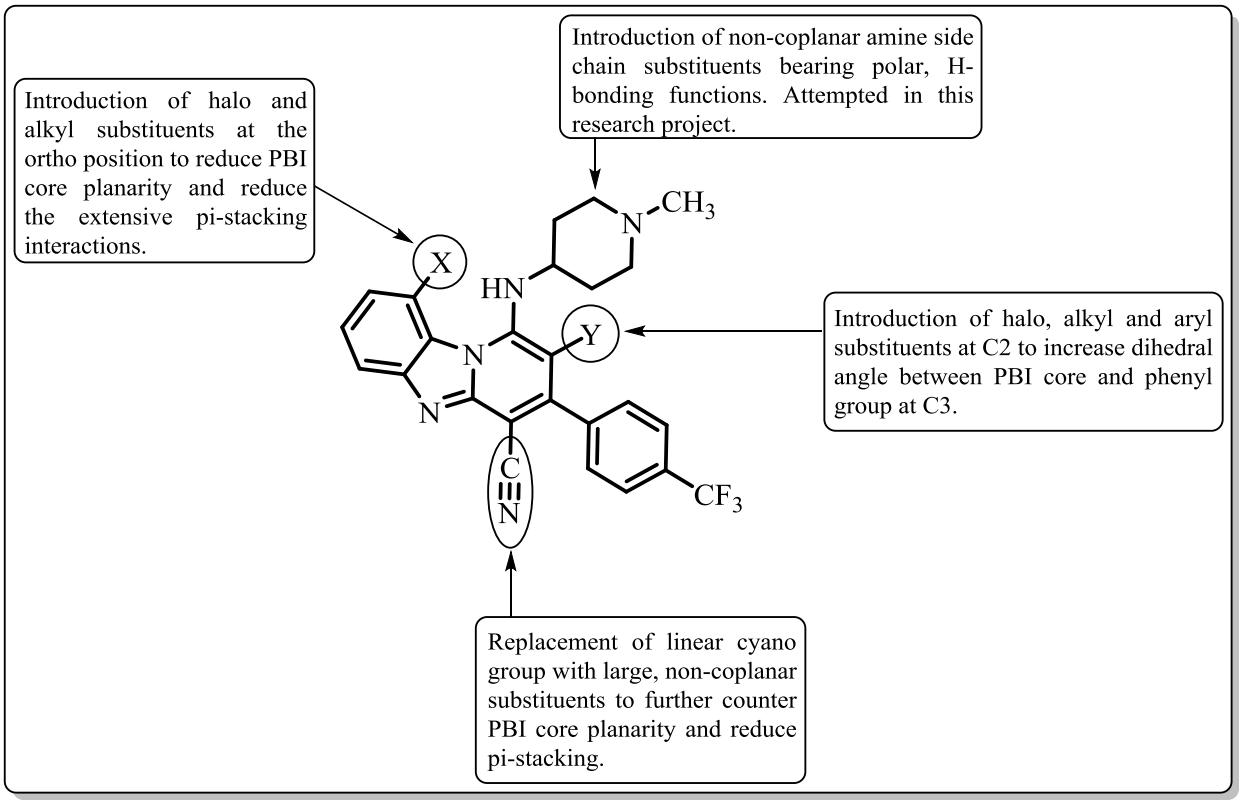

Fig. 4.1: Suggested substitutions around the **5c** molecule aimed at reducing planarity and subsequent π-stacking interactions in PBIs.

CHAPTER 5: EXPERIMENTAL

5.1 Materials and equipment.

All commercially available chemicals were purchased from Sigma-Aldrich or Combi-Blocks and were of analytical quality. These were used without further purification. Reactions were monitored by thin layer chromatography (TLC) using Fluka or Merck F254 aluminium-backed pre-coated silica gel plates and were visualized under UV light at 254 or 366 nm. Silica gel column chromatography was performed using Merck kieselgel by gravity column chromatography. Melting points were determined using a Reichert-Jung Thermovar hot-stage microscope or Stuart SMP-40 automatic melting point machine and are uncorrected.

All compounds synthesized were characterized by ^{1}H NMR, ^{13}C NMR, COSY and LC-MS.

^{1}H NMR spectra were recorded on a Varian Mercury (300 MHz), a Bruker Ultrashield-Plus (400 MHz) spectrometer or a Bruker (600 MHz) with Me_4Si as internal standard. ^{13}C NMR spectra were recorded on the same instruments at 101 MHz or 151 MHz with Me_4Si as internal standard. NMR samples were dissolved in deuterated dimethylsulfoxide (DMSO-d_6), chloroform ($CDCl_3$) or Methanol (MeOD). Chemical shifts (δ) are reported in parts per million (ppm) to 2 decimal places downfield from TMS as the internal standard. Coupling constants (*J*) are reported in Hertz (Hz) to one decimal place. Abbreviations used in assigning ^{1}H-NMR signals are: d (doublet), dd (doublet of doublets), ddd (doublet of doublet of doublets), m (multiplet), q (quartet), s (singlet), t (triplet) or td (triplet of doublets). Axial and equatorial protons on chair-conformed amine substituents are labeled as “a” and “e” respectively.

LC-MS data was obtained on an Agilent LC-MS system with the following chromatographic conditions: an X-bridge C18 2.5 µm column, 3 mm diameter × 50 mm in length and injection volume 2 µL. Mobile phase: 10 mM NH_4OAc buffer (0.4% Acetic acid) in water (Solvent A) and 10 mM NH_4OAc (0.4% Acetic acid), 90% MeOH in water (Solvent B). Flow rate 0.9 ml/min for 7 min; 90% A +10% B run for 2 min, then 5% A + 95% B run from the 3rd to 5th min, 5% A + 95% B run again from the 5th min for one and a half mins then finally reverted to 90% A + 10% B up to the end of the 7th minute. Purity of the compounds was determined using the Agilent infinity diode array detector (DAD) with an absorption wavelength range of 210-640 nm. Column temperature was maintained at 40 ºC. MS spectra were obtained both by electron spray

ionization (ESI), spray chamber conditions: gas temperature 310 ºC, vaporizer 210 ºC; and atmospheric pressure chemical ionization (APCI).

Thermomicroscopy was performed on a Linkam THMS600 hot stage, Linkam TP92 temperature control unit and Nikon SMZ-10 stereoscopic microscope. Thermogravimetric analysis (TGA) was carried out over an appropriately chosen temperature range using the TA Q500 thermogravimetric analyzer. A sample ranging in weight between 2-5 mg was weighed on a clean alumina crucible for TGA analysis. Data obtained was analyzed using the program TA Instruments Universal Analysis version 4.7A.

Differential scanning calorimetry (DSC) was done using the TA Q200 instrument. A sample was taken from under the mother liquor, rapidly dried on filter paper and weighed on the Platinum pan. The weighed sample was then heated at constant rate. Data obtained was analyzed by TA Universal Analysis as in TGA. The result is a heat flux versus temperature curve, with endothermic or exothermic changes represented as negative or positive peaks respectively.

The Bruker KAPPA APEX II Duo four-circle x-ray diffractometer, using graphite-monochromated Mo-Kα radiation (λ=0.71073 Å), was used for determination of unit cell dimensions and single crystal intensity data collection. Unit cells of the solvated crystals were determined at low temperature (100 ± 2 K) after their removal form mother liquor. Data collections were carried out in the same temperature range using Cryostream coolers (Oxford Cryosystems UK). Single crystals were mounted on a nylon loop and coated with paratone oil to prevent solvent loss.

For the intensity data collected above, space group symmetry was determined by examining systematic absences using the program XPREP.[128] Structure solution and refinement was done by direct methods using *SHELXL-2000* and *SHELXS* which employ full-matrix least-squares minimization of the sum of the squares of the differences between observed and calculated intensities.[129] All structures were refined by the full-matrix least-squares techniques using the programs above and the graphic interface program X-Seed.[130]

Structural visualization, graphical representation and determination of structural parameters were performed using the programs POV-Ray and PLATON. POV-Ray was used to generate ORTEP (Oak Ridge Thermal Ellipsoid Plot) diagrams of molecules with atoms represented as ellipsoids

of 50% probability.[131] Bond lengths, geometry, π-stacking and hydrogen bonding interactions were calculated using PLATON 10.[132]

5.2 Synthesis and characterization.

5.2.1 General procedures and characterization of intermediate compounds

1-hydroxy-3-(4-(trifluoromethyl)phenyl)benzo[4,5]imidazo[1,2-*a*]pyridine-4-carbonitrile(3)

A mixture of 2-benzimidazole acetonitrile (563 mg, 3.58 mmol), ethyl (4-trifluoromethylbenzoyl) acetate (1g, 4.30 mmol) and NH_4OAc (552 mg, 7.16 mmol) was triturated at 150 ºC for 1h and then allowed to cool to 90 ºC. MeCN (10 ml) was added and the mixture was stirred for 15 min, allowed to cool to r.t. and cooled on ice. The cold mixture was filtered and the residue washed with cold MeCN (4 × 10 ml) then dried in vacuo.

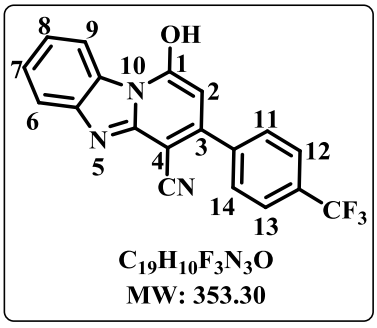

$C_{19}H_{10}F_3N_3O$
MW: 353.30

Tan silvery powder (905 mg, 72%), M.P. >350 ºC; R_f 0.4 (40% EtOAc/Hex); ^{1}H NMR (400 MHz, DMSO) δ 13.84 (s, 1H, O*H*), 8.63 (d, *J* = 8.1 Hz, 1H, ArH^9), 7.93 (d, *J* = 8.3 Hz, 2H, ArH^{12,13}), 7.88 (d, *J* = 8.3 Hz, 2H, ArH^{11,14}), 7.62 – 7.57 (m, 2H, ArH^{6,7}), 7.43 (t, *J* = 8.4 Hz, 1H, ArH^8), 6.12 (s, 1H, H^2); ^{13}C NMR (101 MHz, DMSO) δ 158.6, 151.5, 147.9, 141.5, 132.4, 130.4, 130.1, 129.7, 128.1, 127.4, 126.1, 126.0, 125.9, 123.2, 117.0, 116.7, 112.1, 105.3, 68.5; MS: *m/z* 354.1 $[M+H]^+$; Purity 99% by LC (t_R 4.58 min).

1-chloro-3-(4-(trifluoromethyl)phenyl)benzo[4,5]imidazo[1,2-*a*]pyridine-4-carbonitrile (4).

A mixture of compound **3** (760 mg, 2.15 mmol) and $POCl_3$ (4 ml, 43.02 mmol) was heated to reflux at 130 ºC for 2h. Excess $POCl_3$ was removed under reduced pressure and 20 ml ice-cold water was added to the mixture with stirring to yield a precipitate. The mixture was neutralized with saturated $NaHCO_3$ and filtered. The resulting solid was washed with ice-cold water (4 × 15 ml) and dried in vacuo.

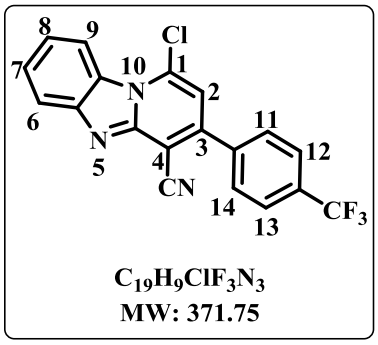

$C_{19}H_9ClF_3N_3$
MW: 371.75

Yellow solid (795 mg, 99%), M.P. 274-276 ºC; R_f 0.3 (20% EtOAc/Hex); ^{1}H NMR (400 MHz, DMSO) δ 8.69 (d, *J* = 8.5 Hz, 1H, ArH^9), 8.07 – 7.99 (m, 5H, ArH^{6,11,12,13,14}), 7.70 (t, *J* = 7.3 Hz, 1H, ArH^7), 7.59 (s, 1H, H^2), 7.54 (t, *J* = 7.4 Hz, 1H, ArH^8); ^{13}C NMR (101 MHz, DMSO) δ 148.3, 147.8, 145.0, 139.5, 135.2, 130.4, 129.8, 129.7, 129.6, 129.5, 127.6, 126.4, 126.3, 123.1, 120.3, 116.3, 115.4, 112.9, 97.6; MS *m/z* 372.0 $[M + H]^+$; Purity 99% by LC (t_R 4.62 min).

2-(5,7-dichloro-1H-benzo[d]imidazol-2-yl)acetonitrile (1a)

A mixture of 3, 5-dichlorobenzene-1, 2-diamine (870 mg, 4.91 mmol) and ethyl cyanoacetate (1,667 mg, 14.73 mmol) in DMF (5 ml) was heated at 160 ºC under reflux for 24 hr. The reaction mixture was then diluted with ethyl acetate (30 ml) and washed with distilled water (5 × 150 ml). The organic layer was dried over $MgSO_4$, filtered and concentrated. The resulting residue was purified by column chromatography.

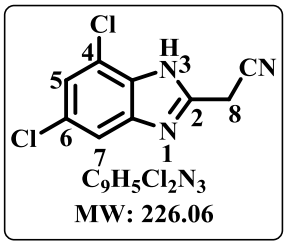

$C_9H_5Cl_2N_3$
MW: 226.06

Light brown solid (1,032 mg, 74%), M.P 239-240 ºC; R_f 0.3 (40% EtOAc/Hex); ^{1}H NMR (300 MHz, DMSO) δ 13.17 (s, 1H, N*H*), 7.63 (s, 1H, H^5), 7.39 (d, *J* = 1.8 Hz, 1H, H^7), 4.44 (s, 2H, H^8); ^{13}C NMR (101 MHz, DMSO) δ 147.9, 147.8, 139.0, 133.6, 127.2, 122.1, 116.6, 112.9, 18.9; MS *m/z* 226.0, 227.9, 229.0; Purity 93% by LC (t_R 3.24 min).

7,9-dichloro-1-hydroxy-3-(4-(trifluoromethyl)phenyl)benzo[4,5]imidazo[1,2-*a*]pyridine-4-carbonitrile (3a)

A mixture of compound **1a** (1,075 mg, 4.75 mmol), ethyl (4-trifluoromethylbenzoyl) acetate (1,484 mg, 5.7 mmol) and NH_4OAc (733 mg, 9.5 mmol) was triturated at 150 ºC for 1 hr and then allowed to cool to 90 ºC. MeCN (10 ml) was added and the mixture was stirred for 15 min, allowed to cool to r.t. and cooled on ice. The cold mixture was filtered and the residue washed with cold MeCN (4 × 10 ml) then dried in vacuo.

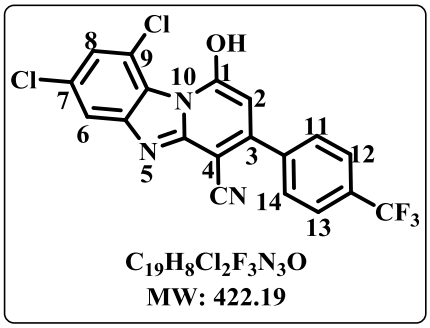

Green-yellow solid (983 mg, 49%), M.P 386-388 ºC; R_f 0.2 (70% EtOAc/Hex); ^{1}H NMR (300 MHz, DMSO) δ 8.52 (d, *J* = 2.0 Hz, 1H, H^8), 7.90 (d, *J* = 8.3 Hz, 2H, $H^{12,13}$), 7.83 (d, *J* = 8.2 Hz, 2H, $H^{11,14}$), 7.66 (d, *J* = 2.0 Hz, 1H, H^6), 5.90 (s, 1H, H^2); ^{13}C NMR (101 MHz, DMSO) δ 159.1, 152.3, 142.4, 130.8, 130.1, 129.68, 125.9, 125.8, 125.4, 125.3, 125.2, 125.0, 124.9, 123.2, 118.6, 118.0, 114.7, 102.4, 70.6; MS *m/z* 420.0, 422.0, 424.0; Purity >98% by LC (t_R 4.67 min).

1,7,9-trichloro-3-(4-(trifluoromethyl)phenyl)benzo[4,5]imidazo[1,2-*a*]pyridine-4-carbonitrile (4a)

A mixture of compound **3a** (989 mg, 2.34 mmol) and $POCl_3$ (4 ml, 46.8 mmol) was heated to reflux at 130 ºC for 2h. Excess $POCl_3$ was removed under reduced pressure and 20 ml ice-cold water was added to the mixture with stirring to yield a precipitate. The mixture was neutralized with saturated $NaHCO_3$ and filtered. The resulting solid was washed with ice-cold water (4 × 15 ml) and dried in vacuo.

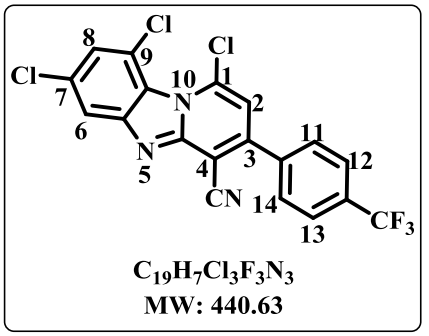

Green-yellow solid (983 mg, 95%), M.P 266-268 °C; Rf 0.5 (20% EtOAc/Hex); ^{1}H NMR (400 MHz, DMSO) δ 8.69 (s, 1H, H^8), 8.05 (d, *J* = 8.4 Hz, 2H, $H^{12,13,}$), 8.01 (d, *J* = 8.5 Hz, 2H, $H^{11,14}$), 7.91 (s, 1H, H^6), 7.66 (s, 1H, H^2); ^{13}C NMR (101 MHz, DMSO) δ 149.5, 149.0, 141.2, 139.2, 135.3, 131.4, 131.1, 130.9, 130.3, 129.6, 129.4, 127.1, 126.4, 126.3, 124.9, 115.1, 114.8, 114.2, 98.4; MS *m/z* 441.9 $[M + H]^+$; Purity >98% by LC (t_R 4.89 min).

2-(5,6-dichloro-1H-benzo[d]imidazol-2-yl)acetonitrile (1b)

A mixture of 4, 5-dichloro-o-phenylenediamine (835 mg, 4.71 mmol) and ethyl cyanoacetate (1,599 mg, 14.14 mmol) in DMF (5 ml) was heated at 150 ºC under reflux for 12 hr. The reaction mixture was then diluted with ethyl acetate (30 ml) and washed with distilled water (5 × 150 ml). The organic layer was dried over $MgSO_4$, filtered and concentrated. The resulting residue was purified by column chromatography.

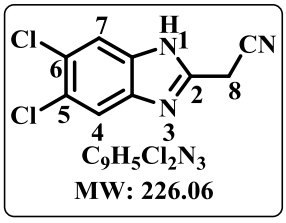

Brown powder (610 mg, 57%), M.P >300 ºC; R_f 0.2 (50% EtOAc/Hex); ^{1}H NMR (300 MHz, DMSO) δ 12.91 (s, 1H, N*H*), 7.87 (s, 2H, $H^{4,7}$), 4.43 (s, 2H, H^8); ^{13}C NMR (101 MHz, DMSO) δ 148.4, 145.2, 143.4, 120.4, 116.7, 116.0, 113.5, 110.2, 18.9; MS *m/z* 224.0, 226.0, 227.0; Purity 93% by LC (t_R 3.15 min).

7,8-dichloro-1-hydroxy-3-(4-(trifluoromethyl)phenyl)benzo[4,5]imidazo[1,2-*a*]pyridine-4-carbonitrile (3b)

A mixture of compound **1b** (578 mg, 2.56 mmol), ethyl (4-trifluoromethylbenzoyl) acetate (798 mg, 3.07 mmol) and NH_4OAc (394 mg, 5.11 mmol) was triturated at 150 ºC for 4 hours and then allowed to cool to 90 ºC. MeCN (10 ml) was added and the mixture was stirred for 15 min, allowed to cool to r.t. and cooled on ice. The cold mixture was filtered and the residue washed with cold MeCN (4 × 10 ml) then dried in vacuo.

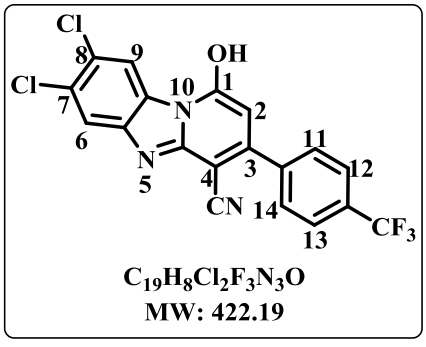

Grey powder (621 mg, 57%), M.P >270 ºC; R_f 0.4 (50% EtOAc/Hex); ^{1}H NMR (300 MHz, DMSO) δ 8.65 (s, 1H, H^9), 7.85 (q, *J* = 8.3 Hz, 4H, $H^{11,12,13,14}$), 7.75 (s, 1H, H^6), 5.73 (s, 1H, H^2); ^{13}C NMR (101 MHz, DMSO) δ 159.6, 153.3, 151.9, 143.0, 141.7, 129.8, 129.6, 129.4, 127.5, 126.0, 125.8, 125.7, 123.3, 121.4, 119.1, 116.7, 116.2, 100.2, 70.8; MS *m/z* 420.0, 422.0 [M^+], 423.9; Purity >98% by LC (t_R 4.87 min).

1,7,8-trichloro-3-(4-(trifluoromethyl)phenyl)benzo[4,5]imidazo[1,2-*a*]pyridine-4-carbonitrile (4b)

A mixture of compound **3b** (621 mg, 1.47 mmol) and $POCl_3$ (3 ml, 29.40 mmol) was heated to reflux at 130 ºC for 4 hr. Excess $POCl_3$ was removed under reduced pressure and 20 ml ice-cold water was added to the mixture with stirring to yield a precipitate. The mixture was neutralized with saturated $NaHCO_3$ and filtered. The resulting solid was washed with ice-cold water (4 × 15 ml) and dried in vacuo.

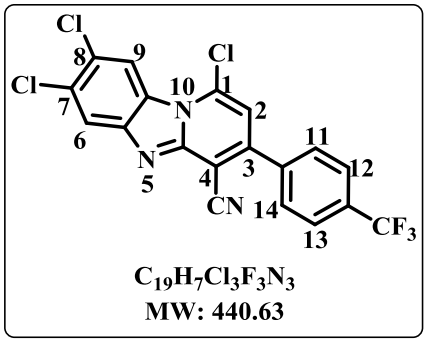

Yellow solid (520 mg, 80%), M.P 237-238 ºC; R_f 0.5 (20% EtOAc/Hex); ^{1}H NMR (300 MHz, DMSO) δ 8.83 (s, 1H, H^9), 8.32 (s, 1H, H^6), 8.03 (s, 4H, $H^{11,12,13,14}$), 7.69 (s, 1H, H^2); ^{13}C NMR (101 MHz, DMSO) δ 149.5, 149.3, 144.3, 139.1, 135.4, 130.6, 130.4, 130.3, 129.0, 126.4, 126.3, 125.7, 125.2, 121.2, 121.0, 117.5, 115.0, 113.7, 97.7; MS *m/z* 441.0, 442.0; Purity >98% by LC (t_R 5.13 min).

2-(7-chloro-1H-benzo[d]imidazol-2-yl)acetonitrile (1c)

A mixture of 3-chlorobenzene-1, 2-diamine (803 mg, 5.63 mmol) and ethyl cyanoacetate (1,909 mg, 16.89 mmol) in DMF (5 ml) was heated at 150 ºC under reflux for 3 hr. The reaction mixture was then diluted with ethyl acetate (30 ml) and washed with distilled water (5 × 150 ml). The organic layer was dried over $MgSO_4$, filtered and concentrated. The resulting residue was purified by column chromatography.

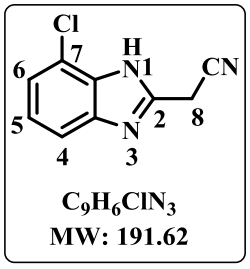

Brown powder (670 mg, 62%), M.P. 233-235 °C; R_f 0.3 (50% EtOAc/Hex); ^{1}H NMR (300 MHz, DMSO) δ 12.94 (s, 1H, N*H*), 7.48 (d, *J* = 7.2 Hz, 1H,H^4), 7.22 (d, *J* = 7.8 Hz, 1H, H^6), 7.12 (t, *J* = 7.9 Hz, 1H, H^5), 4.44 (s, 2H, H^8); ^{13}C NMR (101 MHz, DMSO) δ 162.2, 127.3, 125.8, 123.9, 121.9, 116.4, 111.1, 26.6, 18.8; MS *m/z* 192.0 $[M+H]^+$; Purity >98% by LC (t_R 3.18 min).

9-chloro-1-hydroxy-3-(4-(trifluoromethyl)phenyl)benzo[4,5]imidazo[1,2-*a*]pyridine-4-carbonitrile (3c)

A mixture of compound **1c** (655 mg, 3.42 mmol), ethyl (4-trifluoromethylbenzoyl) acetate (1141 mg, 4.10 mmol) and NH_4OAc (527 mg, 6.84 mmol) was triturated at 150 ºC for 3 hours and then allowed to cool to 90 ºC. MeCN (10 ml) was added and the mixture was stirred for 15 min, allowed to cool to r.t. and cooled on ice. The cold mixture was filtered and the residue washed with cold MeCN (4 × 10 ml) then dried in vacuo.

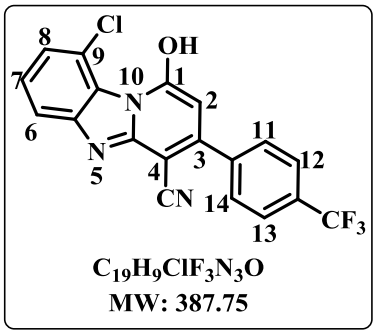

Grey powder (1096 mg, 83%), M.P. 241-244 °C; R_f 0.3 (30% EtOAc/Hex); ^{1}H NMR (300 MHz, DMSO) δ 8.61 (d, *J* = 7.2 Hz, 1H, H^8), 7.93 (d, *J* = 8.2 Hz, 2H, $H^{12,13}$), 7.85 (d, *J* = 8.1 Hz, 2H, $H^{11,14}$), 7.64 (d, *J* = 7.1 Hz, 1H, H^6), 7.41 (t, *J* = 8.1 Hz, 1H, H^7), 6.13 (s, 1H, H^2); ^{13}C NMR (101 MHz, DMSO) δ 158.5, 152.3, 144.5, 141.6, 130.4, 129.8, 127.1, 126.6, 126.0, 125.9, 125.7, 125.3, 125.1, 124.2, 124.0, 116.8, 116.4, 115.5, 69.6; MS *m/z* 388.0 $[M+H]^+$; Purity >98% by LC (t_R 1.75 min).

1,9-dichloro-3-(4-(trifluoromethyl)phenyl)benzo[4,5]imidazo[1,2-*a*]pyridine-4-carbonitrile (4c)

A mixture of compound **3c** (1310 mg, 3.38 mmol) and $POCl_3$ (6 ml, 67.60 mmol) was heated to reflux at 130 ºC for 3 hr. Excess $POCl_3$ was removed under reduced pressure and 20 ml ice-cold water was added to the mixture with stirring to yield a precipitate. The mixture was neutralized with saturated $NaHCO_3$ and filtered. The resulting solid was washed with ice-cold water (4 × 15 ml) and dried in vacuo.

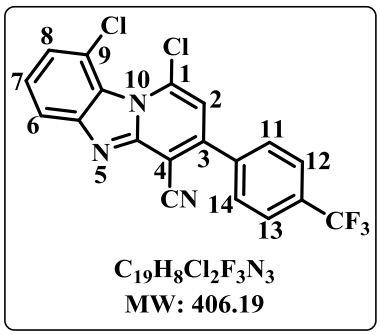

Green-yellow powder (1293 mg, 94%), M.P. 261-263 °C; R_f 0.4 (30% EtOAc/Hex); ^{1}H NMR (300 MHz, DMSO) δ 8.66 (d, *J* = 8.2 Hz, 1H, H^8), 8.04 (s, 4H, H^{11-14}), 7.80 (d, *J* = 8.2 Hz, 1H, H^6), 7.69 (s, 1H, H^2), 7.56 – 7.46 (m, 1H, H^7); ^{13}C NMR (101 MHz, DMSO) δ 149.1, 148.3, 142.2, 139.3, 135.3, 131.3, 130.9, 130.7, 130.4, 129.2, 127.1, 126.4, 126.3, 124.0, 123.6, 115.4, 115.1, 113.8, 98.2; MS *m/z* 406.0 $[M^+]$; Purity >98% by LC (t_R 5.17 min).

5.2.2 General procedure for synthesis of LHS-unsubstituted final compounds 5a-5u:

The appropriate amine (2 equiv.) was added to a stirred mixture of compound **4** (1 equiv.) and triethylamine (2 equiv.) in THF (5 ml). The mixture was irradiated in microwave (150 W) at 80 ºC for 20 min. THF was removed under reduced pressure and the resulting solid purified by column chromatography then recrystallized from acetone or ethanol, filtered and washed with a minimal amount ice-cold acetone or ethanol.

1-(4-hydroxypiperidin-1-yl)-3-(4-(trifluoromethyl)phenyl)benzo[4,5]imidazo[1,2-*a*]pyridine-4-carbonitrile (5a)

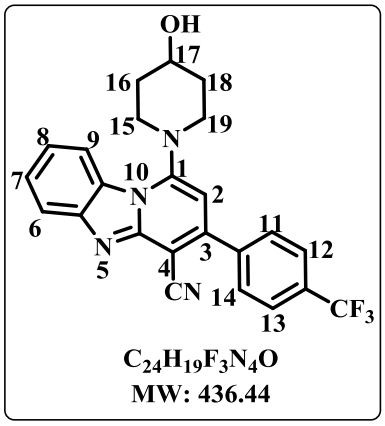

$C_{24}H_{19}F_3N_4O$
MW: 436.44

Yellow powder (164 mg, 55%); MP 307-309 ºC; R_f 0.4 (80% EtOAc/Hex); ^{1}H NMR (400 MHz, DMSO) δ 8.33 (d, *J* = 8.3 Hz, 1H, H^9), 8.02 (d, *J* = 8.3 Hz, 2H, $H^{12,13}$), 7.96 (d, *J* = 8.3 Hz, 2H, $H^{11,14}$), 7.93 (d, *J* = 8.1 Hz, 1H, H^6), 7.62 (t, *J* = 7.7 Hz, 1H, H^7), 7.50 (t, *J* = 7.2 Hz, 1H, H^8), 6.72 (s, 1H, H^2), 3.82 – 3.68 (m, 1H, H^{17}), 3.56 (s br, 1H, O*H*), 3.22 – 3.18 (m, 1H, H^{16e}), 2.98 – 2.89 (m, 2H, $H^{18e,16a}$), 2.16 – 2.02 (m, 2H, $H^{18a,15e}$), 1.95 – 1.76 (m, 2H, $H^{15a,19e}$), 1.65 – 1.54 (m, 1H, H^{19a}); ^{13}C NMR (101 MHz, DMSO) δ 153.6, 149.7, 148.8, 145.1, 141.0, 130.3, 129.1, 126.7, 126.2, 122.2, 122.0, 119.7, 119.6, 116.3, 116.0, 100.8, 100.4, 67.0, 63.1, 49.6, 46.4, 34.4, 32.4, 31.1; MS *m/z* 437.1 $[M + H]^+$; Purity 99% by LC (t_R 4.44 min). VT-^{1}H NMR was recorded at 30, 50 and 70 ºC due to occurrence of rotamers. The spectrum at 50 ºC was used as it showed no duplication of the singlet corresponding to the H^2 proton (δ 6.72).

1-(3-hydroxypyrrolidin-1-yl)-3-(4-(trifluoromethyl)phenyl)benzo[4,5]imidazo[1,2-*a*]pyridine-4-carbonitrile (5b)

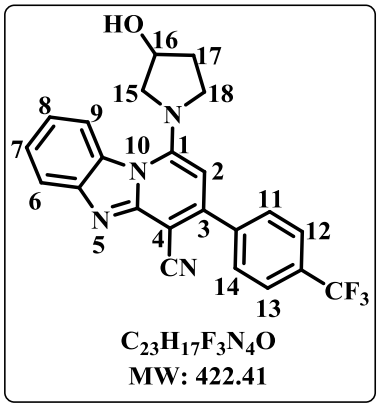

$C_{23}H_{17}F_3N_4O$
MW: 422.41

Silvery brown powder (108 mg, 46%) MP 260-262 ºC; R_f 0.3 (80% EtOAc/Hex); ^{1}H NMR (400 MHz, DMSO) δ 8.23 (d, *J* = 8.3 Hz, 1H, H^9), 8.02 (d, *J* = 8.8 Hz, 2H, $H^{12,13}$), 7.99 (d, *J* = 8.9 Hz, 2H, $H^{11,14}$) 7.91 (d, *J* = 7.8 Hz, 1H, H^6), 7.61 (t, *J* = 7.2 Hz, 1H, H^7), 7.44 (t, *J* = 7.2 Hz, 1H, H^8), 6.75 (s, 1H, H^2), 5.25 – 5.20 (m, 1H, H^{16}), 4.56 (s, 1H, O*H*), 3.74 (d, *J* = 10.0 Hz, 1H, H^{15e}), 3.59 (d, *J* = 10.8 Hz, 1H, H^{15a}), 3.43 – 3.35 (m, 2H, $H^{18a,18e}$), 2.36 – 2.25 (m, 1H, H^{17e}), 2.03 – 1.94 (m, 1H, H^{17a}); ^{13}C NMR (101 MHz, DMSO) δ 151.9, 149.8, 149.4, 145.4, 141.3, 130.6, 130.3, 129.4, 126.5, 126.3, 126.2, 126.1, 125.9, 121.5, 119.3, 117.0, 116.7, 98.6, 89.6, 69.6, 59.5, 49.8, 34.2; MS *m/z* 423.1 $[M + H]^+$; Purity 99% by LC (t_R 4.43 min).

1-((1-methylpiperidin-4-yl)amino)-3-(4-(trifluoromethyl)phenyl)benzo[4,5]imidazo[1,2-*a*]pyridine-4-carbonitrile (5c)

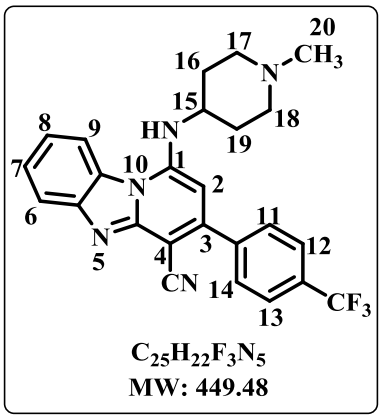

$C_{25}H_{22}F_3N_5$
MW: 449.48

Crystalline yellow solid (151 mg, 51%) MP 215-217 ºC; R_f 0.4 (10% MeOH/DCM); ^{1}H NMR (400 MHz, DMSO) δ 8.41 (d, *J* = 8.3 Hz, 1H, H^9), 7.96 (s, 4H, $H^{11,12,13,14}$), 7.85 (d, *J* = 8.1 Hz, 1H, H^6), 7.58 (t, *J* = 7.7 Hz, 1H, H^7), 7.40 (t, *J* = 7.4 Hz, 1H, H^8), 6.34 (s, 1H, H^2), 3.88 – 3.78 (m, 1H, H^{15}), 2.88 – 2.78 (m, 2H, $H^{17e,18e}$), 2.24 (s, 3H, methyl H^{20}), 2.17 (t, *J* = 10.6 Hz, 2H, $H^{17a,18a}$), 2.10 – 2.01 (m, 2H, $H^{16e,19e}$), 1.92 (t, *J* = 9.6 Hz, 2H, $H^{16a,19a}$); ^{13}C NMR (101 MHz, DMSO) δ 150.6, 149.6, 148.98, 145.4, 142.0, 141.9, 130.3, 130.2, 130.0, 128.7, 128.6, 126.4, 126.2, 126.1, 126.0, 120.7, 118.8, 117.7, 117.6, 116.1, 91.6, 54.4, 50.7, 46.3, 31.1; MS *m/z* 450.2 [M + H]+; Purity 99% by LC (t_R 4.03 min).

1-((1-methylpiperidin-4-yl)oxy)-3-(4-(trifluoromethyl)phenyl)benzo[4,5]imidazo[1,2-*a*]pyridine-4-carbonitrile (5d)

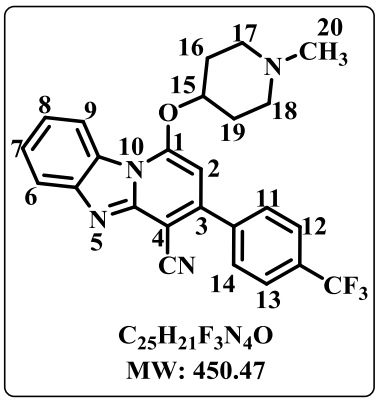

$C_{25}H_{21}F_3N_4O$
MW: 450.47

Yellow powder (41 mg, 10%); MP 304-306 ºC; R_f 0.4 (5% MeOH/DCM); ^{1}H NMR (400 MHz, MeOD) δ 8.35 (d, *J* = 8.3 Hz, 1H, H^9), 7.94 (d, *J* = 8.1 Hz, 2H, $H^{12,13}$), 7.88 (d, *J* = 8.5 Hz, 2H, $H^{11,14}$), 7.84 (d, *J* = 8.2 Hz, 1H, H^6), 7.59 (t, *J* = 7.8 Hz, 1H, H^7), 7.41 (t, *J* = 7.4 Hz, 1H, H^8), 6.65 (s, 1H, H^2), 5.24 – 5.16 (m, 1H, H^{15}), 2.86 (t, *J* = 11.1 Hz, 2H, $H^{17e,18e}$), 2.57 (t, *J* = 11.4 Hz, 2H, $H^{17a,18a}$), 2.40 (s, 3H, methyl H^{20}), 2.38 – 2.30 (m, 2H, $H^{16e,19e}$), 2.26 – 2.18 (m, 2H, $H^{16a,19a}$); ^{13}C NMR (101 MHz, MeOD) δ 154.2, 152.0, 147.9, 144.0, 140.5, 140.0, 131.6, 131.3, 129.4, 128.5, 128.1, 126.5, 125.4, 125.3, 122.7, 122.0, 118.2, 116.1, 114.9, 91.1, 89.3, 77.2, 51.9, 44.7, 29.8; MS *m/z* 451.2 $[M + H]^+$; Purity 98% by LC (t_R 4.04 min).

1-(3-(methylamino)piperidin-1-yl)-3-(4-(trifluoromethyl)phenyl)benzo[4,5]imidazo[1,2-*a*]pyridine-4-carbonitrile (5e)

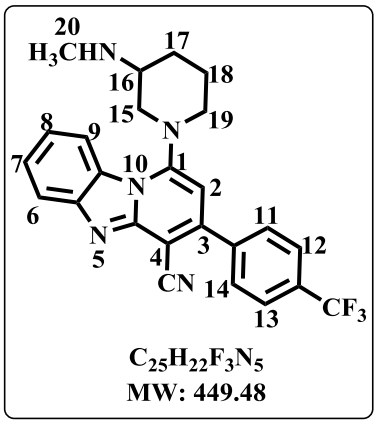

$C_{25}H_{22}F_3N_5$
MW: 449.48

Yellow solid (81 mg, 21%); MP 215-216 ºC; R_f 0.5 (10% MeOH/DCM); ^{1}H NMR (400 MHz, DMSO,) δ 8.31 (d, *J* = 8.3 Hz, 1H, H^9), 8.07 – 8.00 (m, 4H, $H^{11,12,13,14}$), 7.96 (d, J = 7.8 Hz, 1H, H^6), 7.64 (t, *J* = 7.2 Hz, 1H, H^7), 7.52 (t, *J* = 7.2 Hz, 1H, H^8), 6.83 (s, 1H, H^2), 3.92 – 3.85 (m, 1H, H^{15e}), 3.75 – 3.62 (m, 1H, H^{16}), 3.57 – 3.49 (m, 1H, H^{15a}), 3.00 (t, *J* = 11.1 Hz, 1H, H^{19e}), 2.79 (t, *J* = 10.8 Hz, 1H, H^{19a}), 2.61 (s, 3H, methyl H^{20}), 2.41 – 2.32 (m, 1H, H^{17e}), 2.15 – 1.95 (m, 2H, $H^{17a,18e}$), 1.69 – 1.56 (m, 1H, H^{18a}); ^{13}C NMR (101 MHz, DMSO) δ 152.8, 149.6, 148.5, 145.1, 140.9, 130.5, 130.4, 130.3, 128.9, 126.8, 126.3, 122.5, 119.8, 117.0, 116.2, 101.6, 100.0, 93.3, 54.2, 51.6, 51.0, 30.0, 26.7, 25.2, 22.9; MS *m/z* 450.2 $[M + H]^+$; Purity 99% by LC (t_R 4.13 min). VT-^{1}H NMR was recorded at 30, 50 and 70 ºC due to occurrence of rotamers. The spectrum at 50 ºC was used as it showed no duplication of the singlet corresponding to the H^2 proton (δ 6.83).

1-((1-acetylpiperidin-4-yl)amino)-3-(4-(trifluoromethyl)phenyl)benzo[4,5]imidazo[1,2-*a*]pyridine-4-carbonitrile (5f)

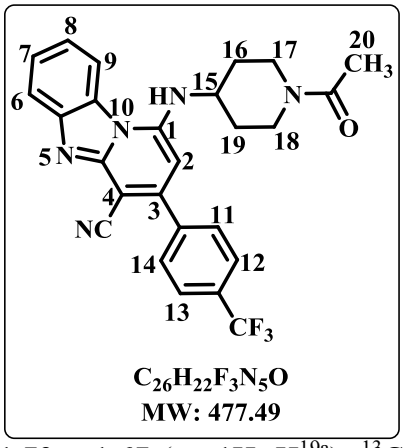

Yellow powder (142 mg, 48%); MP 253-255 ºC; R_f 0.5 (5% MeOH/DCM); ^{1}H NMR (400 MHz, DMSO) δ 8.39 (d, *J* = 8.4 Hz, 1H, H^9), 8.00 – 7.93 (m, 4H, $H^{11,12,13,14}$), 7.86 (d, *J* = 8.0 Hz, 1H, H^6), 7.59 (t, *J* = 7.5 Hz, 1H, H^7), 7.42 – 7.34 (m, 2H, H^8, N*H*), 6.48 (s, 1H, H^2), 4.44 – 4.34 (m, 1H, H^{17e}), 4.21 – 4.10 (m, 1H, H^{18e}), 3.93 – 3.84 (m, 1H, H^{15}), 3.30 – 3.20 (m, 1H, H^{17a}), 2.85 – 2.73 (m, 1H, H^{18a}), 2.17 – 2.08 (m, 2H, $H^{16e,19e}$), 2.05 (s, 3H, methyl H^{20}), 1.90 – 1.81 (m, 1H, H^{16a}), 1.79 – 1.67 (m, 1H, H^{19a}); ^{13}C NMR (101 MHz, DMSO) δ 168.6, 150.9, 149.4, 148.7, 145.4, 141.9, 130.4, 130.2, 130.1, 128.5, 126.5, 126.1, 126.0, 123.2, 120.8, 118.9, 117.4, 116.0, 91.5, 83.7, 50.7, 50.6, 45.1, 31.7, 30.9, 21.7; MS *m/z* 478.2 $[M + H]^+$; Purity 99% by LC (t_R 4.35 min).

1-(4-(methylamino)piperidin-1-yl)-3-(4-(trifluoromethyl)phenyl)benzo[4,5]imidazo[1,2-*a*]pyridine-4-carbonitrile (5g)

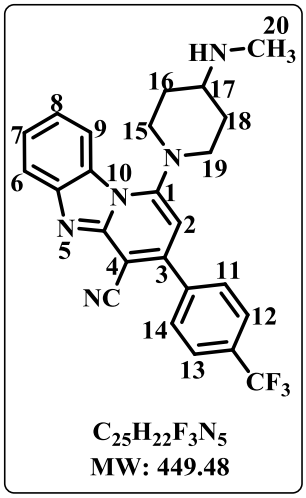

Brown powder (53 mg, 17%); MP 247-249 ºC; R_f 0.3 (10% MeOH/DCM); ^{1}H NMR (400 MHz, DMSO) δ 8.35 (d, *J* = 8.1 Hz, 1H, H^9), 8.04 (d, *J* = 8.5 Hz, 2H, $H^{12,13}$), 7.99 (d, *J* = 8.5 Hz, 2H, $H^{11,14}$), 7.96 (d, *J* = 8.3 Hz, 1H, H^6), 7.65 (t, *J* = 7.6 Hz, 1H, H^7), 7.49 (t, *J* = 7.6 Hz, 1H, H^8), 6.78 (s, 1H, H^2), 3.66 (t, *J* = 11.6 Hz, 2H, $H^{15e,19e}$), 3.61 – 3.50 (m, 1H, H^{17}), 2.99 (t, *J* = 11.5 Hz, 2H, $H^{15a,19a}$), 2.66 (s, 3H, methyl H^{20}), 2.59 (s, 1H, N*H*), 2.39 – 2.30 (m, 2H, $H^{16e,18e}$), 2.26 – 2.09 (m, 2H, $H^{16a,18a}$); ^{13}C NMR (101 MHz, DMSO) δ 153.1, 149.6, 149.5, 149.2, 148.6, 148.5, 145.2, 140.9, 130.3, 129.0, 126.8, 126.2, 122.2, 119.8, 116.3, 116.2, 115.8, 101.2, 92.8, 54.8, 49.3, 47.6, 29.8, 27.4, 26.4; MS *m/z* 450.2 $[M + H]^+$; Purity 99% by LC (t_R 4.16 min). VT-^{1}H NMR was recorded at 30, 50 and 70 ºC due to occurrence of rotamers. The spectrum at 50 ºC was used as it showed no duplication of the singlet corresponding to H^2 proton (δ 6.78).

1-(3-hydroxyazetidin-1-yl)-3-(4-(trifluoromethyl)phenyl)benzo[4,5]imidazo[1,2-*a*]pyridine-4-carbonitrile (5h)

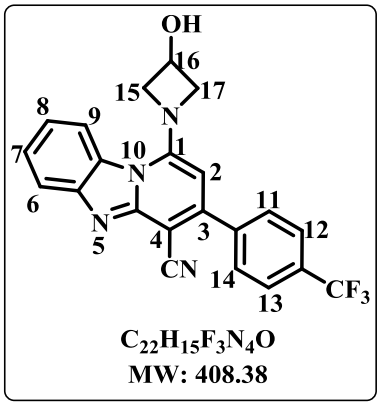

$C_{22}H_{15}F_3N_4O$
MW: 408.38

Crystalline brown solid (173 mg, 57%) MP 289-290 ºC; R_f 0.3 (60% EtOAc/Hex); ^{1}H NMR (400 MHz, DMSO) δ 8.20 (d, *J* = 8.3 Hz, 1H, H^9), 8.03 – 7.97 (m, 4H, $H^{11,12,13,14}$), 7.89 (d, *J* = 8.2 Hz, 1H, H^6), 7.60 (t, *J* = 7.2 Hz, 1H, H^7), 7.45 (t, *J* = 7.2 Hz, 1H, H^8), 6.56 (s, 1H, H^2), 5.92 (d, *J* = 6.2 Hz, 1H, O*H*), 4.75 – 4.69 (m, 1H, H^{16}), 4.48 (d, *J* = 9.0 Hz, 2H, $H^{15e,17e}$), 4.01 (d, *J* = 9.0 Hz, 2H, $H^{15a,17a}$); ^{13}C NMR (101 MHz, DMSO) δ 152.8, 149.9, 149.3, 145.5, 141.4, 130.6, 130.2, 129.9, 128.8, 126.5, 126.2, 126.1, 125.9, 123.2, 121.5, 119.1, 116.9, 116.5, 96.1, 88.1, 64.1, 60.6; MS *m/z* 409.1 $[M + H]^+$; Purity 99% by LC (t_R 4.42 min).

1-(piperidin-4-ylamino)-3-(4-(trifluoromethyl)phenyl)benzo[4,5]imidazo[1,2-*a*]pyridine-4-carbonitrile (5i)

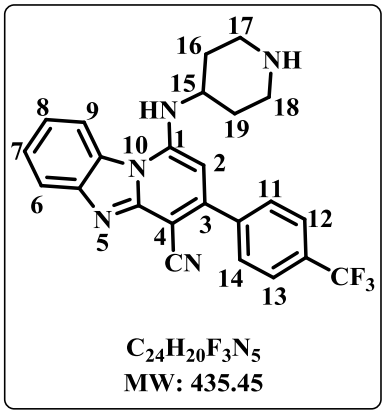

$C_{24}H_{20}F_3N_5$
MW: 435.45

Yellow solid (336 mg, 83%) MP >270 ºC; R_f 0.1 (30% MeOH/DCM); ^{1}H NMR (300 MHz, DMSO) δ 8.68 (d, *J* = 8.0 Hz, 1H, H^9), 7.93 – 7.82 (m, 4H, $H^{11,12,13,14}$), 7.61 (d, *J* = 7.7 Hz, 1H, H^6), 7.35 (t, *J* = 7.1 Hz, 1H, H^7), 7.15 (t, *J* = 7.2 Hz, 1H, H^8), 5.88 (s, 1H, H^2), 3.90 – 3.81 (m, 1H, H^{15}), 3.31 – 3.20 (m, 2H, $H^{17e,18e}$), 3.00 – 2.88 (m, 2H, $H^{17a,18a}$), 2.09 – 1.97 (m, 2H, $H^{16e,19e}$), 1.83 – 1.68 (m, 2H, $H^{16a,19a}$); ^{13}C NMR (101 MHz, DMSO) δ 151.7, 150.5, 148.4, 145.6, 143.7, 130.4, 129.8, 129.6, 129.3, 126.1, 125.8, 125.7, 124.6, 123.4, 120.2, 119.1, 116.9, 116.7, 91.2, 72.7, 66.8, 50.6, 43.5, 31.2; MS *m/z* 436.1 $[M + H]^+$; Purity >98% by LC (t_R 3.40 min).

1-((4-hydroxycyclohexyl)amino)-3-(4-(trifluoromethyl)phenyl)benzo[4,5]imidazo[1,2-*a*]pyridine-4-carbonitrile (5j)

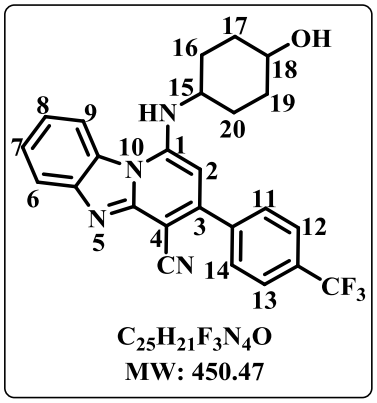

$C_{25}H_{21}F_3N_4O$
MW: 450.47

Yellow solid (57 mg, 16%) MP 244-246 ºC; R_f 0.3 (3% MeOH/DCM); ^{1}H NMR (300 MHz, DMSO) δ 8.36 (d, *J* = 8.2 Hz, 1H, H^9), 7.96 (s, 4H, $H^{11,12,13,14}$), 7.84 (d, *J* = 8.1 Hz, 1H, H^6), 7.58 (t, *J* = 7.8 Hz, 1H, H^7), 7.39 (t, *J* = 7.9 Hz, 1H, H^8), 7.29 (s, 1H, N*H*), 6.38 (s, 1H, H^2), 4.60 (d, *J* = 4.2 Hz, 1H, O*H*), 3.89 – 3.76 (m, 1H, H^{18}), 3.56 – 3.44 (m, 1H, H^{15}), 2.16 – 2.05 (m, 2H, $H^{17e,19e}$), 1.95 – 1.85 (m, 2H, $H^{17a,19a}$), 1.79 – 1.62 (m, 2H, $H^{16e,20e}$), 1.48 – 1.30 (m, 2H, $H^{16a,20a}$); ^{13}C NMR (101 MHz, DMSO) δ 150.8, 149.5, 148.9, 145.4, 141.9, 130.6, 130.4, 130.2, 128.5, 127.9, 126.4, 126.0, 125.9, 123.2, 120.7, 118.9, 117.5, 115.9, 114.4, 91.4, 83.2, 68.6, 52.1, 34.1, 29.9; MS *m/z* 451.2 $[M + H]^+$; Purity >98% by LC (t_R 4.44 min).

1-(4-oxopiperidin-1-yl)-3-(4-(trifluoromethyl)phenyl)benzo[4,5]imidazo[1,2-*a*]pyridine-4-carbonitrile (5k)

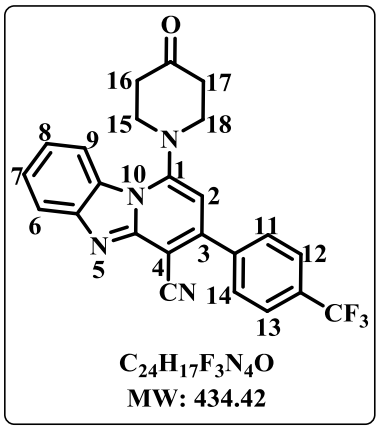

$C_{24}H_{17}F_3N_4O$
MW: 434.42

Yellow solid (72 mg, 21%) MP >270 ºC; R_f 0.2 (40% EtOAc/Hex); ^{1}H NMR (300 MHz, $CDCl_3$) δ 8.37 (d, *J* = 8.1 Hz, 1H, H^9), 8.11 (d, *J* = 7.9 Hz, 1H, H^6), 7.84 (s, 4H, $H^{11,12,13,14}$), 7.66 (t, *J* = 7.2 Hz, 1H, H^7), 7.49 (t, *J* = 7.2 Hz, 1H, H^8), 6.53 (s, 1H, H^2), 4.01 – 3.89 (m, 2H, $H^{16e,17e}$), 3.40 – 3.26 (m, 2H, $H^{16a,17a}$), 3.16 – 3.00 (m, 2H, $H^{15e,18e}$), 2.78 – 2.65 (m, 2H, $H^{15a,18a}$); ^{13}C NMR (101 MHz, $CDCl_3$) δ 204.1, 151.7, 151.6, 148.7, 145.5, 145.2, 139.9, 138.7, 129.7, 129.0, 128.9, 126.8, 126.1, 126.0, 122.4, 120.8, 117.6, 114.8, 114.4, 102.4, 100.1, 95.4, 50.8, 40.3; MS *m/z* 435.1 $[M + H]^+$; Purity >98% by LC (t_R 4.23 min).

1-(3-(methylamino)pyrrolidin-1-yl)-3-(4-(trifluoromethyl)phenyl)benzo[4,5]imidazo[1,2-*a*]pyridine-4-carbonitrile (5l)

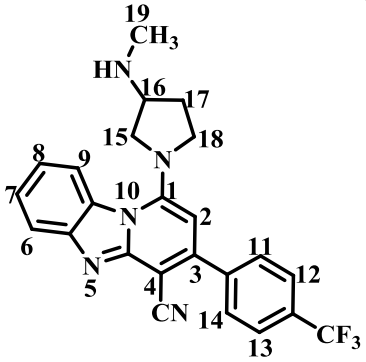

$C_{24}H_{20}F_3N_5$
MW: 435.45

Brown solid (244 mg, 70%) MP 225-228 ºC; R_f 0.3 (6% MeOH/DCM); ^{1}H NMR (300 MHz, MeOD) δ 8.16 (d, *J* = 8.2 Hz, 1H, H^9), 7.97 – 7.82 (m, 5H, $H^{6,11,12,13,14}$), 7.59 (t, *J* = 7.2 Hz, 1H, H^7), 7.45 (t, *J* = 7.2 Hz, 1H, H^8), 6.70 (s, 1H, H^2), 3.73 – 3.63 (m, 1H, H^{16}), 3.63 – 3.54 (m, 2H, $H^{15e,18e}$), 3.54 – 3.43 (m, 1H, H^{15a}), 3.32 – 3.27 (m, 1H, H^{18a}), 2.53 – 2.40 (m, 4H, H^{17e} and methyl H^{19}), 2.05 – 1.90 (m, 1H, H^{17a}); ^{13}C NMR (101 MHz, MeOD) δ 151.4, 150.4, 149.0, 144.4, 140.7, 131.5, 131.2, 129.3, 128.9, 126.2, 125.4, 125.3, 122.7, 121.5, 118.2, 116.2, 115.2, 98.6, 90.2, 58.5, 55.7, 49.8, 33.3, 30.5; MS *m/z* 436.2 $[M + H]^+$; Purity 97% by LC (t_R 3.42 min).

1-((4-hydroxy-4-methylcyclohexyl)amino)-3-(4-(trifluoromethyl)phenyl)benzo[4,5]imidazo[1,2-*a*]pyridine-4-carbonitrile (5m)

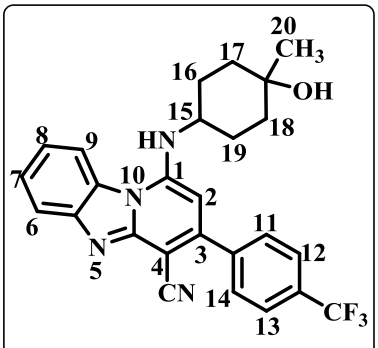

$C_{26}H_{23}F_3N_4O$
MW: 464.49

Yellow solid (34 mg, 27%) MP >270 ºC; R_f 0.2 (60% EtOAc/Hex); ^{1}H NMR (300 MHz, DMSO) δ 8.36 (d, *J* = 8.4 Hz, 1H, H^9), 7.97 (s, 4H, $H^{11,12,13,14}$), 7.86 (d, *J* = 7.7 Hz, 1H, H^6), 7.60 (t, *J* = 7.4 Hz, 1H, H^7), 7.49 – 7.34 (m, 2H, H^8 and N*H*), 6.41 (s, 1H, H^2), 3.99 – 3.84 (m, 1H, H^{15}), 2.08 – 1.96 (m, 2H, $H^{17e,18e}$), 1.90 – 1.74 (m, 2H, $H^{17a,18a}$), 1.71 – 1.49 (m, 4H, H^{17} and H^{18}), 1.24 (s, 3H, methyl H^{20}); ^{13}C NMR (101 MHz, DMSO) δ 150.9, 149.3, 149.0, 144.7, 141.8, 130.4, 130.2, 130.1, 128.4, 126.6, 126.1, 126.0, 123.2, 121.0, 118.6, 117.3, 115.9, 115.6, 114.9, 92.0, 83.0, 68.4, 51.7, 37.9, 28.2, 27.3; MS *m/z* 465.2 $[M + H]^+$; Purity >98% by LC (t_R 4.49 min).

1-((1-(methylsulfonyl)piperidin-4-yl)amino)-3-(4-(trifluoromethyl)phenyl)benzo[4,5]imidazo[1,2-*a*]pyridine-4-carbonitrile (5n)

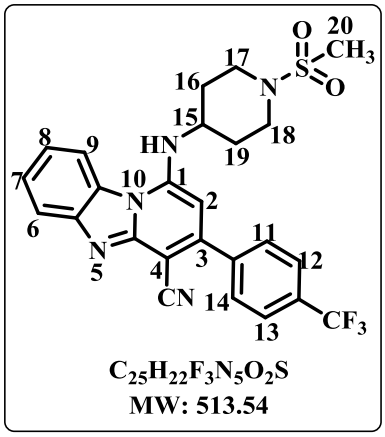

Brown solid (222 mg, 56%) MP >270 ºC; R_f 0.2 (60% EtOAc/Hex); ^{1}H NMR (300 MHz, DMSO) δ 8.39 (d, *J* = 8.4 Hz, 1H, H^9), 7.96 (s, 4H, $H^{11,12,13,14}$), 7.86 (d, *J* = 7.6 Hz, 1H, H^6), 7.59 (t, *J* = 7.7 Hz, 1H, H^7), 7.51 – 7.37 (m, 2H, H^8 and N*H*), 6.43 (s, 1H, H^2), 4.09 – 3.99 (m, 1H, H^{15}), 3.72 – 3.60 (m, 2H, $H^{17e,18e}$), 3.03 – 2.93 (m, 2H, $H^{17a,18a}$), 2.91 (s, 3H, methyl H^{20}), 2.25 – 2.13 (m, 2H, $H^{16e,19e}$), 2.05 – 1.87 (m, 2H, $H^{16a,19a}$); ^{13}C NMR (101 MHz, DMSO) δ 150.8, 149.4, 148.7, 145.4, 141.9, 130.4, 130.2, 128.5, 127.9, 126.5, 126.1, 126.0, 123.2, 120.9, 119.0, 117.3, 116.1, 114.4, 91.6, 83.9, 55.4, 50.2, 44.9, 35.1, 30.5; MS *m/z* 514.1 $[M + H]^+$; Purity 97% by LC (t_R 4.19 min).

1-((4-(2-hydroxypropan-2-yl)cyclohexyl)amino)-3-(4-(trifluoromethyl)phenyl)benzo[4,5]imidazo[1,2-*a*]pyridine-4-carbonitrile (5o)

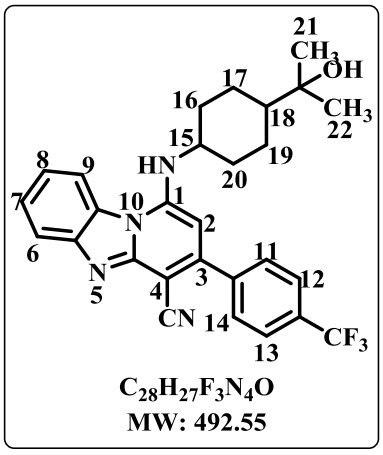

Yellow solid (259 mg, 66%) MP 277-280 ºC; R_f 0.3 (2% MeOH/DCM); ^{1}H NMR (300 MHz, DMSO) δ 8.37 (d, *J* = 8.1 Hz, 1H, H^9), 7.96 (s, 4H, $H^{11,12,13,14}$), 7.85 (d, *J* = 8.3 Hz, 1H, H^6), 7.58 (t, *J* = 7.7 Hz, 1H, H^7), 7.43 – 7.30 (m, 2H, H^8 and N*H*), 6.38 (s, 1H, H^2), 4.07 (s, 1H, O*H*), 3.84 – 3.73 (m, 1H, H^{15}), 2.24 – 2.13 (m, 2H, $H^{17e,19e}$), 1.94 – 1.82 (m, 2H, $H^{17a,19a}$), 1.71 – 1.54 (m, 2H, $H^{16e,20e}$), 1.31 – 1.15 (m, 3H, H^{18} and $H^{16a,20a}$), 1.07 (s, 6H, methyl $H^{21,22}$); ^{13}C NMR (101 MHz, DMSO) δ 150.8, 149.5, 148.9, 145.4, 141.9, 130.3, 130.2, 130.0, 129.7, 128.7, 128.5, 126.4, 126.0, 125.9, 123.2, 120.7, 118.9, 117.5, 115.9, 100.0, 91.4, 83.0, 71.0, 53.1, 48.4, 32.1, 27.5, 26.2; MS *m/z* 493.2 $[M + H]^+$; Purity >98% by LC (t_R 4.90 min).

1-((1,1-dioxidotetrahydro-2H-thiopyran-4-yl)amino)-3-(4-(trifluoromethyl)phenyl)benzo[4,5]imidazo[1,2-*a*]pyridine-4-carbonitrile (5p)

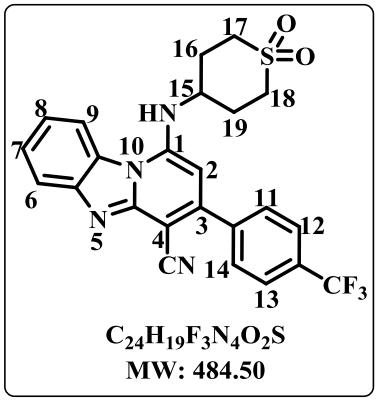

Yellow solid (132 mg, 35%) MP >270 ºC; R_f 0.2 (60% EtOAc/Hex); ^{1}H NMR (300 MHz, DMSO) δ 8.46 (d, *J* = 8.4 Hz, 1H, H^9), 8.02 – 7.92 (m, 4H, $H^{11,12,13,14}$), 7.86 (d, *J* = 8.3 Hz, 1H, H^6), 7.63 – 7.53 (m, 2H, H^7 and N*H*), 7.41 (t, *J* = 7.4 Hz, 1H, H^8), 6.45 (s, 1H, H^2), 4.34 – 4.19 (m, 1H, H^{15}), 3.46 – 3.35 (m, 2H, $H^{17e,18e}$), 3.27 – 3.14 (m, 2H, $H^{17a,18a}$), 2.49 – 2.30 (m, 4H, H^{16} and H^{19}); ^{13}C NMR (101 MHz, DMSO) δ 150.9, 149.3, 148.6, 145.3, 141.9, 130.8, 130.5, 130.2, 128.5, 126.5, 126.1, 126.0, 125.9, 123.2, 120.9, 118.9, 117.3, 116.2, 91.5, 84.2, 82.1, 49.8, 49.5, 29.0; MS *m/z* 485.1 $[M + H]^+$; Purity >98% by LC (t_R 3.96 min).

1-(((1,1-dioxidotetrahydro-2H-thiopyran-4-yl)methyl)amino)-3-(4-(trifluoromethyl)phenyl)benzo[4,5]imidazo[1,2-*a*]pyridine-4-carbonitrile (5q)

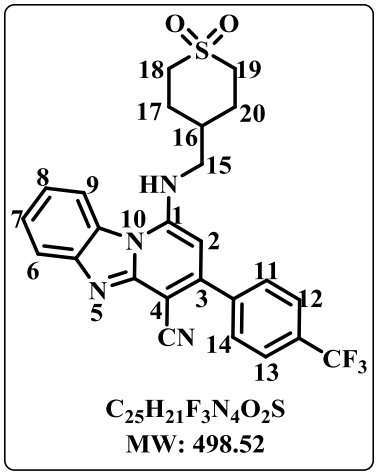

Brown solid (115 mg, 30%) MP >270 ºC; R_f 0.4 (100% EtOAc); ^{1}H NMR (300 MHz, DMSO) δ 8.53 (d, *J* = 8.4 Hz, 1H, H^9), 7.98 (s, 4H, $H^{11,12,13,14}$), 7.87 (d, *J* = 7.4 Hz, 1H, H^6), 7.73 (t, *J* = 6.3 Hz, 1H, N*H*), 7.60 (t, *J* = 7.4 Hz, 1H, H^7), 7.41 (t, *J* = 7.3 Hz, 1H, H^8), 6.39 (s, 1H, H^2), 3.57 (t, *J* = 6.4 Hz, 2H, H^{15}), 3.21 – 3.01 (m, 4H, H^{18} and H^{19}), 2.28 – 2.11 (m, 3H, H^{16} and $H^{17e,20e}$), 1.88 – 1.70 (m, 2H, $H^{17a,20a}$); ^{13}C NMR (101 MHz, DMSO) δ 150.7, 149.5, 149.2, 145.4, 141.9, 130.4, 130.2, 130.1, 128.4, 126.5, 126.1, 126.0, 123.2, 121.0, 119.0, 117.5, 115.3, 114.4, 90.9, 83.2, 55.4, 50.2, 47.2, 33.8, 28.1; MS *m/z* 499.1 $[M + H]^+$; Purity 95% by LC (t_R 4.03 min).

1-(((tetrahydro-2H-pyran-4-yl)methyl)amino)-3-(4-(trifluoromethyl)phenyl)benzo[4,5]imidazo[1,2-*a*]pyridine-4-carbonitrile (5r)

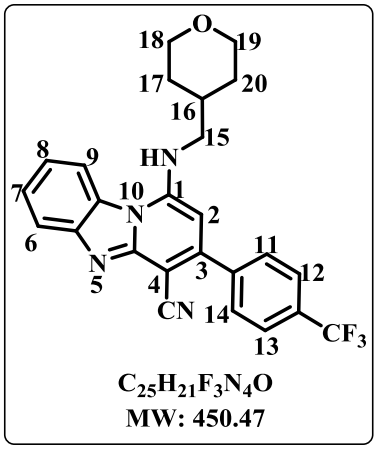

$C_{25}H_{21}F_3N_4O$
MW: 450.47

Crystalline brown solid (213 mg, 61%) MP 227-229 ºC; R_f 0.2 (60% EtOAc/Hex); ^{1}H NMR (300 MHz, DMSO) δ 8.50 (d, *J* = 8.4 Hz, 1H, H^9), 7.96 (s, 4H, $H^{11,12,13,14}$), 7.86 (d, *J* = 7.4 Hz, 1H, H^6), 7.68 (s, 1H, N*H*), 7.58 (t, *J* = 7.3 Hz, 1H, H^7), 7.41 (t, *J* = 7.2 Hz, 1H, H^8), 6.35 (s, 1H, H^2), 3.93 – 3.84 (m, 2H, $H^{18e,19e}$), 3.50 (d, *J*=7.1 Hz, 2H, H^{15}), 3.38 – 3.33 (m, 1H, $H^{18a,19a}$), 3.29 – 3.25 (m, 1H, H^{16}), 2.17 – 2.10 (m, 1H, H^{17e}), 1.80 – 1.69 (m, 2H, $H^{17a,20e}$), 1.44 – 1.26 (m, 2H, H^{20a}); ^{13}C NMR (101 MHz, DMSO) δ 150.6, 149.5, 145.4, 141.9, 130.7, 130.4, 130.2, 129.8, 128.6, 128.4, 126.4, 126.1, 126.0, 125.9, 123.2, 120.9, 118.9, 117.6, 115.3, 90.9, 82.9, 67.2, 48.9, 34.3, 31.1; MS *m/z* 451.2 $[M + H]^+$; Purity >98% by LC (t_R 4.58 min).

1-(4-aminopiperidin-1-yl)-3-(4-(trifluoromethyl)phenyl)benzo[4,5]imidazo[1,2-*a*]pyridine-4-carbonitrile (5s)

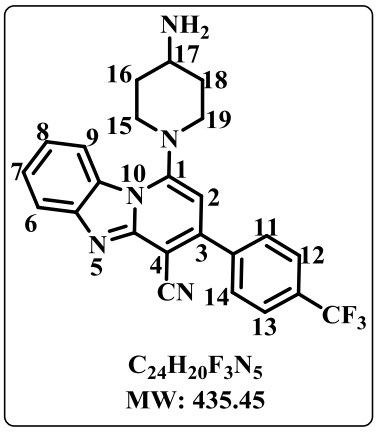

$C_{24}H_{20}F_3N_5$
MW: 435.45

Yellow solid (150 mg, 85%) MP 233-235 ºC; R_f 0.2 (10% MeOH/DCM); ^{1}H NMR (300 MHz, DMSO) δ 8.33 (d, *J* = 8.5 Hz, 1H, H^9), 8.08 – 7.85 (m, 5H, H^6 and $H^{11,12,13,14}$), 7.62 (t, *J* = 7.2 Hz, 1H, H^7), 7.50 (t, *J* = 7.2 Hz, 1H, H^8), 6.73 (s, 1H, H^2), 3.56 – 3.45 (m, 2H, $H^{15e,19e}$), 2.99 – 2.85 (m, 2H, $H^{15a,19a}$), 2.84 – 2.73 (m, 1H, H^{17}), 2.07 – 1.88 (m, 2H, $H^{16e,18e}$), 1.81 – 1.63 (m, 2H, $H^{16a,18a}$); ^{13}C NMR (101 MHz, DMSO) δ 153.9, 149.7, 148.8, 145.1, 141.0, 130.7, 130.3, 129.1, 126.7, 126.2, 125.9, 123.2, 122.1, 119.7, 116.3, 116.0, 100.7, 91.9, 66.9, 50.3, 48.8, 47.1, 35.2, 33.1; MS *m/z* 436.2 $[M + H]^+$; Purity 99% by LC (t_R 3.54 min).

1-(piperazin-1-yl)-3-(4-(trifluoromethyl)phenyl)benzo[4,5]imidazo[1,2-*a*]pyridine-4-carbonitrile (5t)

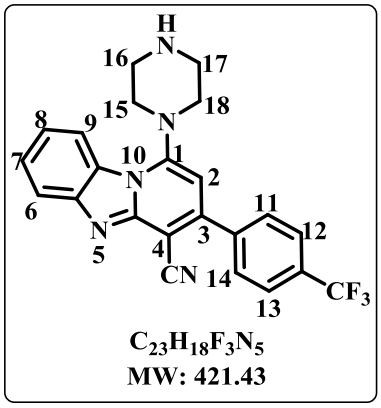

$C_{23}H_{18}F_3N_5$
MW: 421.43

Dark yellow solid (221 mg, 52%) MP >270 ºC; R_f 0.3 (6% MeOH/DCM); ^{1}H NMR (300 MHz, DMSO) δ 8.36 (d, *J* = 8.2 Hz, 1H, H^9), 8.07 – 7.96 (m, 4H, $H^{11,12,13,14}$), 7.93 (d, *J* = 8.1 Hz, 1H, H^6), 7.62 (t, *J* = 7.1 Hz, 1H, H^7), 7.50 (t, *J* = 7.2 Hz, 1H, H^8), 6.74 (s, 1H, H^2), 3.50 – 3.40 (m, 2H, $H^{16e,17e}$), 3.16 – 3.03 (m, 4H, $H^{16a,17a}$ and $H^{15e,18e}$), 3.03 – 2.90 (m, 2H, $H^{15a,18a}$); ^{13}C NMR (101 MHz, DMSO) δ 153.5, 149.7, 148.8, 145.1, 141.0, 130.7, 130.5, 130.4, 130.3, 129.0, 128.6, 126.7, 126.2, 126.1, 125.9, 122.1, 119.6, 116.3, 100.5, 91.9, 66.9, 51.7, 45.0; MS *m/z* 422.1 $[M + H]^+$; Purity 97% by LC (t_R 3.29 min).

1-(4-methylpiperazin-1-yl)-3-(4-(trifluoromethyl)phenyl)benzo[4,5]imidazo[1,2-*a*]pyridine-4-carbonitrile (5u)

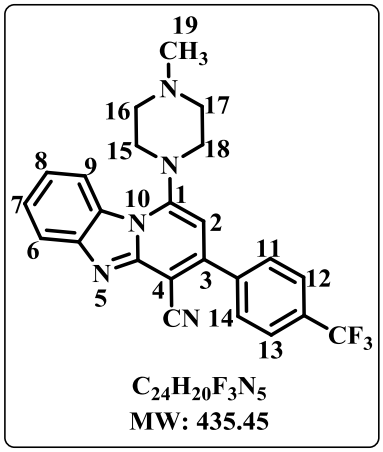

$C_{24}H_{20}F_3N_5$
MW: 435.45

Bright yellow solid (223 mg, 70%) MP 232-234 ºC; R_f 0.4 (4% MeOH/DCM); ^{1}H NMR (300 MHz, DMSO) δ 8.33 (d, *J* = 8.0 Hz, 1H, H^9), 8.04 – 7.92 (m, 5H, H^6 and $H^{11,12,13,14}$), 7.63 (t, *J* = 7.1 Hz, 1H, H^7), 7.51 (t, *J* = 7.2 Hz, 1H, H^8), 6.77 (s, 1H, H^2), 3.55 – 3.46 (m, 2H, $H^{16e,17e}$), 3.16 – 3.04 (m, 2H, $H^{16a,17a}$), 2.90 – 2.89 (m, 2H, $H^{15e,18e}$), 2.75 – 2.72 (m, 2H, $H^{15a,18a}$), 2.35 (s, 3H, methyl H^{19}); ^{13}C NMR (101 MHz, DMSO) δ 167.2, 153.2, 143.0, 132.3, 130.3, 128.9, 126.8, 126.7, 126.3, 125.0, 124.4, 122.5, 122.2, 119.7, 119.2, 116.3, 109.3, 105.8, 100.6, 54.1, 50.4, 46.1, 36.3, 31.1; MS *m/z* 436.1 $[M + H]^+$; Purity 96% by LC (t_R 3.70 min).

5.2.3 General procedure for synthesis of LHS-substituted final compounds 5v-6a:

The appropriate amine (2 equiv.) was added to a stirred mixture of the appropriate substituted chloro-intermediate **4a**, **4b** or **4c** (1 equiv.) and triethylamine (2 equiv.) in THF (5 ml). The mixture was irradiated in microwave (150 W) at 80 ºC for 30 min. Confirmation of reaction completion was done by TLC after 30 min. The reaction mixture was irradiated for a further 10 min in cases where large amounts of starting material were present. THF was then removed under reduced pressure and the resulting solid purified by column chromatography then recrystallized from acetone or ethanol, filtered and washed with a minimal amount of ice-cold acetone or ethanol.

7,8-dichloro-1-((1-methylpiperidin-4-yl)amino)-3-(4-(trifluoromethyl)phenyl)benzo[4,5]imidazo[1,2-*a*]pyridine-4-carbonitrile (5v)

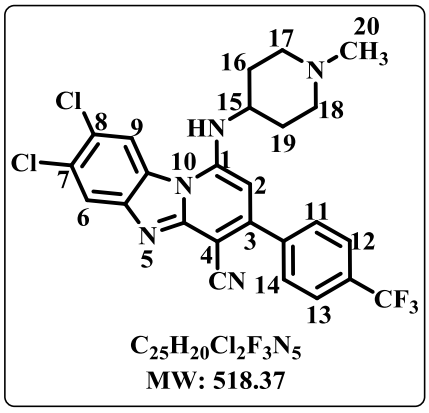

$C_{25}H_{20}Cl_2F_3N_5$
MW: 518.37

Brown solid (227 mg, 61%), M.P 264-266 ºC; R_f 0.4 (5% MeOH/DCM); ^{1}H NMR (400 MHz, DMSO) δ 8.69 (s, 1H, N*H*), 8.08 (s, 1H, H^9), 8.03 (s, 1H, H^6), 7.93 (s, 4H, $H^{11,12,13,14}$), 6.30 (s, 1H, H^2), 4.10 – 4.03 (m, 1H, H^{15}), 4.01 – 3.86 (m, 2H, $H^{17e,18e}$), 2.61 (s, 3H, methyl H^{20}), 2.41 – 2.30 (m, 2H, $H^{17a,18a}$), 2.20 – 2.12 (m, 2H, $H^{16e,19e}$), 2.04 – 1.96 (m, 2H, $H^{16a,19a}$); ^{13}C NMR (101 MHz, DMSO) δ 150.9, 145.3, 142.2, 139.5, 133.7, 131.7, 130.5, 130.2, 129.9, 129.7, 129.5, 126.3, 126.0, 125.9, 122.3, 121.7, 121.0, 118.9, 117.6, 92.8, 63.2, 53.7, 37.2, 30.4, 30.1; MS *m/z* 518.1 [M^+]; Purity 96% by LC (t_R 4.08 min).

7,9-dichloro-1-(piperidin-4-ylamino)-3-(4-(trifluoromethyl)phenyl)benzo[4,5]imidazo[1,2-*a*]pyridine-4-carbonitrile (5w)

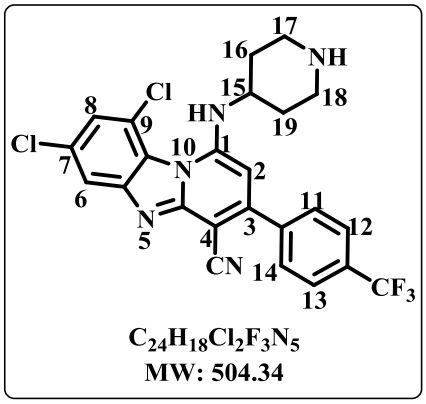

$C_{24}H_{18}Cl_2F_3N_5$
MW: 504.34

Brown powder (27 mg, 8%), M.P 262-263 ºC; R_f 0.2 (30% MeOH/DCM); ^{1}H NMR (300 MHz, DMSO) δ 8.84 (s, 1H, H^8), 7.90 – 7.78 (m, 5H, H^6 and $H^{11,12,13,14}$), 7.43 (s, 1H, N*H*), 7.31 (s, 1H, H^2), 3.88 – 3.81 (m, 1H, H^{15}), 3.38 – 3.35 (m, 2H, $H^{17e,18e}$), 3.16 – 3.04 (m, 2H, $H^{17a,18a}$), 2.07 – 1.98 (m, 2H, $H^{16e,19e}$), 1.84 – 1.72 (m, 2H, $H^{16a,19a}$); ^{13}C NMR (101 MHz, DMSO) δ 151.2, 144.1, 141.8, 132.4, 129.7, 129.5, 129.1, 128.8, 128.5, 127.1, 126.9, 126.1, 125.7, 125.6, 123.4, 123.1, 121.6, 119.8, 115.5, 92.3, 66.8, 50.2, 42.6, 30.1; MS *m/z* 504.0 [M^+]; Purity >98% by LC (t_R 3.95 min).

1-(4-aminopiperidin-1-yl)-7,9-dichloro-3-(4-(trifluoromethyl)phenyl)benzo[4,5]imidazo[1,2-*a*]pyridine-4-carbonitrile (5x)

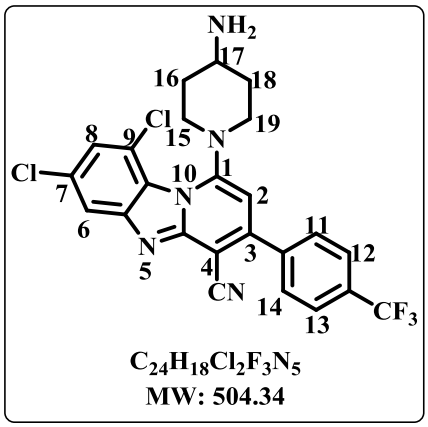

$C_{24}H_{18}Cl_2F_3N_5$
MW: 504.34

Brown powder (119 mg, 32%), M.P 247-248 ºC; R_f 0.2 (8% MeOH/DCM); ^{1}H NMR (400 MHz, DMSO) δ 8.24 (d, *J* = 1.9 Hz, 1H, H^8), 8.04 – 7.98 (m, 4H, $H^{11,12,13,14}$), 7.84 (d, *J* = 1.8 Hz, 1H, H^6), 6.85 (s, 1H, H^2), 3.54 – 3.50 (m, 2H, $H^{15e,19e}$), 2.99 – 2.90 (m, 2H, $H^{15a,19a}$), 2.88 – 2.78 (m, 1H, H^{17}), 2.04 – 1.94 (m, 2H, $H^{16e,18e}$), 1.69 – 1.56 (m, 2H, $H^{16a,18a}$); ^{13}C NMR (101 MHz, DMSO) δ 153.8, 150.9, 149.9, 149.8, 141.6, 141.1, 140.6, 130.3, 130.1, 129.0, 126.3, 126.2, 126.1, 125.8, 125.7, 123.9, 123.7, 115.9, 115.0, 114.8, 102.3, 50.4, 48.6, 34.9; MS *m/z* 504.0 [M^+]; Purity 97% by LC (t_R 4.08 min).

7,9-dichloro-1-(4-cyclopentylpiperazin-1-yl)-3-(4-(trifluoromethyl)phenyl)benzo[4,5]imidazo[1,2-*a*]pyridine-4-carbonitrile (5y)

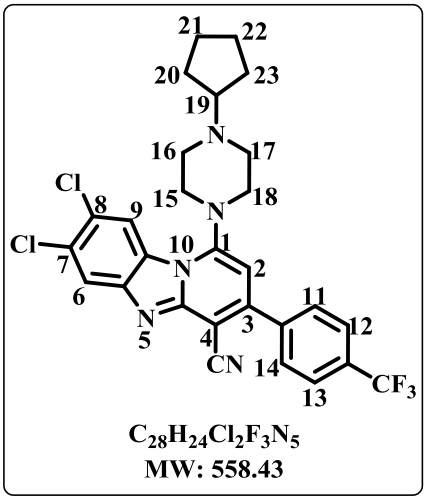

Brown powder (90 mg, 39%), M.P 209-211 ºC; R_f 0.3 (40% EtOAc/Hex); ^{1}H NMR (300 MHz, DMSO) δ 8.47 (s, 1H, H^9), 8.26 (s, 1H, H^6), 8.02 (d, J = 3.7 Hz, 2H, $H^{12,13}$), 7.32 (d, J = 4.2 Hz, 2H, $H^{11,14}$), 6.86 (s, 1H, H^2), 3.55 – 3.45 (m, 4H, H^{15} and H^{18}), 3.14 – 3.02 (m, 5H, $H^{16,17}$ and H^{19}), 1.78 – 1.52 (m, 8H, $H^{20,21,22,23}$); ^{13}C NMR (101 MHz, DMSO) δ 153.0, 150.9, 150.6, 144.8, 140.7, 130.3, 129.4, 128.4, 128.3, 127.9, 127.0, 126.9, 126.2, 124.0, 120.6, 117.5, 115.8, 101.8, 92.6, 67.0, 51.1, 50.8, 31.7, 30.2, 29.4, 29.1, 24.1, 22.5; MS *m/z* 558.1 [M^+]; Purity >98% by LC (t_R 5.34 min).

9-chloro-1-(3-(methylamino)pyrrolidin-1-yl)-3-(4-(trifluoromethyl)phenyl)benzo[4,5]imidazo[1,2-*a*]pyridine-4-carbonitrile (5z)

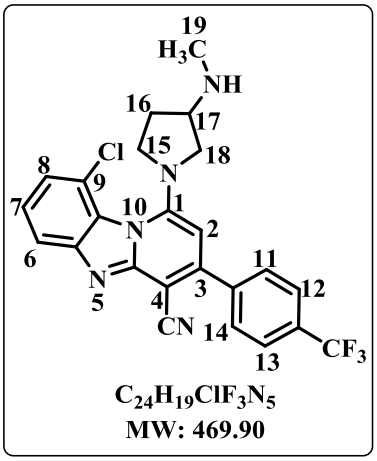

Dark yellow solid (210 mg, 58%), M.P. >270 °C; R_f 0.3 (5% MeOH/DCM); ^{1}H NMR (300 MHz, DMSO) δ 8.19 (d, J = 8.2 Hz, 1H, H^8), 7.98 (s, 4H, $H^{11\text{-}14}$), 7.66 (d, J = 7.8 Hz, 1H, H^6), 7.38 (t, J = 8.1 Hz, 1H, H^7), 6.78 (s, 1H, H^2), 3.67 – 3.53 (m, 2H, $H^{15e,18e}$), 3.50 – 3.44 (m, 2H, $H^{15a,18a}$), 2.32 (s, 3H, Methyl H^{19}), 2.30 – 2.22 (m, 1H, H^{17}), 2.01 – 1.50 (m, 2H, H^{16}); ^{13}C NMR (101 MHz, DMSO) δ 151.9, 150.5, 149.9, 142.3, 141.0, 137.9, 133.5, 130.5, 130.2, 126.2, 126.0, 125.9, 123.1, 122.6, 122.0, 116.5, 116.0, 99.4, 89.7, 59.3, 56.6, 50.2, 34.9, 31.23; MS *m/z* 470.1 [M+H]$^+$; Purity >98% by LC (t_R 4.18 min).

9-chloro-1-(3-(methylamino)piperidin-1-yl)-3-(4-(trifluoromethyl)phenyl)benzo[4,5]imidazo[1,2-*a*]pyridine-4-carbonitrile (6a)

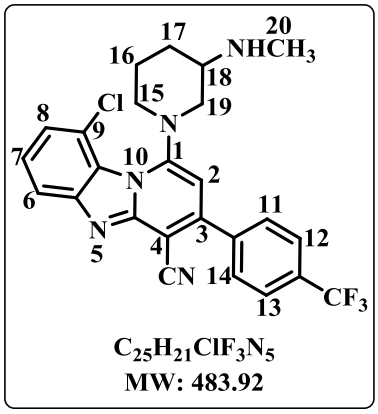

$C_{25}H_{21}ClF_3N_5$
MW: 483.92

Brown powder (268 mg, 74%), M.P. >270 °C; R_f 0.3 (6% MeOH/DCM); ^{1}H NMR (300 MHz, DMSO) δ 8.27 (d, *J* = 8.4 Hz, 1H, H^8), 8.09 – 7.97 (m, 4H, $H^{12\text{-}14}$), 7.72 (d, *J* = 7.5 Hz, 1H, H^6), 7.53 – 7.41 (m, 1H, H^7), 6.86 (s, 1H, H^2), 3.80 – 3.70 (m, 1H, H^{18}), 3.23 – 3.08 (m, 2H, $H^{15e,19e}$), 2.92 – 2.76 (m, 1H, H^{19a}), 2.70 – 2.55 (m, 1H, H^{16e}), 2.38 (s, 3H, methyl H^{20}), 2.23 – 2.13 (m, 1H, H^{17e}), 2.01 – 1.87 (m, 2H, H^{16a}), 1.42 – 1.28 (m, 1H, H^{17a}); ^{13}C NMR (101 MHz, DMSO) δ 153.5, 150.4, 149.2, 142.1, 140.7, 133.5, 130.9, 130.6, 130.3, 130.2, 126.3, 125.8, 123.1, 122.7, 116.1, 115.8, 115.2, 102.0, 92.7, 55.4, 54.8, 51.3, 32.7, 29.7, 23.4; MS *m/z* 484.1 $[M+H]^+$; Purity >98% by LC (t_R 4.22 min).

5.3 Pharmacological activity and solubility testing protocols

5.3.1 *In vitro* antiplasmodial activity

The test samples were tested in triplicate on one occasion against chloroquine-sensitive (CQS) NF54 strain of *Plasmodium falciparum*. Continuous *in vitro* cultures of asexual erythrocyte stages of *P. falciparum* were maintained using a modified version of the Trager and Jensen method.[129] Quantitative assessment of antiplasmodial activity *in vitro* was determined via the parasite lactate dehydrogenase assay.[133]

The test samples were prepared to a 20 mg/ml stock solution in 100% DMSO. Samples were tested as suspensions if not completely dissolved. Stock solutions were stored at -20 °C. Further dilutions were prepared on the day of the experiment. Chloroquine (CQ) and artesunate were used as the reference drugs in all experiments. A full dose-response was performed for all compounds to determine the concentration inhibiting 50% of parasite growth (IC_{50} value). Test samples were tested at a starting concentration of 100 µg/ml, which was then serially diluted 2-fold in complete medium to give 10 concentrations; with the lowest concentration being 0.2 µg/ml. The same dilution technique was used for all samples. Reference drugs were tested at a starting concentration of 1000 ng/ml. The highest concentration of solvent to which the parasites

were exposed had no measurable effect on parasite viability. The IC_{50} values were obtained using a non-linear dose-response curve fitting analysis via GraphPad Prism v.4.0 software.

5.3.2 Beta-hematin inhibition assay

This assay quantifies the inhibition of beta-hematin formation at a particular drug concentration. It involves addition of pyridine solution which complexes with free heme (absorbance at 405 nm) but not beta-hematin, allowing for quantification of hemozoin formation. The controls used are chloroquine (CQ) and amodiaquine, both known beta-hematin inhibiting antimalarials, and the non-inhibitor pyrimethamine.

Stock solutions of controls and test compounds were made to 20 mM concentration in DMSO. A solution containing water/305.5 μM NP40/DMSO at a v/v ratio of 70%/20%/10%, respectively was added to every well in columns 1-11 while 140 μL of water and 40 μL of 305.5 μM NP40 were added to column 12 to mediate the formation of beta-hematin. Twenty microliters of drug (20 mM) was added to column 12 and 100 μL of this solution serially diluted to column 2, with column 1 left as the blank (0 μM of compound). In case the compound was colored, a pre-reading of the plate was done by measuring absorbance at 405 nm on a SpectraMax plate reader. A 178.8 μL aliquot of hematin stock was suspended in 20 ml of a 1 M acetate buffer, pH 4.9 and 100 μL of this hematin suspension added into each well. Plates were then incubated for 5 hours at 37°C after which 32 μL of pyridine solution (20% water, 20% acetone, 10% 2M HEPES buffer (pH 7.4), 50% pyridine) was added. This was followed by addition of 60 μL of acetone to all wells. Plates were again read at 405 nm and IC_{50} values plotted using GraphPad software.

5.3.3 Cytotoxicity

Compounds were tested for *in vitro* cytotoxicity against the mammalian Chinese hamster ovarian (CHO) cell line using the 3-(4,5-dimethylthiazol-2-yl)-2,5-diphenyltetrazoliumbromide (MTT) assay. The MTT assay is used as a colorimetric assay for cellular growth and survival, and compares well other available assays.[134,135] The test samples were tested in triplicate on one occasion.

The test samples were prepared to a 2 mg/ml stock solution in 10% Methanol or 10% DMSO and were tested as a suspension if not completely dissolved. Test compounds were stored at -20 °C

until use. Emetine was used as the reference drug in all experiments. The initial concentration of emetine was 100 µg/ml, which was serially diluted in complete medium with 10-fold dilutions to give 6 concentrations, the lowest being 0.001 µg/ml. The same dilution technique was applied to all the test samples. The highest concentration of solvent to which the cells were exposed had no measurable effect on cell viability.

The half-maximal inhibitory concentration (IC_{50}) values were obtained from full dose-response curves using a non-linear dose-response curve fitting analysis via GraphPad Prism v.4 software.

5.3.4 Single-point *in vitro* metabolic stability

All compounds were prepared to a 10 mM stock solution in DMSO.

The test compound (1 µM) was incubated at 37 °C in a solution containing 0.35 mg/ml microsomes (MLM – male mouse BALB/c, Xenotech; RLM – male rat IGS, Xenotech or HLM – mixed gender, Xenotech) and NADPH (1 mM) in phosphate buffer (100 mM, pH 7.4) for 30 min while shaking. The samples were then prepared by cold-ice acetonitrile precipitation containing 0.1 µM carbamazepine (internal standard), centrifuged and filtered for LC-MS analysis. The incubations were performed in triplicate and three controls (propranolol, midazolam and MMV390048) were also included. Results are reported as percentage remaining unchanged after 30 min incubation and as predicted half-life using Obach's formula.

LC-MS/MS analysis was performed on a 4000 Q-TRAP (AB SCIEX) equipment with a Turbo V® ion source coupled to an Agilent 1200 Rapid Resolution (600 bar) HPLC system. Electron spray ionization mode was used for all synthetic compounds. Analyst 1.5.1 software was used for instrument control and data acquisition. Metabolic stability analysis was performed using a Kinetex PFP column, 2.1 mm × 50 mm, 2.6 µm particles (Phenomenex) or a Kinetex C18 column, 2.1 mm × 50 mm, 2.6 µm particles (Phenomenex) with gradient of 0.4 ml/min of the mobile phase constituted of 0.1% formic acid (A) and 0.1% formic acid in acetonitrile (B) at 40 °C. Sample tray temperature was 8 °C and the injection volume used was 2 µL. Multiple reaction monitoring (MRM) mode was used for quantification of parent compound before and after incubation in liver microsomes.

5.3.5 Metabolite identification

The test compound (10 µM) was incubated at 37 °C in a solution containing 1 mg/ml microsomes (MLM – male mouse BALB/c, Xenotech; RLM – male rat IGS, Xenotech or HLM – mixed gender, Xenotech), magnesium chloride (10 mM) and NADPH (1 mM) in phosphate buffer (100 mM, pH 7.4) for 1 hour while shaking. The samples were then prepared by cold-ice acetonitrile precipitation, centrifuged and filtered for LC-MS analysis. Controls containing all the sample constituents (not incubated), and in which NADPH, microsomes or the test compound were individually excluded were also prepared and handled similarly to the test compound. Propranolol (10 µM) was incubated concomitantly as a positive control.

LC-MS/MS was performed on similar equipment as used for metabolic stability testing above. Metabolite identification was done using a Poroshell 120 EC –C18, 100 × 4.6 mm, 2.7 µm particles (Agilent) with a gradient of 0.4 ml/min mobile phase constituted of 0.1% formic acid (A) and 0.1% formic acid in acetonitrile (B) at 40 °C. Sample tray temperature of 8 °C and injection volume 10 µL were used.

IDA-EPI (Information-dependent acquisition-Enhanced product ion) scans were performed to obtain fragmentation data of parent and metabolites. MS data acquisition methods were built using Lightsight 2.3 and determined sets of biotransformations. Metabolites formed *in vitro* in microsomal incubations were identified by comparison of the chromatogram after 1 hour incubation (T60) with chromatograms at T0 and in the no-NADPH control using Lightsight 2.3. The tentative identity of the metabolite was deduced by comparison of the product ion spectra of the $[M+H]^+$ ions of the metabolite with that of the parent compounds using Analyst 1.6 and Lightsight 2.3.

5.3.6 Gametocidal activity

Compounds were assayed on two different platforms, ATP and luciferase reporter lines, which measure different metabolic parameters and account for compound diversity in mode of action. Two transgenic parasite lines were employed in the luciferase assays: NF54-PfS16-GFP-Luc and NF54-Mal8p1.16-GFP-Luc. This assay allowed determination of stage-specific gametocidal activity. Additionally, late stage gametocidal activity was assessed by an independent bioluminescent ATP assay. Gametocytes were produced as per Reader *et al*. (2015) and methods therein applied in compound assays.[136]

The **luciferase reporter assay** was established to enable accurate, reliable and quantifiable investigation of the stage-specific action of gametocidal compounds for each of the early and late gametocyte marker cell lines NF54-PfS16-GFP-Luc and NF54-Mal8p1.16-GFP-Luc. Drug assays were set up on day 5 and 10, representing >90% of either early stage I/II/III or mature stage IV/V gametocytes respectively. In each instance, assays were set up using a 2-3% gametocytemia, 1.5% hematocrit culture and 48 hour drug pressure in a gas chamber (90% N_2, 5% O_2 and 5% CO_2) at 37 °C. Luciferase activity was determined in 20 µL parasite lysates by adding 50 µL luciferin substrate (Promega Luciferase Assay System) at room temperature and detection of resultant bioluminescence at an integration constant of 10 s with the GloMax®-Multi+ Detection system with Instinct® software.

For the **ATP assay**, gametocytes representing >90% of the late stage IV/V (predominantly stage V) phase, were enriched using density gradient centrifugation and magnetic separation. Drug dilutions were placed in triplicate in 96-well plates. Approximately 50,000 gametocytes in glucose-rich complete medium were added to each well in a final volume of 100 µL and the plates incubated for 24 hours in a humidified gas chamber (90% N_2, 5% O_2 and 5% CO_2) at 37 °C. Subsequently, the BacTiter-Glo® assay (Promega) was performed according to the manufacturer‟s instructions at room temperature in the dark, with assay substrate incubated for 10 minutes, to detect ATP levels. Bioluminescence was detected at an integration constant of 0.5 s with GloMax®-Multi+ Detection system with Instinct® software.

5.3.7 Liver stage activity

Huh-7 cells, a human hepatoma cell line, were cultured in 1640 RPMI medium supplemented with 10% v/v fetal calf serum (FCS), 1% v/v non-essential amino acids, 1% v/v penicillin/streptomycin, 1% v/v glutamine and 10 mM HEPES buffer (pH 7), and maintained at 37 ºC with 5% CO_2. Inhibition of *P. berghei* liver stage infection was determined by measuring the luminescence of Huh-7 cell lysates 48 hours after infection with a firefly luciferase-expressing *P. berghei* line, PbGFP-Luccon, as previously described.[137,138] Briefly, cells (10×10^3 per well) were seeded in 96-well plates the day before drug treatment and infection. Tested compounds were prepared in the following way: 10 mM stock solutions were obtained by dissolving accurately weighed compounds in DMSO and dilutions subsequently made with medium to the desired concentration. Medium was replaced by fresh medium containing the appropriate concentration of each compound 1 hour prior to infection. Sporozoites (10,000 per well), freshly obtained through disruption of salivary glands of infected female *Anopheles stephensi* mosquitoes, were added to the wells 1 hour after compound addition. Sporozoite addition was followed by centrifugation at 1700 g for 5 min. Parasite load was determined 48 hours after infection by luminescence measurement using Biotium‟s Firefly Luciferase Assay Kit. The effect of the compounds on the viability of Huh-7 cells was assessed by the Alamar Blue assay (Invitrogen, UK), using the manufacturer‟s protocol. Nonlinear regression analysis was employed to fit the normalized results of the dose-response curves, and EC_{50} values were determined using GraphPad software.

5.3.8 Turbidimetric solubility

The assay involved initial dissolution of the test compounds in DMSO to obtain 10 mM stock solutions. Serial dilutions were then prepared on 96-well plates from a concentration range of 0.25 mM to 10 mM, with a blank well of 0 mM included as a reference. This was done in triplicate for all the samples on the pre-dilution plate. From each pre-dilution solution, secondary dilutions of the samples in DMSO and 0.01 M phosphate-buffered saline (PBS, pH 7.4) were then prepared on a second 96-well plate, the turbidimetric assay plate. This plate set up was also done in triplicate. All samples on the assay plate were diluted to a concentration range of 0-200 μM. Hydrocortisone and reserpine were included as positive and negative controls respectively, and were handled in the same manner as the test samples.

The assay plate was then incubated for 2 hours, after which absorbance of the solutions was determined at 620 nm using a SpectraMax 340 PC^{384} microplate reader. Absorbance from the wells containing only DMSO and 2% v/v PBS in DMSO serve as the blank readings. The wavelength of 620 nm is chosen because few organic compounds are known to absorb UV radiation at this value. Any observed absorbance, therefore, is expected to be due to particles which crash out of solution beyond the solubility limit of the particular sample.

By plotting the corrected absorbance versus concentration curves on MS Excel, the apparent solubility of the compounds was determined. This is indicated by the point in the PBS curve at which the plot shows a definite deviation from the baseline and a concomitant increase in corrected absorbance values due to presence of particles in solution as a result of the sample compound‟s insolubility.

5.3.9 Kinetic solubility

The kinetic solubility assay was performed using a miniaturized shake flask method in H3D‟s ADME facilities. Stock solutions (10 mM concentration) of each of the test compounds were used to prepare calibration standards (10-220 μM) in DMSO. These were then used to spike (1:50) duplicate aqueous samples of phosphate buffered saline (pH 7.4), with a final DMSO concentration of 2%. After slow shaking in an incubator (2 hours at 25 °C), the solutions were centrifuged, filtered and analyzed by means of HPLC-DAD (Agilent 1200 Rapid Resolution HPLC with a diode array detector). Best fit calibration curves were constructed using the calibration standards, which were used to determine the aqueous samples‟ solubility.[139]

REFERENCES:

128. XPREP – Data preparation and reciprocal space exploration, Version 5.1, © Bruker Analytical x-ray systems, **1997**.

129. Sheldrick, G. M. A short history of *SHELX*. *Acta Cryst.*, **2008**, *A64*, 112-122.

129. Trager, W.; Jensen, J. B. Human malaria parasites in continuous culture. *Science*, **1976**, *193*, 673-675.

130. Barbour, L. J. X-Seed, A supramolecular tool for supramolecular crystallography. *Supramol. Chem.*, **2001**, *1*, 189-191.

131. POV Ray for windows, version 3.7.0. The Persistence of Vision Raytracer Pty. Ltd. © **1991-2013**.

132. Spek, A. L. PLATON, A multipurpose crystallographic tool, Version 290512, © **1980-2012**.

133. Makler, M. T.; Ries, J. M.; Williams, J. A. et al. Parasite lactate dehydrogenase as an assay for *Plasmodium falciparum* drug sensitivity. *Am. Soc. Trop. Med. Hyg.*, **1993**, *48*, 739-741.

134. Mosmann, T. Rapid colorimetric assay for cellular growth and survival: Application to proliferation and cytotoxicity assays. *J. Immunol. Methods*, **1983**, *65*, 55-63.

135. Rubinstein, L. V.; Shoemaker, R. H.; Paull, K. D. et al. Comparison of *in vitro* anticancer drug screening data generated with a tetrazolium assay against a diverse panel of human tumor cell lines. *J. Natl. Cancer I.*, **1990**, *82*, 1113-1118.

136. Reader, J.; Botha, M.; Theron, A. et al. Nowhere to hide: Interrogating different metabolic parameters of *Plasmodium falciparum* gametocytes in a transmission blocking drug discovery pipeline towards malaria elimination. *Malar. J.*, **2015**, *14*, 213-230.

137. Ploemen, I. H. J.; Prudencio, M.; Douradinha, B. G. et al. Visualization and quantitative analysis of the rodent malaria liver stage by real time imaging. *PLoS One*, **2009**, *4*, e7881.

138. Prudencio, M; Mota, M. M.; Mendes, A. M. A toolbox to study liver stage malaria. *Trends Parasit.*, **2011**, *27*, 565-574.

139. Hill, A. P.; Young, R. J. Getting physical in drug discovery: A contemporary perspective on solubility and hydrophobicity. *Drug Discov. Today*, **2010**, *15*, 648-655.